
Electronic Theses and Dissertations, 2004-2019

2014

A Study Of Compressive Sensing For Application To Structural Health Monitoring

Vaahini Ganesan
University of Central Florida

 Part of the [Mechanical Engineering Commons](#)
Find similar works at: <https://stars.library.ucf.edu/etd>
University of Central Florida Libraries <http://library.ucf.edu>

This Masters Thesis (Open Access) is brought to you for free and open access by STARS. It has been accepted for inclusion in Electronic Theses and Dissertations, 2004-2019 by an authorized administrator of STARS. For more information, please contact STARS@ucf.edu.

STARS Citation

Ganesan, Vaahini, "A Study Of Compressive Sensing For Application To Structural Health Monitoring" (2014). *Electronic Theses and Dissertations, 2004-2019*. 4546.
<https://stars.library.ucf.edu/etd/4546>

A STUDY OF COMPRESSIVE SENSING FOR APPLICATION TO STRUCTURAL HEALTH
MONITORING

by

VAAHINI GANESAN

Bachelor of Engineering, Anna University - Chennai, India, 2011

A thesis submitted in partial fulfilment of the requirements
for the degree of Master of Science
in the Department of Mechanical and Aerospace Engineering
in the College of Engineering and Computer Science
at the University of Central Florida
Orlando, Florida

Summer Term
2014

© 2014 Vaahini Ganesan

ABSTRACT

One of the key areas that have attracted attention in the construction industry today is Structural Health Monitoring, more commonly known as SHM. It is a concept developed to monitor the quality and longevity of various engineering structures. The incorporation of such a system would help to continuously track health of the structure, indicate the occurrence/presence of any damage in real time and give us an idea of the number of useful years for the same. Being a recently conceived idea, the state of the art technique in the field is straight forward - populating a given structure with sensors and extracting information from them. In this regard, instrumenting with too many sensors may be inefficient as this could lead to superfluous data that is expensive to capture and process.

This research aims to explore an alternate SHM technique that optimizes the data acquisition process by eliminating the amount of redundant data that is sensed and uses this sufficient data to detect and locate the fault present in the structure. Efficient data acquisition requires a mechanism that senses just the necessary amount of data for detection and location of fault. For this reason Compressive Sensing (CS) is explored as a plausible idea. CS claims that signals can be reconstructed from what was previously believed to be incomplete information by Shannon's theorem, taking only a small amount of random and linear non - adaptive measurements. As responses of many physical systems contain a finite basis, CS exploits this feature and determines the sparse solution instead of the traditional least - squares type solution.

As a first step, CS is demonstrated by successfully recovering the frequency components of a simple sinusoid. Next, the question of how CS compares with the conventional Fourier transform is analyzed. For this, recovery of temporal frequencies and signal reconstruction is performed using the same number of samples for both the approaches and the errors are compared. On the

other hand, the FT error is gradually minimized to match that of CS by increasing the number of regularly placed samples. Once the advantages are established, feasibility of using CS to detect damage in a single degree of freedom system is tested under unforced and forced conditions. In the former scenario, damage is indicated when there is a change in natural frequency of vibration of the system after an impact. In the latter, the system is excited harmonically and damage is detected by a change in amplitude of the system's vibration. As systems in real world applications are predominantly multi-DOF, CS is tested on a 2-DOF system excited with a harmonic forcing. Here again, damage detection is achieved by observing the change in the amplitude of vibration of the system. In order to employ CS for detecting either a change in frequency or amplitude of vibration of a structure subjected to realistic forcing conditions, it would be prudent to explore the reconstruction of a signal which contains multiple frequencies. This is accomplished using CS on a chirp signal.

Damage detection is clearly a spatio-temporal problem. Hence it is important to additionally explore the extension of CS to spatial reconstruction. For this reason, mode shape reconstruction of a beam with standard boundary conditions is performed and validated with standard/analytical results from literature. As the final step, the operation deflection shapes (ODS) are reconstructed for a simply supported beam using CS to establish that it is indeed a plausible approach for a less expensive SHM. While experimenting with the idea of spatio-temporal domain, the mode shape as well as the ODS of the given beam are examined under two conditions - undamaged and damaged. Damage in the beam is simulated as a decrease in the stiffness coefficient over a certain number of elements. Although the range of modes to be examined heavily depends on the structure in question, literature suggests that for most practical applications, lower modes are more dominant in indicating damage. For ODS on the other hand, damage is indicated by observing the shift in the recovered spatial frequencies and it is confirmed by the reconstructed response.

TABLE OF CONTENTS

LIST OF FIGURES	viii
LIST OF TABLES	xiv
CHAPTER 1: INTRODUCTION	1
1.1 Objective	1
1.2 Motivation	1
1.3 Temporal measurement techniques	2
1.3.1 Considerations in temporal based measurements	3
1.4 Spatial measurement techniques	4
1.4.1 Proposed idea	5
1.5 Structure of planned experiments	6
CHAPTER 2: LITERATURE REVIEW	7
2.1 Structural Health Monitoring	7
2.2 Vibration Based SHM	11
2.3 Compressive Sensing	19

CHAPTER 3: COMPRESSIVE SENSING	28
3.1 Compressive Sensing - An insight	28
3.2 Mathematical background and modeling	29
3.2.1 Analytical procedure for Compressive Sensing	31
3.3 An example problem	33
CHAPTER 4: RESULTS AND DISCUSSION	35
4.1 First attempt at L1 Minimization	35
4.2 How Compressive Sensing scores over Fourier transform	39
4.2.1 Fourier Transform approach to signal recovery and reconstruction	41
4.2.2 L1 minimization approach	44
4.2.3 L2 minimization approach	46
4.2.3.1 L1 Vs L2 minimizations - Intuitive understanding	47
4.3 Quantitative comparison of FFT to L1 minimization	49
4.4 Single degree of freedom system	56
4.4.1 Unforced undamped SDOF system	57
4.4.2 Forced damped SDOF system	62
4.5 L1 minimization for signals with multiple frequencies	69

4.6 Modeshape reconstruction using L1 minimization	73
4.7 Comparison of modeshape - Analytical versus Finite Element Method	79
4.8 Investigation of Operational deflection shapes	84
4.8.1 ODS of a simply supported beam	84
4.8.1.1 Damage case 1 (Elements 75-80)- SS beam ODS	90
4.8.1.2 Damage case 2 (Elements 25-35) - SS beam ODS	93
4.8.2 ODS of a fixed-fixed beam	96
4.8.2.1 Damage case 1 (Elements 68-78)- FF beam ODS	100
4.8.2.2 Damage case 2 (Elements 20-30) - FF beam ODS	104
CHAPTER 5: CONCLUSION	107
LIST OF REFERENCES	108

LIST OF FIGURES

2.1	A basic Structural Health Monitoring system	7
2.2	Two types of Guided Wave Testing approaches (a) Pulse Echo System (b) Pulse Catch System	8
2.3	Extended and smoothed mode shape obtained from a free-free tested beam [61]	17
2.4	Normalized weighted addition of wavelet coefficients of difference in mode shapes. Basis used - Symlet (65 samples)[61]	18
2.5	Simply supported beam with crack at 'd' and under static loading of $F =$ $100N$ [68]	19
2.6	Plot of Haar wavelet coefficients that indicate the presence and location of damage in figure 2.5[68]	19
2.7	Original image processed conventionally retaining all wavelet coefficients (64 x 64 pixels camera) [69]	20
2.8	Compressed image after eliminating insignificant wavelet coefficients (single pixel camera) [69]	20
2.9	(Row 1) Doppler original signals of length 4096; (Row 2) Reconstructed signal from 1200 samples/projections [71]	22
2.10	(Left) Original Image; (Right)Reconstructed image by total minimum varia- tion [72]	23

2.11	(Left) Original Image; (Center)Reconstructed image from 1% largest wavelet coefficients; (Right) Reconstructed image from 1% largest curvelet coefficients [75]	24
2.12	(Left) Original Image;(Right) Reconstructed image from wave atom coefficients [75]	24
3.1	Single pixel camera with DMD array [91]	33
4.1	Original sinusoidal signal in the time domain: $y(t) = \sin(6.4(2\pi t)) - 0.5\sin(9.3(2\pi t))$ and its recovered frequency components	36
4.2	Original sinusoidal signal in the time domain: $y(t) = \sin(6.4(2\pi t)) - 0.5\sin(9.3(2\pi t))$	37
4.3	Solution of L1 and L2 minimizations	39
4.4	Original sine signal with 2 frequencies	40
4.5	Frequencies recovered by FFT using 8 samples	41
4.6	Reconstructed signal	42
4.7	Reconstructed signal from nine samples	43
4.8	Original signal with the 9 random samples	44
4.9	Solutions of L1 and L2 minimization	45
4.10	Original and Reconstructed signal using L1	46
4.11	Original and Reconstructed signal using L2	47

4.12	Comparison of error in reconstruction - FFT and L1 Minimization approaches	49
4.13	Frequency recovery and signal reconstruction - L1 minimization approach (attempt 2)	52
4.14	Frequency recovery and signal reconstruction - FFT approach (attempt 2) . .	53
4.15	Error in reconstruction - L1 and FFT approaches (attempt 2)	54
4.16	Frequency recovery - FFT approach (attempt 2)	54
4.17	Signal reconstruction using L1 minimization (9 random samples)(attempt 2) .	55
4.18	Signal reconstruction using FFT (Sampling frequency 18 Hz)(attempt 2) . . .	55
4.19	Signal reconstruction using FFT (Sampling frequency 20 Hz)(attempt 2) . . .	56
4.20	Original unforced response of the undamped SDOF system - Undamaged . .	58
4.21	Frequency recovered from L1 minimization and L2 minimization - undamaged	59
4.22	Reconstructed response and original response overlapped - Undamaged . . .	59
4.23	Original unforced response of the undamped SDOF system - Damaged	60
4.24	Frequency recovered from L1 minimization and L2 minimization - Damaged	61
4.25	Reconstructed response and original response overlapped - Damaged	62
4.26	Original forced response of the damped SDOF system - Undamaged	63
4.27	Solutions of L1 and L2 minimizations - Forced damped SDOF system - Un- damaged	64

4.28	Reconstructed response - Undamaged	64
4.29	Original response of the SDOF forced system - Damaged	66
4.30	Solutions of the L1 and L2 minimizations - Damaged	67
4.31	Reconstructed response - Damaged	68
4.32	Input chirp signal	69
4.33	Original response of the SDOF system to the chirp input	70
4.34	Solutions of L1 and L2 minimizations - Chirp input response of SDOF system	71
4.35	Reconstructed response of SDOF system - Chirp excitation	72
4.36	Analytical first modeshape of a simply supported beam - Healthy and damaged cases	75
4.37	Damaged first modeshape of the SS beam with 10 random samples	76
4.38	Solutions to the L1 and L2 minimizations	77
4.39	Reconstructed 1st modeshape and its original superimposed - Damaged . . .	78
4.40	Analytical Vs FEM solution - Mode shape 1 (SS beam)	81
4.41	Analytical Vs FEM solution - Mode shape 2 (SS beam)	82
4.42	Analytical Vs FEM solution - Mode shape 3 (SS beam)	83
4.43	Analytical Vs FEM solution - Mode shape 4 (SS beam)	83
4.44	Analytical Vs FEM solution - Mode shape 5 (SS beam)	84

4.45	ODS of a simply supported beam - Healthy (with 10 random samples)	86
4.46	L1 and L2 minimization solutions	87
4.47	Reconstructed ODS of the SS beam - Healthy	88
4.48	Damage case 1 - ODS of SS beam	90
4.49	Extra frequencies recovered - Damage case 1 of SS beam	91
4.50	Reconstructed ODS - Damage case 1 of SS beam	92
4.51	Reconstructed ODS compared to original ODS - Damage case 1 of SS beam .	92
4.52	Damage case 2 - ODS of SS beam	94
4.53	Extra frequencies recovered - Damage case 2 of SS beam	94
4.54	Reconstructed ODS - Damage case 2 of SS beam	95
4.55	Reconstructed ODS compared to original ODS - Damage case 2 of SS beam .	96
4.56	ODS of a fixed-fixed beam - Healthy (with random samples)	97
4.57	L1 and L2 minimization solutions	98
4.58	Reconstructed ODS of the FF beam - Healthy	99
4.59	Damage case 1 - ODS of FF beam	101
4.60	Extra frequencies recovered - Damage case 1 of FF beam	102
4.61	Reconstructed ODS - Damage case 1 of FF beam	102

4.62	Reconstructed ODS compared to original ODS - Damage case 1 of FF beam .	103
4.63	Damage case 2 - ODS of FF beam	104
4.64	Extra frequencies recovered - Damage case 2 of FF beam	105
4.65	Reconstructed ODS - Damage case 2 of FF beam	106
4.66	Reconstructed ODS compared to original ODS - Damage case 2 of FF beam .	106

LIST OF TABLES

4.1	Details of the first attempt at L1 minimization	38
4.2	Details of simple sine signal - Recovery and reconstruction using FFT and L1 minimization	40
4.3	RMS error - FFT and L1 minimization	50
4.4	RMS error in FFT reconstruction - Increasing number of samples/second . . .	50
4.5	Details of simple sine signal - Recovery and reconstruction using FFT and L1 minimization (second attempt)	51
4.6	Details of the SDOF system from equation 4.5	57
4.7	Details of the SDOF system from equation 4.6	63
4.8	Specifications of the SDOF system for the chirp excitation	70
4.9	Specifications of the simply supported beam	74
4.10	Boundary conditions of different types of beams [99]	79
4.11	Damage cases of SS beam	89
4.12	Elements to beam span reflection	89
4.13	Damage cases of FF beam	100
4.14	Elements to beam span reflection	100

CHAPTER 1: INTRODUCTION

1.1 Objective

The objective of this thesis is to explore compressive sensing as a potential approach to Structural Health Monitoring (SHM) in order to develop a technique that would be cost effective, efficient and elegant. As the name suggests, SHM is the continuous monitoring of the condition and longevity of different types of structures such as bridges, roads, buildings, pillars, etc. It is also important to mention here that methods used in SHM can be extended to smaller scale structures such as parts of machinery - rotor blades, shafts, armature and other such parts.

1.2 Motivation

Some large scale structures that are a part of our daily lives are roads, railway lines, bridges, overpasses, buildings, etc. In the United States alone, as on September 2013, Federal analysis shows that there are 7700 bridges that are in the danger of collapse and about 18000 that are fracture critical and are required to be replaced [97]. Two of the 10 major reasons for structural collapse are parts failure and poor maintenance [98]. In some situations, large bridges have failed due to a simple damage in a small piece. In fact it has been reported widely in the media that most of these accidents that claim a huge number of life and property can be prevented by stringent monitoring of the condition of the structures and their maintenance. Failure of the railway lines due to cracks, wear and tear due to the environmental effects, etc. lead to derailment of trains that claim thousands of lives around the world every year. In addition to these, industries face huge monetary losses due to defective parts of machinery or parts failure due to wear and tear. The solution to the above mentioned problems obviously lies in the installation of an effective structural health monitoring

system. The challenge however (as mentioned earlier) lies in developing a scheme that would be affordable, efficient as well as simple.

Structural health monitoring is a recently conceived idea and hence the present day approaches for its implementation are rudimentary. Literature supports that invariably, all SHM applications today involves embedding the structure in question with arbitrarily placed sensors. Also, the number of sensors employed is not limited by any factor. As mentioned before, such an approach can be considered as an ineffective use of resources. With greater number of sensors comes a greater amount of data to be collected. This calls for a heavy data acquisition system which would require a large amount of power for its functioning. The losses in the system would be tremendous also. Further, storage and processing of a large amount of data is very expensive. Despite all these concerns, choosing such an SHM system could be justified if it were the only way to achieve it. But is there any other approach for the same, only less expensive in terms of cost and time? This is the question will be discussed throughout this thesis.

1.3 Temporal measurement techniques

As mentioned earlier, the state of the art technique in monitoring structures is to populate it with several sensors. Naturally, the following question is which parameter is monitored to ensure structural health or indicate structural damage? An intuitive approach is to observe the natural frequencies of vibration of the structure in question and to look for any changes in them that could most likely be tied to damage. Further exploration in the temporal domain led to the revelation that all modal properties of a structure can provide damage signatures.

Although a pioneer in vibration based SHM, natural frequencies of vibration failed to prove itself efficient because obtaining the natural frequency requires that time histories of data are analyzed,

making it expensive in terms of cost and processing time. Use of frequency response function (FRF) for damage detection and location is explored. However, it is quickly concluded that this route may not favor optimizing the number of sensors because the accuracy of FRF in damage detection and location lies in the proximity of damage to the sensors.

Other time domain based SHM included measuring and monitoring the transmissibility function between the DOFs of a structure that is modeled as a multi-DOF system. Since this parameter denotes how much of the input excitation is transmitted from one part of the structure (element/DOF) to another, any damage in any of the elements would change the value of the parameter for the respective DOF. It is quite evident from the nature of detection that this method would again heavily depend on the modeling of the structure, i.e. the number of elements that it is being divided into which in turn decides the placement and the number of sensors. Correlation coefficients between the time histories of strain data is investigated as a potential SHM parameter. However, it weighs heavily on sampling and computation.

1.3.1 Considerations in temporal based measurements

Temporal domain measurements provide tell-tale signs of damage theoretically. Although experimental results in literature support the viability of some of these approaches, it is quite evident that these may not favor reducing the amount of data sensed. To the contrary, all these techniques will fair better with greater sensor density on the structure. While increased number of sensors pose a problem of expense, lack of a standard approach to deciding on the number of sensors to be used and where they are to be placed on the structure can cause reliability issues on the received data. In the recent times, since SHM is attracting attention globally, there are projects implemented on some well known structures around the globe and these projects are generously funded. Hence, when implemented, the focus is primarily on the outcome, i.e. increasing the accuracy while com-

promising on the cost. While this could be acceptable for an experimental scenario, when it comes to deploying the same system for everyday use on more commonly used structures, the cost might become unaffordable. In addition to this, other problems include increased power demands, complicated installation of a dense maintenance system, need for high capacity data acquisition and storage systems and heavy processing. It should also be kept in mind that a complicated network of sensors may run into repair more often.

1.4 Spatial measurement techniques

The previous section elaborated on the different measurement techniques adopted in the temporal domain. It was also seen that these methods were largely effective either theoretically or in an experimental setup. One of the main reasons for the incomplete nature of temporal measurement methods in practice is that SHM inherently is a spatio-temporal problem. By this we mean that while damage in a system may be reflected in its time-domain response, the spatial-domain response of the system may contain information that could enhance the quality of detection or location. Hence, investigation of spatial measurements for SHM becomes indispensable.

When considering temporal methods, natural frequency of vibration was the first line of identification of damage. Hence it would be intuitive to exploit the feasibility of its spatial counterpart - the mode shape. Literature indicates that mode shape extraction for damage detection and localization is a well established approach. Typically in a system, the lower modes are more dominant over the higher modes. Therefore, it would suffice to observe lower modes for signs of damage. Since modeshapes were found to be not as sensitive to damage as expected, it may be unsafe to depend on this parameter as a first line of defense against structural failure. To overcome this, the first or second order derivatives of the mode shape may be used.

Mode localization is the concentration of modal strain energy to a specific mode. Hence, when the energy of a mode increases to an extent that it suddenly dominates the structure's vibration, damage could be identified. The sensitivity of this approach was quite low. Operation deflection shapes (ODS) is also explored as a plausible approach for damage detection. ODS is very similar to a mode shape. It is a spatial attribute that indicates and locates damage. An ODS is typically a mixture of several modes and the shape it reflects depends upon the dominant mode, which in turn depends on the excitation frequency. An attempt is made to observe ODS of a beam to look for any sign of damage.

1.4.1 Proposed idea

As discussed earlier, most methods that have been explored or experimented so far focus on accuracy of results. While accuracy is undeniably important, compromising on the expense and efficiency of the maintenance system is not viable, especially when implemented on a commercial scale. Literature reveals that most realistic systems can be expressed using a finite basis. This hints that it may not be necessary to collect large amounts of data in order to characterize a system and to identify damage in it. Exploiting this feature could lead to optimizing the number of sensors used in data acquisition. In accordance with this, the alternate SHM method proposed and investigated is to use Compressive Sensing (CS), that allows reconstruction of signals from what was termed as insufficient by the conventional Nyquist-Shannon sampling theorem.

In addition to reduced sampling rate, CS is flexible in the way the samples are obtained also, i.e. it allows for random non-adaptive measurements to be taken to reconstruct a signal. Hence, in addition to reduction in the amount of data sensed, it would be possible to place these sensors randomly along the structure under observation or to place the sensors at regular intervals but activate only a few random sensors at a time to obtain the data for signal reconstruction.

1.5 Structure of planned experiments

This section is devoted to providing an overview of the simulation experiments that have been planned to be carried out in order to test the feasibility of CS in different scenarios.

The first step is to implement CS on a simple sinusoidal signal with just two frequency components. An attempt is made to recover these frequency components using lesser number of samples as compared to the lower bound dictated by the conventional Nyquist-Shannon rule. Following this is a quantified comparison of Fourier transform (FT) and compressive sensing. This is achieved by attempting to recover the frequencies and reconstruct a sinusoidal signal using both the approaches. The percentage error in the reconstruction of both the approaches are compared. Further, the number of samples for the FT approach is gradually increased so as to match the error for CS. This step provides a visual idea of how advantageous CS is when compared to FT.

The next step is to apply CS to recover the frequency and reconstruct the response of an SDOF system under forced and unforced situations. This is investigated before and after introducing damage into the system by reduction of stiffness coefficient. In the forced and unforced conditions, the signature of damage differs. Further, CS is tested for robustness by recovering the frequency components of a chirp signal that has multiple frequencies. In the spatial domain, CS is employed to reconstruct the modeshape of a simply supported beam in order to detect the presence of any damage. Damage in the beam is modeled as a change in the stiffness coefficient over a certain span. Forcing is harmonic and the excitation frequency is kept lower than the first mode. The reconstructed response may reflect and locate any damage in the beam. A similar approach is adopted for the reconstruction of the ODS as well. Here, the excitation frequency is lower than the first mode so that the ODS resembles the first mode. Any damage would cause a change in the spatial frequency obtained or produce additional frequencies and distort the reconstruction thus allowing to locate the damage.

CHAPTER 2: LITERATURE REVIEW

The thesis discusses a central objective of optimizing the amount of data sensed or measured in order to detect and locate damage in structures and the various concepts explored in relation to this. The literature review is divided in subsections, each discussing about a specific concept and how these are related to one another and to the central objective also.

2.1 Structural Health Monitoring

SHM is a smart damage assessment system that can be broken down into two components [Figure 2.1] - on board network of sensors for data acquisition and central processing unit for analyzing the acquired data [1]. Raghavan et al. discussed state of the art in SHM using Guided Waves or Guided Wave Testing (GWT).

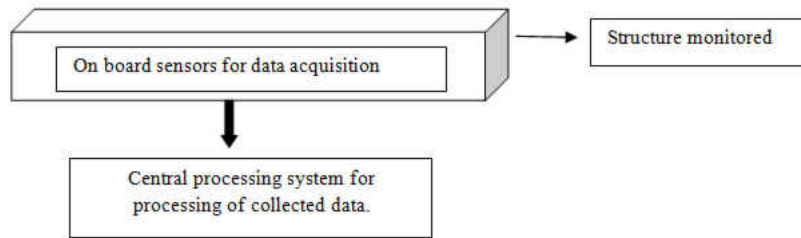


Figure 2.1: A basic Structural Health Monitoring system

The central processing system can be of 2 types - Active and Passive. The former makes use of sensors for both actuating as well as detecting (Eg. guided wave testing), while the latter uses no actuators at all (Eg. acoustic emission, strain/load monitoring). The main disadvantage in passive systems is the high density of sensors on the structures being monitored. Hence in the recent

times the research focus is on active SHM systems, i.e. guided wave testing (GWT). There are 2 basic approaches to GWT - Pulse echo and Pulse catch [Figure 2.2]. The former consists of an actuator that generates a narrow bandwidth pulse of guided wave. This wave propagates through the structure, detects a discontinuity and is reflected back to the sensor. By removing the base signal from the test signal, the presence of a discontinuity is detected and the wave speed is used to determine the location. The latter is a simpler approach where the signal generated by the actuator is detected and analyzed by a sensor on the other end after its propagation through the structure. Damages are identified based on changes in the features of this propagated pulse [1].

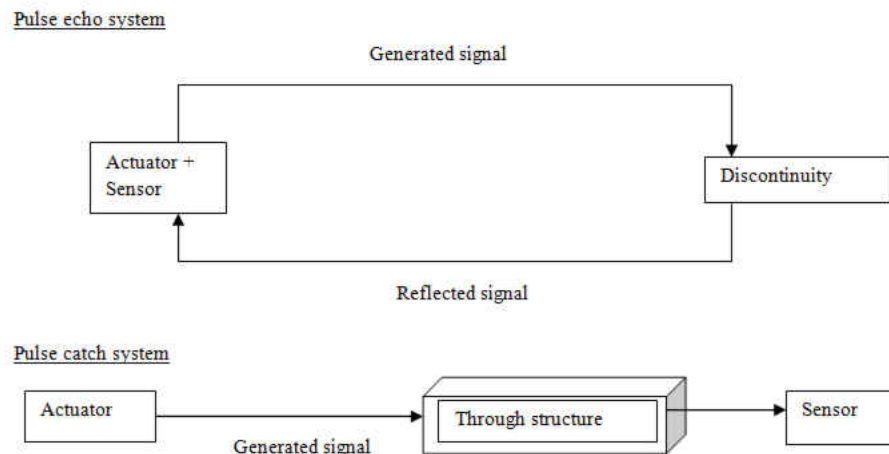


Figure 2.2: Two types of Guided Wave Testing approaches (a) Pulse Echo System (b) Pulse Catch System

GWT comes with its own challenges such as blind zone area near the actuator and sensor, restriction to the use of lower GW modes and susceptibility to noise in the measured data [1]. Ideally, SHM of civil structures must detect and locate the damage in a structure as it occurs. NDE techniques such as GWT, eddy current methods, etc. are local health monitoring methods that can arguably be unnecessary to locate the damage in a structure. More often, global monitoring meth-

ods can detect the presence of damage and further physical examination would suffice to locate the damage [2]. This is cost as well as time efficient. Most global health monitoring techniques are based on changes in the modal parameters of the structure. Significant damage or loss of important members of a fault does appear in mode shape or natural frequency changes, almost to as much as thirty percent. However, if a member plays no role in the fundamental mode, damage to that member will reflect no changes in that modal frequency.

Shifts in the fundamental frequency may result from environmental changes. Hence, this shift has to be much greater in order for a damage to be detected [2]. One way to overcome the problem of sensitivity in detection can be to monitor and observe changes in the first and second derivatives of the mode shape [3]. In case of the damage being distributed throughout the structure, measurement of the deflection profile would prove to be more beneficial [4], [5]. A novel method for damage detection is imaging and pattern recognition [6]. Since the amount of light cracks reflect and absorb are different as compared to the neighboring undamaged regions, it would be possible to ascertain cracks from images. However, it can be quite complicated as it is difficult to set fixed optimal threshold gray levels for the interior image of a structure [2].

Since the concept of SHM is very new, it is a fertile area where a lot of questions are yet to be addressed, solutions extracted. A lot of research is still going on in order to make the existing crude SHM systems to be more elegant, efficient, robust and reliable. One of the areas in this regard is to test the system using different types of guided waves. Some options explored so far are Lamb waves (most common), Love waves, Stanley waves, Rayleigh and Schulte waves. On the other hand, research also focuses on the different types of transducers that can be used for the purpose such as piezoelectric (very common), Comb, electromagnetic acoustic, Hertz contact and laser transducers [Wiki]. The state of art SHM systems employ bulk PZTs as they can act as actuators as well as transducers. However, these are not cost efficient, malign to the environment as they contain lead and require significant power to operate [7]. In situ MEMS based transducers for

ultrasonic flaw detection is a superior technology that can be used to intercept damages by detecting flaws from the reflected ultrasonic energy [8]. This can be of particular help in the form of phased array in metal structures. Low impedance MEMS transducer called Capacitive Micromachined Ultrasonic Transducer (CMUT) is explored as an alternative in Guldiken et al. [7]. Fiber Bragg Grating (FBG) sensors have undergone rapid development to emerge as a reliable in situ transducer for NDE as they have a strong immunity to Electromagnetic Interference and ground loops. They are used for a number of applications such as strain measurement, humidity measurement, early cement shrinkage, etc. FBGs are however non-standard - the prime reason for their lack of viability in the market. Further, their cost of interrogation in the present market is high [9].

The next direction of study was routed to the different topologies of sensor networks that can be incorporated in the structure and also the method adopted to analyze the detected signal. While the techniques for SHM measurements are abundant in the research world, significantly less literature is dedicated to the area of topology. An elaborate review of the little literature in this area reveals that all practical experiments are carried out not using any specific topology, rather flooding the entire structure with as many sensors as possible [10], [11], [7], [12].

One of the reasons for such a non - elegant approach is that the quantity of data measured heavily influences the accuracy and reliability of results obtained. This however is arguably inefficient because embedding a large number of sensors on a single structure increases complexity and cost of installation and maintenance. Greater number of sensors mean greater amount of power consumption, increased electrical hazards and handling of large amount of redundant data (as will be explained in Chapter three). This in turn leads to necessity of a data acquisition system of abundant capacity and increased processing cost and time. More importantly, such a non - conservative approach for damage detection would be highly expensive and practically unwise as well as impossible to realize for structures on a commercial scale. Thus stems the need for optimization of sensing for SHM, the central objective of this thesis. Section 2.1 discusses two main classifications

of SHM techniques GWT and Vibration based. Reduction of sensors employed for detection in GWT is impractical because these are local monitoring methods that retrieve damage signatures over a smaller area of examination. Increased sensor density shows an unambiguous damage indication in the region. It can hence be extended that employing this technique for larger structures would incur a big budget.

It is worth to note that the frequency of GW used plays a significant role in damage detection. Higher frequency provides high sensitivity and resolution, while lower frequency reduces attenuation. Additionally, propagation of GWs are prone to attenuation, losses and interference with environmental noise. These effects can be reduced by the use of fiber optics for carrying the waves. But this, apart from increasing the cost of maintenance would render it unsuitable for existing or old structures. Vibration based SHM therefore seems to be a promising path to reducing the amount of sensed data as will be discussed in the following subsection.

2.2 Vibration Based SHM

Vibration based SHM employs suitable in situ active or passive transducers in order to analyze the characteristics of the structure in time, frequency and modal domains [13]. Earliest approaches to this type of SHM involved comparison of modal properties of the damaged structure against an undamaged baseline of the same structure. Even though these methods are theoretically feasible, realizing them in practice is not straight forward. Vibration based SHM has been successfully implemented for rotary machines using the algorithm of pattern recognition. Such a scenario enjoys benefits of easy accessibility, small scale implementation and better control over environmental factors [14]. The attractive areas for application of this technique are civil engineering structures such as bridges and wind turbines [15],[16],[17],[18],[19],[20]. However, noisy measurements, difficulties in instrumentation especially in hostile environments, uncontrollable environmental in-

fluences on system features are some reasons that hold back this technique to be applied to a larger scale [13]. All vibration based SHM methods heavily depend on time history response of a structure that can be acquired using sensors such as accelerometers, strain gauges, etc. Modal parameters are then extracted once the response is transformed into the frequency domain. The most commonly used domain transformation is the Fourier transforms [21]. This essentially means that irrespective of the analysis domain, in the existing algorithm, the data is initially acquired in the time domain only. Since these methods require time histories of the sensed data, this ultimately leads to acquiring a large amount of data, most of which will be vestigial as will be explained in Chapter three.

Frequency Response Functions (FRF) of the response of a structure can provide comprehensive information that help to identify as well as locate damage [22],[23],[24]. However it can be argued that unless the out-of range modes in the structure's response lie very close together, use of FRFs that provide a wide frequency range is practically void [13], [25]. Besides, the FRF of the structure would vary with forcing and measurement distance from damage. Also, its accuracy will depend on the number and location of sensors [26]. This in turn would make the efforts to reduce number of sensors on the structure futile. An elaborate literature review on vibration based SHM reveals that extraction and examination of modal parameters such as mode shapes and natural frequencies of a structure are strongly backed. This can be attributed to the ease of their interpretation [13], [27], [28], [29].

Changes in the natural frequency of vibration of a structure remained a pioneer in vibration based SHM. Since damage is always modeled as a change in the stiffness (spring constant) or mass of a structure, the natural frequency was analytically the most direct parameter that would reflect a change. Although it is theoretically flawless, this primitive method of damage detection suffered even in application to simple beams under laboratory conditions. It was shown that when the severity of damage was increased beyond 60%, the natural frequency exhibited a more distributed shift

as opposed to localizing damage [27], [30], [31]. Further, it was observed that the geometry of the damage played an important role in this shift [32], [33]. It was experimentally proved that the fundamental frequencies can show a change of 5-10% due to mere natural ambient variations. Hence, lower shifts are insignificant. Therefore, if damage occurs to an important part of the structure that brings about less than 10% change in the natural frequency, it would stand unrecognized [34]. Experimental proofs are obtained by conducting tests on the I-40 Bridge [35] and T-beam slab bridge necks [36], [37]. In this regard, some researchers try to advance the technique by filtering out environmental effects from the data observed [38]. However, this is a by-pass that is subject to a lot of inaccuracy and unreliability.

Mode shape extraction from the response of structures for detection and localization of damage gained popularity in the field of SHM. There are several techniques that are employed for this purpose [39], [21]. The first is a direct comparison between a specific mode shape of a structure in its healthy and damaged states using either Modal Assurance Criterion (MAC) or Coordinate Assurance Modal Criterion (COMAC) [40], [41]. MAC measures the similarity between two mode shapes. A MAC value of 0 indicates complete dissimilarity and hence severe damage, while a value of 1 indicates complete similarity between the two compared mode shapes. Experiments were conducted in this regard on a reinforced concrete bridge under healthy and damaged states [42]. Although MAC is an indication of damage, it doesn't help in localization. COMAC, an advancement of MAC, measures the difference between the two mode shapes point-to-point and hence clearly locates the damage. Like the MAC, this method again takes values between 0 and 1 to indicate the presence and severity of damage [20]. One of the main disadvantages of mode shapes based SHM is the large amount of data that is required in order to make reliable and accurate detection [13]. Hence, this method becomes unsuitable to be used in situations where accessibility of measurement or ease of placement of greater number of sensors is difficult. Additionally, mode shape data is often heavily polluted with noise and measurement errors that affect their sensitivity

to damage [43], [44]. A solution to by-pass this problem of sensitivity to damage can be to measure the first (slope) or second (curvature) derivatives of the mode shape itself. Of the two, the curvature is said to exhibit more localized effects due to damage. The curvature of a mode shape is calculated by equation 2.1,

$$\phi''_{ji} = \frac{\phi_{(j+1)i} - 2\phi_{ji} + \phi_{(j-1)i}}{L^2} \quad (2.1)$$

where, i Mode shape number, j Node number and L Distance between the nodes [13], [45]. Other experimental tests were conducted on civil engineering structures [46], [47], [48], [49], [50], [51], [42], [52] that provide sufficient room for claiming that mode shape curvature measurements are indeed promising.

Operational Deflection Shapes (ODS) are similar to mode shapes, except they provide a physical view of the vibration of a structure. This method of SHM died out quickly owing to many difficulties such as their dependence on number and location of excitation, distance of damage from excitation point, boundary conditions of the structure and the mere complexity of their measurement itself [13], [53].

Mode localization is yet another feature that can be beneficial to detect as well as locate damage in a structure. The modal strain energy confined to a specific mode is analytically expressed by equation 2.2,

$$U_i = \frac{1}{2} \int_0^l EI \left(\frac{\partial^2 \phi_i}{\partial x^2} \right)^2 dx \quad (2.2)$$

Experiments were conducted to test the validity and reliability of this method [51], [54], [55], [14], [56], [57]. These tests can be termed successful only to an extent because they were conducted on small structures and in laboratory conditions. It was further found that although damage was indicated unfailingly, its location almost always depended on the location of sensors and quantity of data collected. This laid importance on intensive sampling [58]. But, as discussed before, such a technique will fail to be accepted at a commercial level. In addition, this technique recognized

variation in material properties along a dimension as damage especially when the severity of the actual damage was quite low [59], [60]. This implies that unless the damage inflicted the structure deeply, the results from observing modal strain energy cannot be trusted. Hence, employing this method for practical uses is questionable.

Observing the measure of correlation coefficients between time histories of strain data of a structure before and after damage can be a useful tool for damage detection as well its localization [10]. This technique is quite similar to the MAC or COMAC measurement discussed earlier. However, the correlation coefficient takes values between +1 and -1, with the former indicating highest correlation or no damage and the latter indicating maximum severity of damage. This was developed as a method to extract and analyze useful information from the abundant data collected by the numerous sensors loaded on the structure. The new data is compared against the time histories in order to calculate the correlation coefficient in real time using the equation 2.3,

$$\rho_{ij}(t_n) = \frac{\sum_{k=n-N_w}^n (s_i(t_k) - \mu_i)(s_j(t_k) - \mu_j)}{\sqrt{\sum_{k=n-N_w}^n (s_i(t_k) - \mu_i)^2} \sqrt{\sum_{k=n-N_w}^n (s_j(t_k) - \mu_j)^2}} \quad (2.3)$$

where, $\rho_{ij}(t_n)$ = correlation coefficient between sensor i and sensor j at time instant t_n for the last N_w measurements, n = number of observations in time domain, $s_i(t_k)$ and $s_j(t_k)$ are the values of sensors i and j respectively at time instant t_k and μ_i and μ_j are the mean values from sensors i and j respectively [10]. This technique was successfully applied to a four span model bridge under laboratory conditions as well as to the Sunrise Boulevard Bridge (practical application). Both attempts produced reliable results for damage indication as well as localization. An important advantage of this technique is its independence of knowledge of loading conditions. However, it depends heavily on time history data and hence intensive sampling. Additionally, calculation of correlation coefficients in real time employs heavy computation of dynamic matrices. Therefore, even though the technique proved valid for real life application, the cost of implementation on a

commercial level would be unaffordable. Further, it is independent of loading. Therefore, if it were to be employed without closing the structure to regular traffic, analysis and conclusions can be reached only after long term monitoring.

As discussed previously, extraction and analysis of mode shapes for damage detection and location is a promising avenue in the field of Structural Health Monitoring. A novel extension to this approach is the further incorporation of Continuous Wavelet Transform (CWT) in order to analyze the mode shapes in the wavelet domain, i.e. to decompose the mode shapes into its wavelet coefficients [61]. This technique requires an initial baseline set of mode shapes, i.e. mode shapes of the healthy structure. Once damage occurs, the difference between the damaged and baseline mode shapes are CWT to obtain the coefficients in the wavelet domain. It should be noted that mode shapes are almost always contaminated with noise [13], [43], [44]. In order to reduce the effect of such contamination, the mode shape data obtained is smoothed using `mslowess` built in function in MatLab [35 from `cont wave analysis`]. This process works by attaching weights to each data point along the beam span (refer equation 2.4) [61],

$$W_i = \left(1 - \left(\frac{x - x_i}{dx}\right)^3\right)^3 \quad (2.4)$$

$i = 1, 2, \dots, n$, where W_i is the weight attached to each point 'i', 'x' is the location on the span of the beam to be smoothed, x_i is the location of point 'i' and 'dx' is the span of the beam [61].

Further, in order to apply CWT to the mode shape, it has to be first extended in order to represent a periodic (sinusoidal in this case) signal in the spatial domain. This also helps to eliminate edge effect [63], [64], [65], [66], [67]. Figure 2.3 represents a smoothed and extended mode shape ready for CWT.

The same procedure is applied for mode shapes of the healthy as well as the damaged structure.

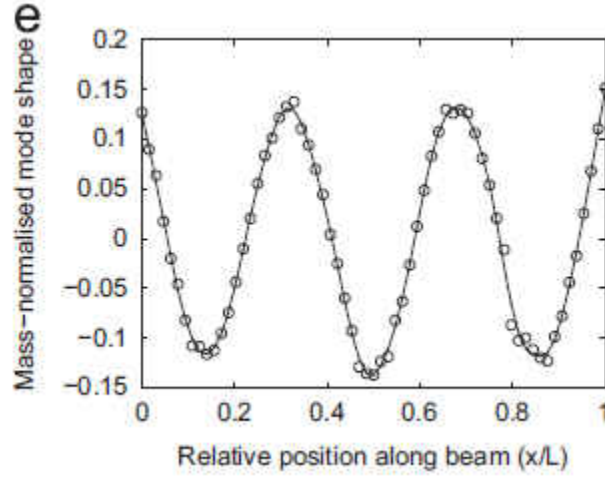


Figure 2.3: Extended and smoothed mode shape obtained from a free-free tested beam [61]

The difference between these two cases is calculated by equation 2.5 [61],

$$\phi_{diff,ext}(x) = \phi_{s,ext,d}(x) - \phi_{s,ext,u}(x) \quad (2.5)$$

where, $\phi_{s,ext,d}(x)$ is the mode shape of the damaged structure and $\phi_{s,ext,u}(x)$ is the mode shape of the same structure in the undamaged case. This modeshape difference is the parameter that is transformed into the wavelet domain by equation 2.6 [61],

$$CWT^i_{\phi_{diff,ext}}(u, s) = \frac{1}{\sqrt{(s)}} \int_{-\infty}^{+\infty} \phi^i_{diff,ext}(x) \Psi^*\left(\frac{x-u}{s}\right) dx \quad (2.6)$$

Although the noise was reduced by smoothing the mode shape immediately after data acquisition, it is worth to mention that even this reduced noise level can still cause significant masking of a damage that may not be very severe. Therefore, the weighted CWT coefficients of all the mode shapes are added for damage detection. In addition to suppressing noise, this step also enhances

damage so that even minute changes can be detected.

$$CWT_{sum}(u, s) = \sum_{i=1}^N CWT_{\phi_{diff}}^i(u, s) \cdot \left(1 - \frac{\omega_u^i}{\omega_d^i}\right)^2 \quad (2.7)$$

The results of applying this methodology for damage detection are represented in Figure 2.4.

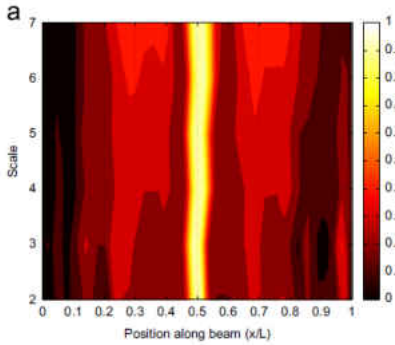


Figure 2.4: Normalized weighted addition of wavelet coefficients of difference in mode shapes. Basis used - Symlet (65 samples)[61]

Wavelet transform is also applied to the displacement response of a structure in order to detect and locate damage. This methodology is formulated on the grounds that damages such as cracks in a beam reflect themselves as local perturbations in the displacement profile of a structure. Although this perturbation is very minute, especially when the damage is not as severe, transformation into their wavelet coefficients will make these damage signatures more pronounced. Experimental tests were carried out on a beam with crack under both static as well as dynamic loads. It was observed that the existence of damage caused an abrupt change in the wavelet coefficients [68]. Figure 2.5 represents the beam and the location of damage while figure 2.6 show the plot of wavelet coefficients that indicate the presence as well as location of the damage.

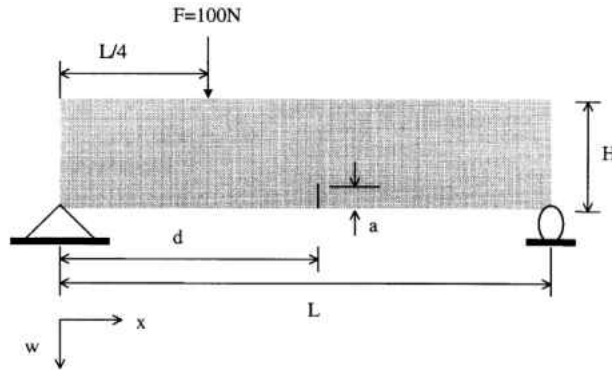


Figure 2.5: Simply supported beam with crack at 'd' and under static loading of $F = 100\text{N}$ [68]

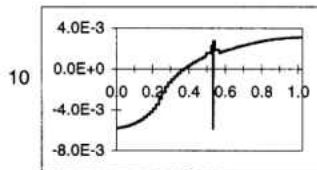


Figure 2.6: Plot of Haar wavelet coefficients that indicate the presence and location of damage in figure 2.5[68]

2.3 Compressive Sensing

Section 2.2 is an exhaustive literature review of various vibration based SHM techniques that are being tested both in a laboratory setting as well as on a real life structure. While some of these techniques died out as fast as they were developed (e.g. Matrix Updation methods), others such as examination of modal parameters and modeshapes seem promising. In all these methods, one common setback is the need to collect abundant amount of data to get complete modal information. However, the question arises How much information do we really need to detect and localize damage? Seeking an answer to this question will lead us to adopt a technique and develop an

algorithm that will be elegant, cost as well as time efficient on a commercial level, i.e. a technique that will require just the sufficient amount of data to serve this purpose. The answer to this question, although for a different application, gave birth to the concept of Compressive Sensing (CS).

CS was originally developed to improve the compactness of images. A sophisticated camera with a high megapixel specification captures a beautiful image that is produced from a million measurements. However, for all practical purposes these images are then compressed into a smaller file. This is brought about by elimination of those measurements that do not or contribute insignificantly to the original image and retention of only those measurements that really matter. CS was conceived as a method to directly make only that many number of measurements that just suffice to produce the image [69]. Hence the name, Compressive Sensing. Figure 2.7 and Figure 2.8 illustrate the reliability of CS.



Figure 2.7: Original image processed conventionally retaining all wavelet coefficients (64 x 64 pixels camera) [69]



Figure 2.8: Compressed image after eliminating insignificant wavelet coefficients (single pixel camera) [69]

The measurements are transformed into the wavelet domain. The former shows an image that is produced using a 64 x 64 pixels camera and conventionally processed without eliminating any of the wavelet coefficients while the latter is from a single pixel camera after the elimination of insignificant wavelet coefficients.

Magnetic Resonance (MR) images are inherently sparse. Hence, it was seen as one of the most viable areas for the practical application of CS. When the MR images are transformed into a suitable domain in which most of the coefficients are closer to zero, i.e. a sparse representation, all these coefficients can be eliminated, thus retaining only the few non-zero measurements. Random under-sampling of the image (treated here as the signal) was performed and it was reconstructed using L1-minimization. Experiments were conducted for sampling and reconstruction of Multi-Slice fast spin echo brain imaging and 3D contrast angiography. It was observed that although the results were successful, the reconstruction was computationally intensive as it is purely iterative in nature [70]. This necessitates the development of faster linear as well as non-linear algorithms for signal reconstruction from under-sampled data.

Most salient information of any real world signal is confined within few of its random projections. In fact it is also possible to reconstruct under-sampled signals that are contaminated with noise [71]. Developing a suitable recovery algorithm in this regard would enable use of CS in applications such as A/D conversion and remote sensing in which the data is highly prone to noise infiltration [72], [73], [74]. As an intermediate step, the data from the sensors is transformed into k random projection coefficients called Rademacher projection. This sequence is then transmitted to the target as opposed to direct transmission of the raw sampled data over the channel. By placing error bounds (lower and higher) at the receiver, noise can be identified and eliminated. Thus, from the rest of the coefficients (Rademacher projections), the original signal can be reconstructed. Figure 2.9 illustrates the results of this process [71].

The first row of images show the Doppler signal of original length (4096) while the second row of images represent the compressed reconstruction from 1200 samples.

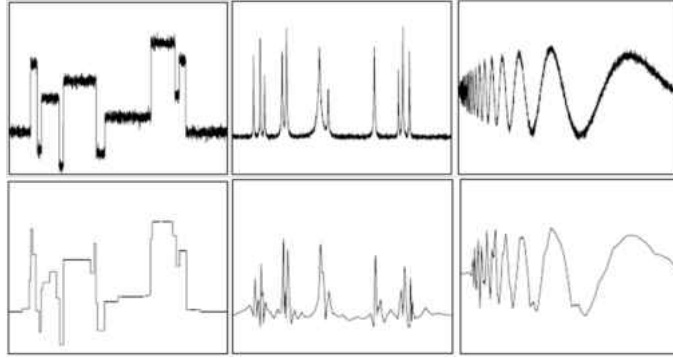


Figure 2.9: (Row 1) Doppler original signals of length 4096; (Row 2) Reconstructed signal from 1200 samples/projections [71]

The concept of CS can be extended to practically any domain as far as the signal that is being reconstructed is sparse in that domain. An exact reconstruction of a signal is attempted from its incomplete frequency information in the Fourier domain [72]. The recovery is posed as a convex optimization problem and thus solved.

$$\min_g \sum_{t=0}^{N-1} |g(t)| \quad s.t. \quad g(\hat{\omega}) = f(\hat{\omega}) \quad \text{for all } \omega \in \Omega \quad (2.8)$$

The solution to equation 2.8, i.e. the result of the convex optimization implies that given a signal with $|T|$ spikes, it can be reconstructed from any set of frequencies of size $O(|T|.logN)$ [72]. Experimental tests were conducted to verify the validity of the proposed idea. Reconstruction of 1D as well as 2D signals from partial frequency information was achieved. Additionally, it was observed that there lay a lower bound on the extent of the incomplete information, i.e. there were a minimum number of samples required to guarantee reconstruction. This lower bound would depend on the incoherence between the measurement and synthesis bases. The greater the incoherence, the lesser the number of samples required. It should however be noted that there will always exist a

small percentage of error in the reconstruction. But with a choice of highly incoherent bases, this error can be reduced to produce almost exact reconstruction. Illustrations for this could be seen in Figure 2.10 [72].

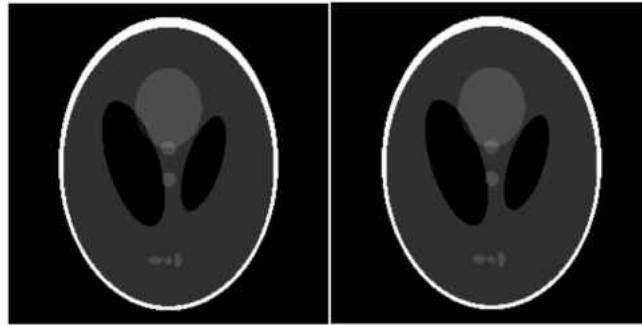


Figure 2.10: (Left) Original Image; (Right)Reconstructed image by total minimum variation [72]

Compressive Sensing, because of its powerful feature of reducing data acquisition is welcome in every field of sensing. One such notable avenue is surface metrology. Once again, the problem is posed as a convex optimization iterative problem. A suitable geometric recovery algorithm is used in this technique to characterize scratched and textured surfaces. Three types of surfaces are identified and characterized – straight scratches, curved scratches and textured surfaces. Hence, three different sparse domains are chosen – ridgelets, curvelets and wave atom transforms respectively. Figure 2.11 contains 3 images. On the left, the original image of the scratched surface, center, the reconstruction of the same from 1% largest wavelet coefficients and right, the reconstruction from 1% largest curvelet coefficients. Figure 2.12 shows the image of the original textured surface and its wave atom reconstruction [75].

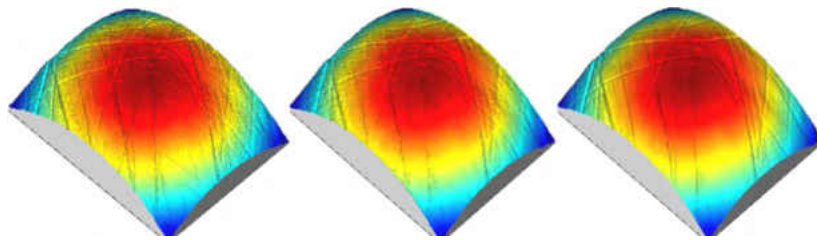


Figure 2.11: (Left) Original Image; (Center)Reconstructed image from 1% largest wavelet coefficients; (Right) Reconstructed image from 1% largest curvelet coefficients [75]

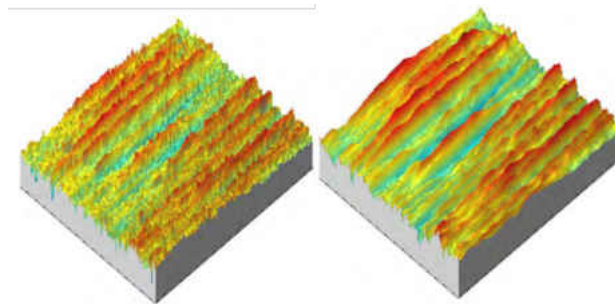


Figure 2.12: (Left) Original Image;(Right) Reconstructed image from wave atom coefficients [75]

As discussed previously, the necessity for CS stemmed from the need to produce compact images directly instead of abundant sampling and then eliminating insignificant coefficients. Hence, shortly after its conception, compressive sensing was widely applied to fields that required imaging. One such application was MRI [70]. Another equally important area is radar imaging. The idea here is straightforward. The image (signal/wave) is obtained from a few necessary measurements and is then represented in its suitable sparse domain. As mentioned earlier [72], the greater the incoherence between the bases, the lesser is the number of required measurements. The signal is then reconstructed using linear programming. The application of CS enhances the performance of radar imaging in the sense that it eliminates the use of pulse compression match filter and reduces the amount of A/D conversion at the receiver. Additionally, it ensures that the A/D con-

version can be performed at a rate lower than that proposed by Nyquist theorem thus resulting in the development of a radar sensing and imaging system that is simple and cost effective [76].

However, such a system when realized in practice has numerous challenges. The echo signal from the target must be sparse in nature or there must be a suitable basis in which this reflected signal can be sparsely represented. It was observed in [71] that most of the real-world signals are invariably contaminated with noise. Hence there arises a need to develop faster signal recovery algorithms with immunity to noise. Another challenge specific to this application is that there exists a sort of proportional relationship between the sampling rate and the range of operation of radar using CS. Hence, for sensing over longer distances, there is a compromise with the extent to which the sampling rate can be reduced [76].

An interesting application for CS is in the field of reconstruction of seismic wave propagation. Here, the wavefield extrapolation process is represented as the convex optimization problem which is yet again solved by a suitable non-linear programming algorithm. The signal is represented in the curvelet basis and a suitable incoherent measurement basis is chosen Helmholtz operators. The wavefield is reconstructed from incomplete modal information. Experimental tests are conducted for reconstruction of the wavefield extrapolation in 2D in a laboratory setting. Although the results were quite successful, the application of this method to large scale scenarios is held back due to some issues. As discussed in many of the previous applications, it can be argued that the success of the CS technique depend to a large extent, on the efficiency or speed of the recovery algorithm. Although it the sampling in CS is claimed to be completely random, devising a smart-learning sampling strategy will help to enhance its performance. Application of this technique to 3D wavefield extrapolation is theoretically simple. However, it has not been realized in practice yet.

Periodic non-uniform sampling becomes impractical when applied to wideband sparse signals. Non-uniform sampling process is based on the assumption that the samples are chosen from the entire range or band of frequencies. However, this may not be the case while considering analog wideband signals. Hence a new strategy of sampling needed to be developed. The alternative idea multiplies the signal to be reconstructed with a random square wave. This is performed at the Nyquist rate. Essentially, the system acts as a low-pass filter that samples the given signal a lower rate than suggested by Nyquist. The system consists of certain parameters, which when chosen appropriately (based on specified conditions), help in efficient reconstruction from the undersampled data [77].

Implementation of compressive sensing to sample and reconstruct wideband signals was discussed in [77]. However, this application considered the environment to be noiseless. When such a task is to be undertaken in a noisy ambiance, several challenges arise, one of which is the design of a radio receiver for wideband sparse signals [78]. It was observed that while CS indeed helped to reduce the number of required measurements, it made the system (receiver) vulnerable to noise. Every time the sampling rate was halved, the noise figure of the receiver dropped by 3 dB. However this was compensated for, as CS greatly enhances the performance of the A/D converters, thus allowing operation over a longer dynamic range [78].

The idea of compressive sensing was also attempted at network feedback control. The strategy in this application is to compress the control vectors that bring about feedback control in the system without compromising on the performance. These vectors were obtained as the solution to the L1 optimization problem using a suitable recovery algorithm called the Fast Iterative Shrinkage Thresholding Algorithm (FISTA)[79]. A controller was designed in order to achieve two important objectives. First, to reduce the tracking error between the reference input and the output signals in a given time interval. Second, to minimize the size of the control vector, i.e. to compress it. It was observed that there existed a trade-off between these two objectives both could not be

satisfied simultaneously. A highly sparse solution to the L1 minimization problem (control vector) produced a large error. To by-pass this difficulty, the problem was posed as the following (equation 2.9) [80],

$$J(u_k) := \| y_k - r_k \|_2^2 + \mu \| u_k \|_0 \quad (2.9)$$

where $\mu > 0$ is an additional regularization parameter that softens the trade-off between minimization of tracking error and minimization of control vector. Simulation tests were carried out to verify the effectiveness of the proposed technique in network feedback control systems. It was observed that the proposed technique was indeed successful and feedback control was achieved by transmission of the compressed control vectors over the rate limited channels [80]. However, this did not automatically guarantee stability.

CHAPTER 3: COMPRESSIVE SENSING

Compressive sensing (CS) is a technique of reconstructing signals from what was originally conceived to be incomplete information. CS or L1 minimization allows frequency recovery and reconstruction of a sparse signal from undersampled random, linear and non-adaptive measurements. They are random, meaning unlike the conventional method, here even the undersampled measurements need not be taken at regular fixed intervals. Non-adaptivity refers to the fixed nature of the measurement matrix that does not change as long as the frequency range of operation and resolution remain the same. This chapter provides an in-depth understanding of CS followed by simulation results and discussion of application of the concept to different signals.

3.1 Compressive Sensing - An insight

Conventionally, signals were reconstructed in line with Shannon's sampling theorem which states that a signal can be faithfully reconstructed only when it is sampled at a rate that is at least twice its highest frequency content [81]. Although theoretically feasible, under practical circumstances, it is seen that the sampling rate has to be at least 10 times the highest frequency content of the signal under reconstruction. Nevertheless, the number of samples collected for the purpose of reconstruction is abundant, and in many cases redundant.

A standing example of this scenario is the number of pixels that are used to capture an image using a sophisticated camera. Today, there are 60 megapixel digital cameras in the market that capture vivid pictures. Although brilliant, for all practical purposes, these heavily loaded images need to be compressed. In this process, all those samples that do not significantly contribute to the image are discarded, while retaining only those that are predominant. Thus, in order to halt this

'arms race' of making a million measurements and retaining only ten thousands while processing, mathematicians about a decade ago explored the possibility of reconstructing images (signals in a more general perspective) from lesser or just the sufficient number of samples [69].

Compressive sensing thus aims at reducing the number of samples obtained at the source, thereby alleviating the burden on the sensing and data acquisition machinery. As discussed in Section 2.3, this breakthrough has opened up several avenues of data acquisition and processing where efficiency and elegance were missing.

3.2 Mathematical background and modeling

As mentioned earlier, Compressive Sensing allows for reconstruction of signals when sampled at a rate much lower than that dictated by Shannon's theorem. However, it is worth mentioning that only sparse signals can be accommodated by this process. Fortunately, most real world signals are sparse when represented in a suitable domain. This means that, when a signal is expanded using a certain basis (or domain), most of the coefficients are zero. To be more specific, a signal is called k -sparse when there are at most k non-zero coefficients in its representation in that domain. Mathematically, the support of a vector x is denoted by equation 3.1[82].

$$\text{supp}(x) = \{j : x_j \neq 0\} \quad (3.1)$$

Since the sparsity of a vector (signal) is expressed in terms of the number of non-zero coefficients, it is wise to calculate the zero-norm (l_0) of that vector x (or signal) (equation 3.2)[82].

$$\|x\|_0 := |\text{supp}(x)| \quad (3.2)$$

Hence, the vector x can be claimed to be k -sparse is $\|x\|_0 \leq k$ [82]. Now, it is quite obvious that the vector x can be compressed by retaining only its non-zero coefficients while discarding the rest. However, this seems to be possible only when complete information of x is initially available. In fact, this is the process of compression used in many imaging techniques such as JPEG and MPEG. In contrast, the idea of Compressive Sensing aims to acquire only samples or measurements that significantly contribute to the signal reconstruction, i.e. only the k non-zero coefficients without the knowledge of their location.

Let us assume that x is a vector of length N and that we aim to reconstruct x using CS. As a first step, we take m linear and random measurements of x (equation 3.3), where $[A]$ is the measurement matrix and $y \in C^m$ is the measurement vector.

$$y = Ax \tag{3.3}$$

As mentioned earlier, CS is applied for the case when $m \ll N$, i.e. for the undersampled scenario. This implies that, the matrix $[A]$ has more number of rows than the number of columns. When we account for the assumption that the vector x is k -sparse, it can be seen that vector can be faithfully reconstructed. Intuitively, the approach for such a reconstruction would be to seek the sparsest solution of the l_0 minimization problem [82] (equation 3.4).

$$\min \|z\|_0 \text{ subject to } Az = y \tag{3.4}$$

However, this problem is NP-Hard to solve [83][84]. Therefore, an alternative approach to the signal recovery is the basis pursuit or l_1 minimization solution of 3.5 [85].

$$\min \|z\|_1 \text{ subject to } Az = y \tag{3.5}$$

The sparsest solution to equation 3.5 can be obtained using different approaches such as convex optimization techniques [86], greedy algorithms [87][88], etc. Now, given that a sparse vector can indeed be recovered from undersampled measurements, i.e. partial information, the question to be addressed is the minimum number of these measurements. It has been successfully demonstrated that faithful reconstruction of a sparse vector (signal) can be obtained when the number of samples (measurements) abide by equation /refsampleslim.

$$m \geq S \cdot \log(N) \quad (3.6)$$

where, s is the number of measurements, S is the number of frequencies present in the signal and N is the original number of samples required (Shannon's theorem) [89]. The two greatest achievements of compressive sensing can be noted as follows :

1. Recovery of the sparse signal from undersampled measurements using only the k largest or non-zero coefficients without any loss of information.
2. Random and non-adaptive measurements without any prior knowledge of the location of these k non-zero coefficients.

3.2.1 Analytical procedure for Compressive Sensing

Let us assume that $f(t)$ is a signal of length N that is to be recovered from undersampled and random measurements. If we are able to find a suitable orthonormal (or non-orthonormal) basis (domain) in which $f(t)$ can be represented, then we can express the signal by equation 3.7.

$$f(t) = \sum_{i=1}^N x_i \psi_i(t), \quad t = 1, \dots, N. \quad (3.7)$$

It is worth to note that the basis to be chosen will depend upon the type of signal that is to be recovered. Some well known examples are - wavelet expansion for image signals, superposition of spikes, curvelets, sinusoids, B-splines, etc. [90]. The signal $f(t)$ is said to be k -sparse in this chosen domain $\psi(t)$ if and only if the coefficient vector x contains k non-zero entries. It should be noted here that equation 3.7 can be re-written as

$$f = \Psi x \quad (3.8)$$

where, Ψ is an $N \times N$ matrix of rows ψ_i . As discussed previously, if the measurement vector $y \in R^m$ can be expressed as equation 3.9

$$y = \Phi f \quad (3.9)$$

Substituting for $f(t)$ from equation 3.8 in equation 3.9,

$$y = \Phi \Psi x = \Theta x \quad (3.10)$$

where, Θ is a $m \times N$ matrix [91]. Since Ψ represents the domain in which a signal is sparse, it depends on the nature of the signal being measured. However, Φ being the measurement matrix has to be non-adaptive and stable. This is a fertile area of research for mathematicians working with CS. Some approaches for designing a suitable measurement matrix are as follows [92].

1. Choosing k rows randomly and normalizing them from an $N \times N$ orthogonal matrix.
2. Choosing N random unit vectors from a k -D space, thus forming a $K \times N$ random matrix.
3. Choosing random entries from a i.i.d Gaussian matrix.

To make it easier to identify such matrices, mathematically there are two conditions to be fulfilled by qualifying measurement matrices. They are:

1. Restricted isometry property (RIP).
2. Incoherence.

Property (1) is important to ensure that the solution of the l_1 optimization problem is stable despite the reduction in the dimensionality of the original signal. Property (2) on the other hand ensures that the columns or vectors of the Ψ and Φ matrices are independent of one another. In fact, greater the incoherence, greater is the quality of reconstruction [72] [74] [93].

3.3 An example problem

This section describes a practical example from [91]. Assume that the image to be captured is of $N \times N$ resolution. But, instead of taking N measurements, only M linear and non-adaptive measurements are taken [94]. Figure 3.1 represents a single pixel camera with digital micromirror device (DMD) system.

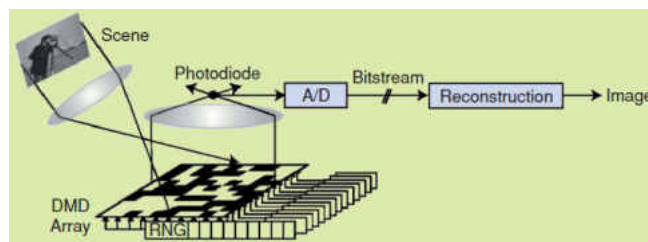


Figure 3.1: Single pixel camera with DMD array [91]

The DMD has array of N mirrors that collect the incident light reflected off of the desired image. It is then focused on to a diode (single pixel) using a secondary lens. Here, CS is realized as follows.

1. The random generator (RNG) generates the numbers 1 and 0 randomly. 1 corresponds to the mirror facing the photodiode, while 0 corresponds to the mirror facing away from it.
2. Thus, the required measurement matrix is created.
3. The random measurements are the voltage reading at the photodiode.
4. This is repeated M number of times.

In this example a specialized reconstruction technique called the total variation optimization is employed [72]. It is very similar to the L1 minimization in the wavelet domain [91].

CHAPTER 4: RESULTS AND DISCUSSION

This chapter deals with presenting and analyzing the results that were obtained from the simulation of various scenarios, ranging from the implementation of L1 minimization (CS) to recover the frequency content of a simple sinusoidal signal to its implementation to recover and reconstruct the operational deflection shape (ODS) of a damaged beam.

The end of this chapter unfolds comparisons between Fourier Transform and L1 minimization (CS) and highlights the advantages of the latter over the former.

4.1 First attempt at L1 Minimization

As mentioned in Chapter 3, Compressive sensing is a novel technique to obtain the sparsest solution to recover and reconstruct a real world signal as far as it can be projected as an L1 minimization problem. Hence, the terms L1 minimization and CS can be interchangeably used. It would be worth mentioning here again that L1 minimization can only be successfully applied to those signals that are inherently sparse, i.e. if a signal were to be treated as a vector, then there exists a domain in which when the signal is expressed, most of its vector components are zero or close to zero. There will be only a very few components that are significantly greater than zero. This implies that, in effect, these are the only components that need to be recovered.

Section 4.1 explains the first attempt at using L1 minimization technique in order to recover the frequency components of a simple sinusoidal signal (Figure 4.1). One underlying objective of this attempt is to understand how CS works and to be able to successfully implement it using a Matlab code. Further, recovery is also attempted using L2 minimization technique in order to observe the significance of L1 over L2.

L1 deals with the sum of the absolute values of the components of a vector (or columns of a matrix). L2 on the other hand, is the sum of the least squares of the vector components (or columns of a matrix). Hence, L2 is used in finding the approximate solution of over-determined systems, i.e. where the number of equations are greater than the number of unknowns. The way L2 works is by minimizing the sum of the squares of the errors resulting from each equation [95][96] .

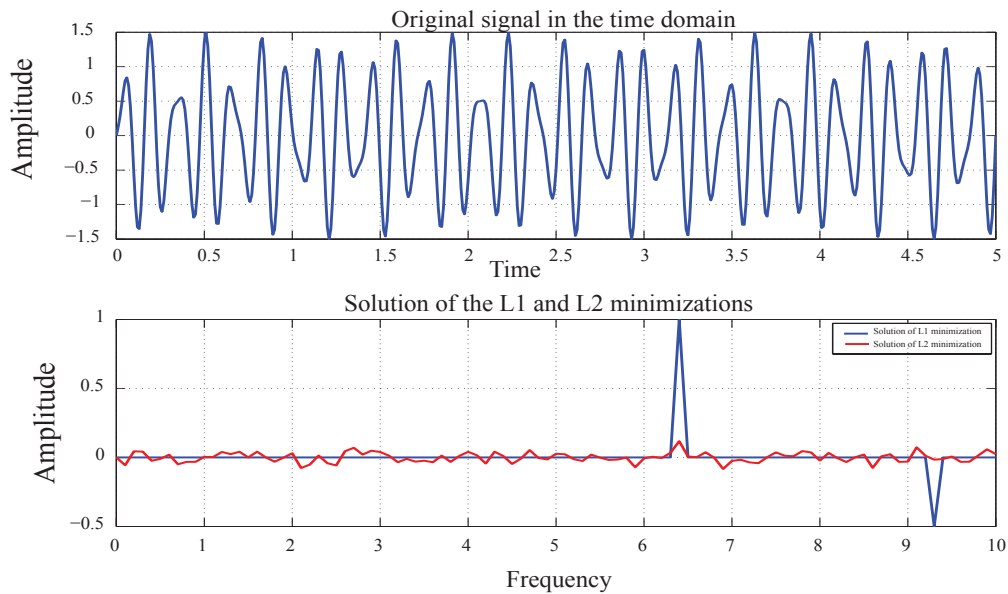


Figure 4.1: Original sinusoidal signal in the time domain: $y(t) = \sin(6.4(2\pi t)) - 0.5\sin(9.3(2\pi t))$ and its recovered frequency components

The original sinusoidal signal in time domain is represented in Figure 4.2. It can be observed from the figure that the signal at hand is not of a single frequency. It is actually a superimposition of more than one sinusoid of possibly different frequencies, amplitude and phase. In this example simulation, the signal is known to us. It has two frequency components – 6.4Hz with an amplitude of 1 and 9.3Hz with an amplitude of 0.5. The two sinusoids are however in phase with each other.

The signal can be mathematically expressed by equation 4.1.

$$y(t) = \sin(6.4(2\pi t)) - 0.5\sin(9.3(2\pi t)) \quad (4.1)$$

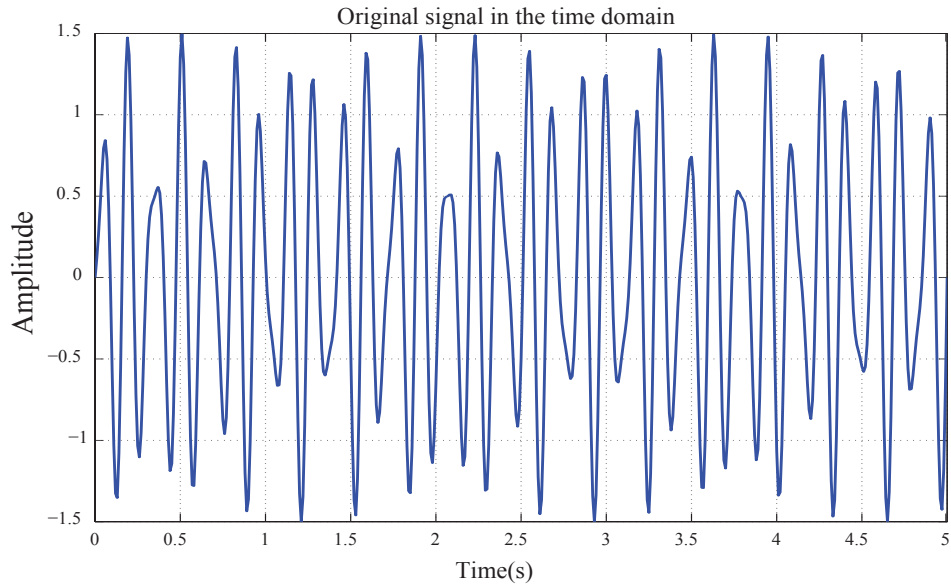


Figure 4.2: Original sinusoidal signal in the time domain: $y(t) = \sin(6.4(2\pi t)) - 0.5\sin(9.3(2\pi t))$

The frequency components of this signal shown in Figure 4.2 were attempted to be recovered using both L1 as well as L2 minimization techniques.

The L1 minimization requires a suitable domain where the signal can be sparse. One such domain for a sinusoidal signal is a measurement matrix of sine and cosine components of frequencies that span over a desired range. Since the signal here is known to us, we know that the highest frequency component is 9.3Hz. Hence, the frequency range to be swept across is chosen to vary from 0 – 10Hz at a resolution of 0.1Hz. Again, the resolution is set depending on the frequency content of the signal to be recovered. While such a signal under the given specifications of frequency

range and resolution requires a total of atleast 100 sinusoids for recovery and reconstruction, the L1 minimization makes it possible to perform the operation with just 10 random samples. It is important to reiterate the significance of the sampling being done at random. Figure 4.3 illustrates both these solutions on a single plot. The details of this simulation are listed in Table 4.1.

Table 4.1: Details of the first attempt at L1 minimization

Type of signal	Sinusoidal
No. of frequency components	2
Frequency components	6.4 Hz, 9.3 Hz
Amplitude components	1, -0.5
Frequency range of operation	0 - 10 Hz
Resolution	0.1Hz
Conventional No. of samples	100
No. of random samples	10

As observed in Figure 4.3, L2 minimization shows no significant spikes in order to distinguish the predominant frequency components of the sinusoidal signal from the passive ones. L1 minimization on the other hand, shows two unambiguous spikes at frequencies 6.4Hz and 9.3Hz. In addition to this, it can be observed that the first spike corresponding to 6.4Hz has an amplitude of 1 in the positive direction, while the second spike, corresponding to 9.3Hz has an amplitude of 0.5 in the negative direction. Thus this is in complete accordance with equation 4.1.

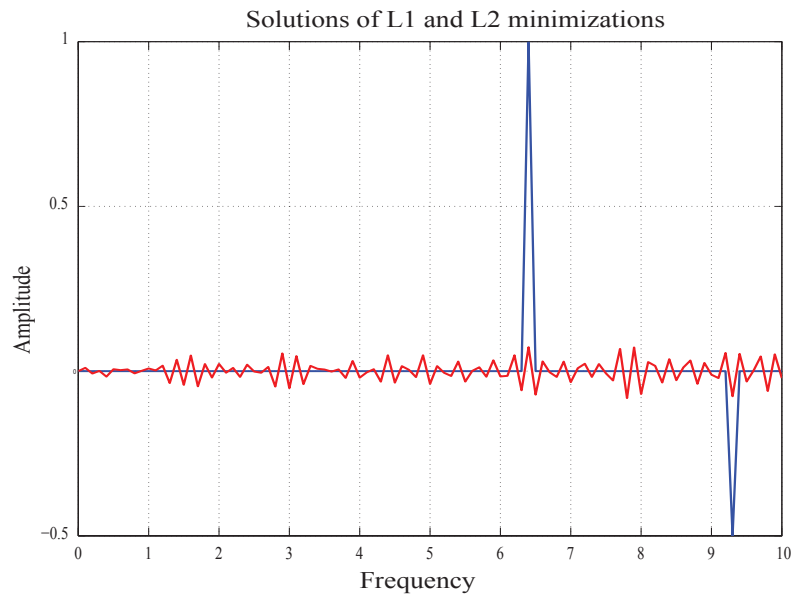


Figure 4.3: Solution of L1 and L2 minimizations

4.2 How Compressive Sensing scores over Fourier transform

So far, the basic concepts of Compressive Sensing or L1 minimization have been discussed in sufficient detail. Sections 3.2 and 3.3 provided a clear understanding of L1 minimization with its mathematical background and an example of its application in real world problems.

Now, the question that naturally arises is despite CS being an effective technique, would it really be necessary to substitute it in place of what is existing conventionally? In other words, if we have been working with Nyquist-Shannon's theorem for so long, what would be the winning attribute of CS (L1 minimization) that would help us decide in its favor? This section 4.2 is devoted to demonstrating this using Matlab simulation, the details of which are given in Table 4.2.

Table 4.2: Details of simple sine signal - Recovery and reconstruction using FFT and L1 minimization

Type of signal	Sinusoidal
No. of frequency components	2
Frequency components	1 Hz, 4 Hz
Amplitude components	0.5, 2
Frequency range of operation	0 - 10 Hz
Resolution	0.1Hz
Conventional	8 samples/sec
No. of random samples	9

As listed in Table 4.2, a simple sinusoidal signal is recovered and reconstructed using two approaches: (a) Fourier Transform and (b) L1 minimization. Figure 4.4 is the sinusoidal signal being handled. It has two frequency components (1 Hz of 0.5 amplitude and 4 Hz of 2 amplitude).

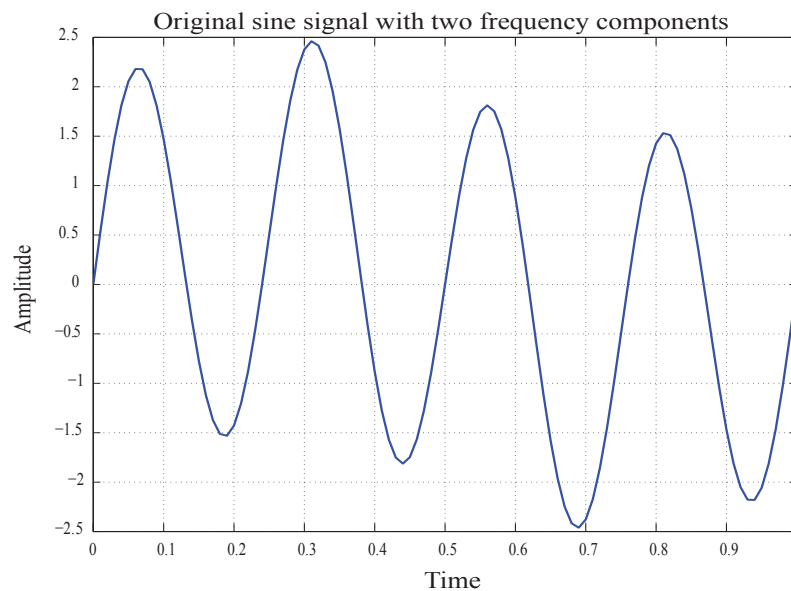


Figure 4.4: Original sine signal with 2 frequencies

4.2.1 Fourier Transform approach to signal recovery and reconstruction

Since the highest frequency component in it is 4 Hz, according to Nyquist-Shannon's theorem, the minimum sampling frequency should be 8 Hz, i.e. 8 samples per second. Since the entire signal is considered only for a time period of 1s, only 8 samples are to be taken at regular intervals.

The frequency components recovered using the FFT technique are represented in Figure 4.5. From the figure, it can be observed that only the lower frequency content of 1 Hz is recovered at 0.5 amplitude. No prominent component is seen anywhere around the expected 4 Hz region. Hence, it can be concluded that the frequency recovery is indeed a failure using just 8 samples a second to recover 2 frequencies, the highest one being 4 Hz.

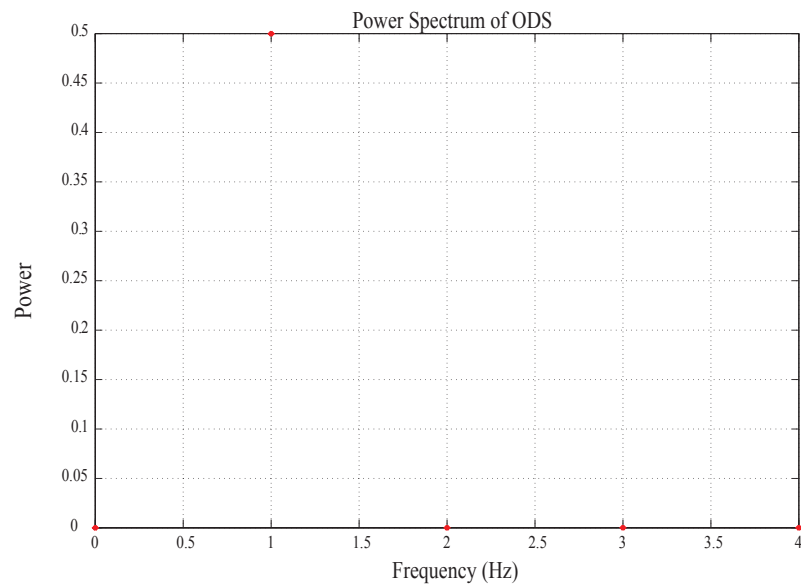


Figure 4.5: Frequencies recovered by FFT using 8 samples

This is however expected because in real world sampling applications, Nyquist criterion doesn't really hold good. In general, the sampling frequency needs to be much higher than the highest

frequency of the signal being reconstructed. Before the idea of FFT is rejected, it would be fair to look into how it performs during signal reconstruction. This is represented in Figure 4.6.

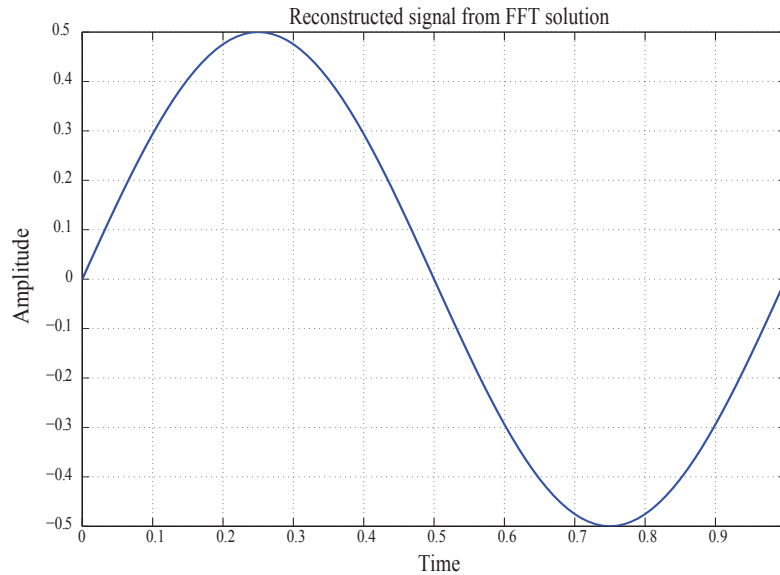


Figure 4.6: Reconstructed signal

As observed in Figure 4.6, Fourier transform does not perform even satisfactorily during the reconstruction process of the original signal. It is seen that the reconstruction is completely different from the original signal in Figure 4.4.

While the original signal is a smooth sinusoid containing two distinct frequencies, the reconstruction simply represents a sinusoid of only 1 Hz. This can be attributed to the fact that during frequency recovery process, only the 1 Hz component showed up. Now, the objective here is to make a valid comparison of Fourier Transform with L1 minimization approach. Recalling equation 3.6, for L1 to work, we would need a minimum of 9 samples/second, i.e. the sampling has to be performed at 9 Hz. The mathematical details of arriving at this number will be discussed

in the sections to come. Therefore, for the FFT approach as well, 9 Hz sampling frequency is chosen, i.e. 9 samples are chosen at regular intervals across the one second signal. The recovery and reconstruction are as shown in Figure 4.7.

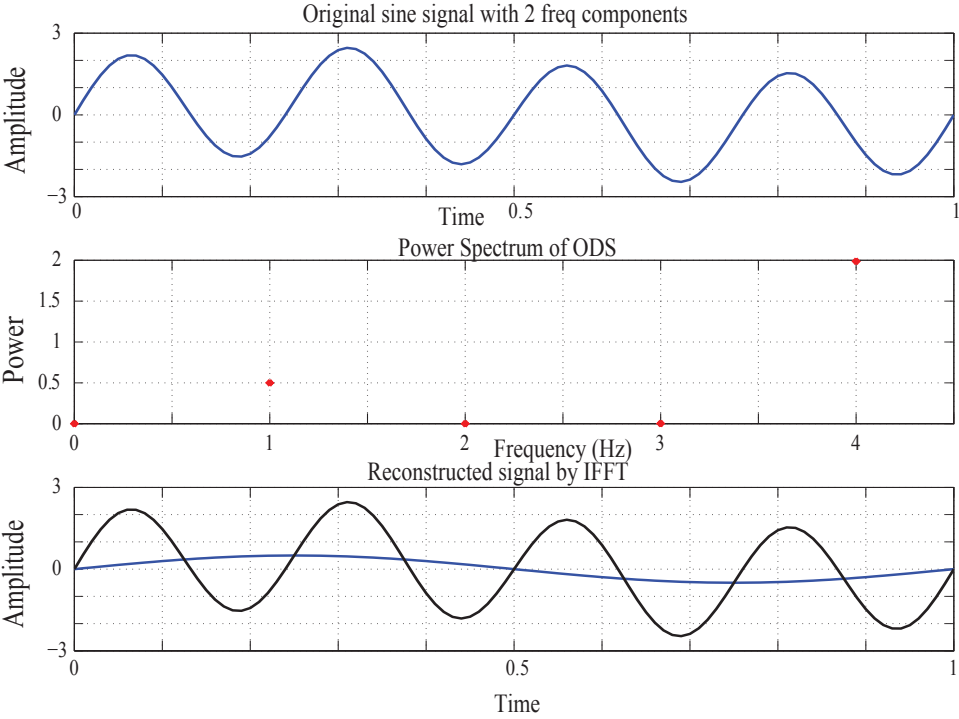


Figure 4.7: Reconstructed signal from nine samples

It can be seen from the figure that with an increased number of samples, the frequency recovery is definitely enhanced - both 1 Hz and 4 Hz components are recovered. However, the reconstructed signal is still different from the original sinusoid.

4.2.2 L1 minimization approach

The next question to address is how will L1 minimization or Compressive Sensing perform under the same circumstances of 8 Hz sampling frequency. As mentioned in Table 4.2, the L1 approach sweeps over a frequency range of 0-10Hz with a resolution of 0.1 Hz in order to obtain the two frequencies of the sinusoid. Hence, conventionally, this would require about 100 samples. But, according to L1 approach, only $S \log(N)$ samples are required. here, $S = 2$ and $N = 100$. Therefore, only 9 samples are required. These samples are represented in Figure 4.8.

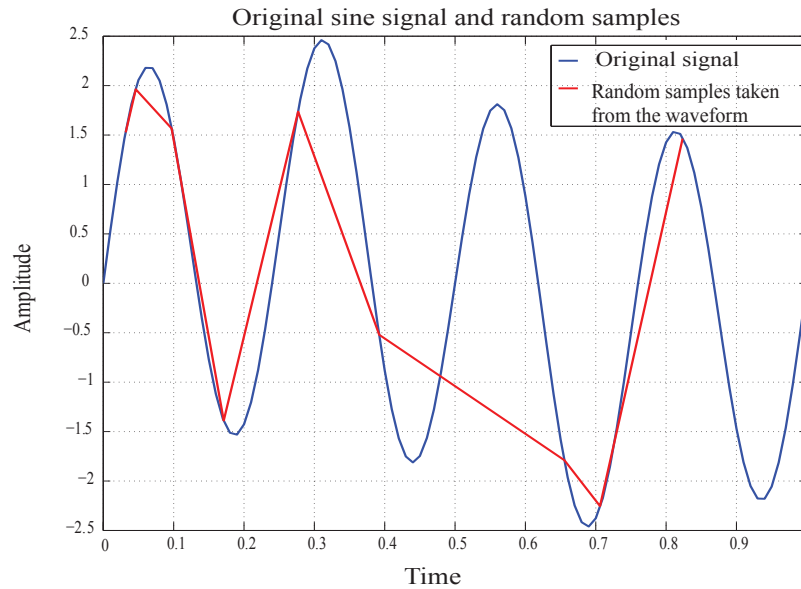


Figure 4.8: Original signal with the 9 random samples

Once these samples are obtained, the L1 minimization recovers the frequencies using the L1 magic Matlab code. These components are represented in Figure 4.9. In fact, this plot shows the frequencies recovered using both L1 as well as L2 minimizations. As expected, the L2 fails to recover any predominant frequency in the signal. The L1 on the other hand performs wonderfully and recovers

both the frequencies distinctly - 1 Hz at an amplitude of 0.5 and 4 Hz at an amplitude of 2.

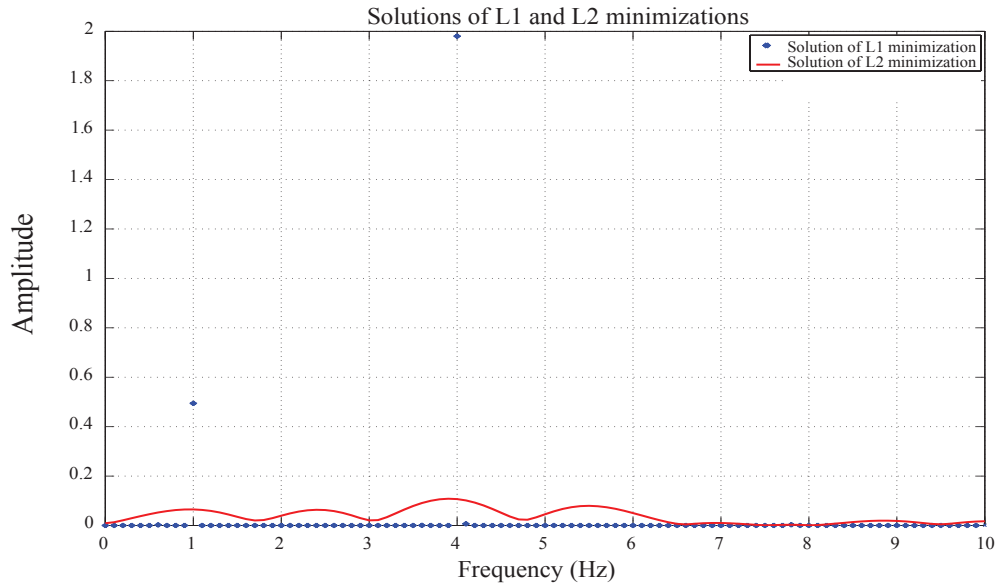


Figure 4.9: Solutions of L1 and L2 minimization

Now that the frequencies are obtained, the last step is to test the actual reconstruction process. The result of this is illustrated in Figure 4.10.

The reconstruction is almost completely coinciding with the original signal. This can be attributed to the fact that even with just 9 samples, L1 minimization was able to recover the dominant frequencies (1 Hz and 4 Hz) in the signal. This indeed is an unambiguous proof of the superiority of L1 over the conventional Nyquist - Shannon theorem of sampling.

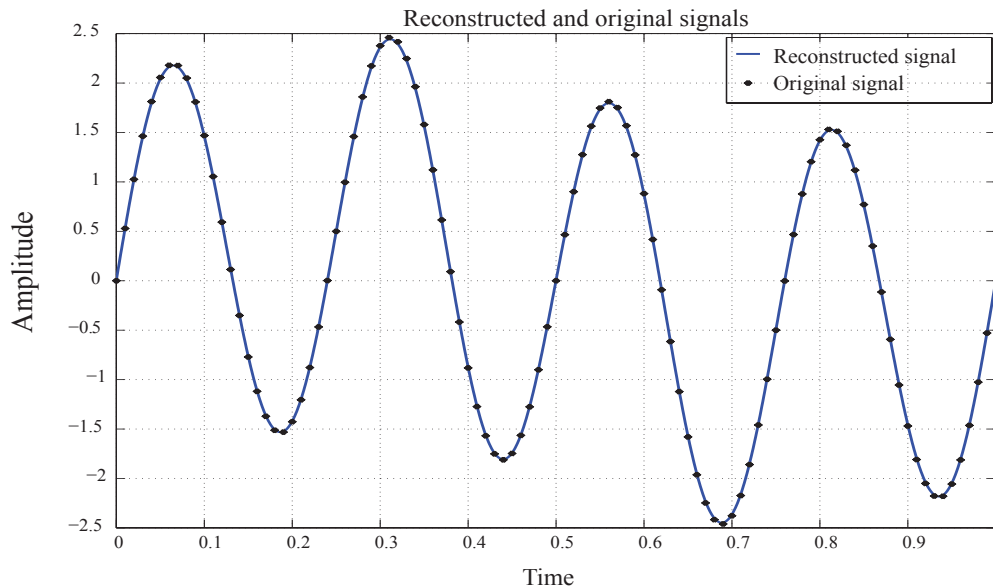


Figure 4.10: Original and Reconstructed signal using L1

4.2.3 L2 minimization approach

Before proceeding any further, it would be wise to investigate the results of L2 minimization as well. Figure 4.9 shows two solutions - frequencies recovered by L1 and L2. While the L1 solution recovers the two expected frequencies (1 Hz and 4 Hz) at respective amplitudes of 0.5 and 2, L2 solution on the other hand recovers no significant frequencies. But before rejecting L2 altogether, the performance of the same in signal reconstruction can be examined first.

Figure 4.11 represents the signal reconstructed from L2 solution. It is very evident that for the same 9 random samples chosen, L2 performs very poorly as compared to L1 minimization. Why is this so? In short, one can say that the reason for the better performance of L1 compared to L2 is because L1 promotes a sparse solution to the optimization problem. In order to understand this

statement, let us look into the details of how L1 and L2 minimizations work.

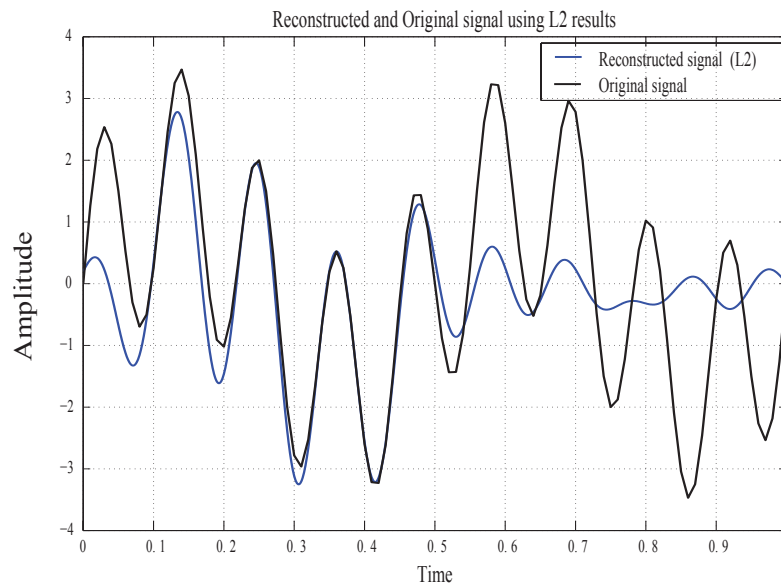


Figure 4.11: Original and Reconstructed signal using L2

4.2.3.1 L1 Vs L2 minimizations - Intuitive understanding

First and foremost, it would be a good idea to clearly define mathematical notations that are to be used in this sub-sub section.

N – Dimensionality of space

p – Type of norm to be defined

X – Vector of dimension N

In general, the p^{th} norm of an n -dimensional vector X is given by equation 4.2.

$$\|X\|_p = \left[\sum_{i=1}^n |x_i|^p \right]^{1/p} \quad (4.2)$$

Following equation 4.2, in 3D space, the L1 and L2 norms are represented as equations 4.3 and 4.4 respectively.

$$\|X\|_1 = |x_1| + |x_2| + |x_3| \quad (4.3)$$

which represents the equation of an octahedron with the center as its origin and

$$\|X\|_2 = \sqrt{|x_1|^2 + |x_2|^2 + |x_3|^2} \quad (4.4)$$

which represents the equation of a sphere with the center as its origin.

Now, while performing L2 minimization of X with the constraint $AX = y$, there is a greater percentage of chance that the minimum energy solution may not lie on any of the axes, thus not providing a sparse solution. In contrast, L1 minimization of the same vector with the same constraint will in fact intersect with the coordinates of the octahedron on any of the axes, thus promoting sparsity. While discussing the sparse solution, it would be wise to mention that L0 norm of a vector is not really a norm as it does not satisfy the conditions for being a norm. In fact, L0 norm of a vector merely returns the number of non-zero entries in it. Hence, when reconstruction is performed from the frequencies recovered from the non-sparse L2 minimization, the signal will no longer be preserved.

4.3 Quantitative comparison of FFT to L1 minimization

In this section, the difference in performance between the FFT and L1 minimization approaches is quantified. In order to fulfill on this, the error in the reconstructed signal is calculated for both the cases (FFT as well as L1). From the previous two sub-sections it can be predicted that indeed, the error from FFT approach would be much higher than the one from L1 minimization approach. Once this is established, the number of samples for the FFT method of reconstruction is gradually enhanced till the point where the errors from both the approaches are comparable. This will give a quantitative idea of the difference between FFT and L1 minimization techniques.

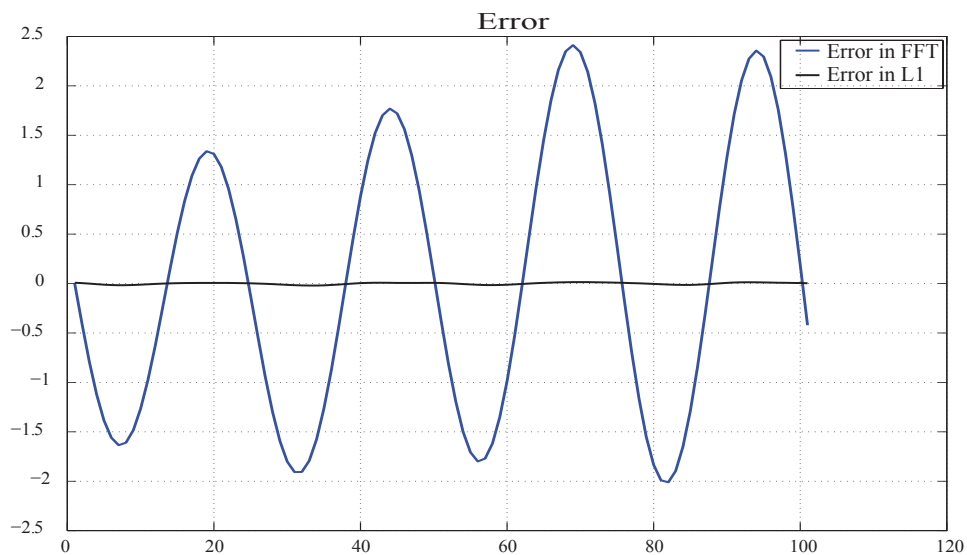


Figure 4.12: Comparison of error in reconstruction - FFT and L1 Minimization approaches

Figure 4.12 illustrates a run in which the L1 minimization approach to signal reconstruction is almost perfect with 9 samples. This can be interpreted from the error curve which is more or less coinciding with the horizontal axis at zero. On the other hand, the error from the FFT approach is

oscillating between -2.5 to +2.5. It should be noted that while calculating the error, equally spaced same data points (along the time axis) are chosen for the reconstructed signal from employing both the techniques. The RMS error in both the cases are listed in Table 4.3.

Table 4.3: RMS error - FFT and L1 minimization

Reconstruction technique	No. of samples	RMS error
FFT	9 samples/sec	1.4072
L1	9 samples	0.0084

This goes to show that for the same number of samples used (9 samples), the L1 indeed is much more superior as compared to FFT. Now, the next step is to gradually increase the number of samples used in the FFT approach to the extent when the RMS error of FFT is comparable to that of L1. Table 4.4 lists the RMS error in the FFT reconstruction for different cases of sampling frequencies (number of samples/second).

From Table 4.4, it can be observed that for the FFT approach, if 16 samples are chosen at regular intervals over a period of one second for the signal, the error is still at 0.0084, i.e. comparable to the L1 error. Although this value of error indeed matches that of L1, it can be clearly observed that this reduction in error comes with a price - an increase in the number of samples.

Table 4.4: RMS error in FFT reconstruction - Increasing number of samples/second

No. of samples/second	RMS error
9	1.4072
16	0.0084

It would be wise to throw light on the applicability and the advantage of L1 in the spatial domain at this juncture. The previous test indicates that the only very few samples (almost one-tenth that of FFT) are required in the time domain for frequency recovery and signal reconstruction. If this were to be extended to the spatial domain, it would not be wrong to predict that only a few randomly placed sensors need to be fired up at any instant, in order to obtain the information required to reconstruct the operational deflection shape (ODS) of a structure like a beam.

Before moving on, it should be highlighted that one of the other advantages of L1 minimization is striking clear when the signal to be reconstructed contains high frequency components. For instance, in the previous example in section 4.2, the signal had a frequency content of 1 Hz and 4 Hz. Hence, the conventional number of equi-spaced samples had to be a minimum of $8/s$ and for the L1, it was fixed at 9. If we consider a case with frequencies of 2 Hz and 9 Hz (with amplitudes 1.5 and 2 respectively), the conventional number of samples would increase to a minimum of $18/s$ while for L1, it would still remain at 9 (using equation 3.6). This is because, for L1 minimization, the number of samples depends on the range of frequencies to be swept across and the resolution at which it will be done. In order to reiterate this significance of L1, a signal of frequency 2 Hz and 9 Hz is attempted to be reconstructed. The details of the reconstruction are as given in table 4.5.

Table 4.5: Details of simple sine signal - Recovery and reconstruction using FFT and L1 minimization (second attempt)

Type of signal	Sinusoidal
No. of frequency components	2
Frequency components	2 Hz, 9 Hz
Amplitude components	1.5, 2
Frequency range of operation	0 - 10 Hz
Resolution	0.1Hz
Conventional	18 samples/sec
No. of random samples	9

Figure 4.13 represents the L1 recovery of frequency components from the sinusoid whose details are listed out in the table 4.5 and the signal reconstruction. As explained earlier, by equation 3.6, only 9 samples/second are taken at random along the length of the 1s signal ($S = 2$ and $N = 100$). These random samples are indicated in the figure itself.

It can be seen that L1 minimization indeed works flawlessly by recovering exactly 2 dominant frequency components, 2 Hz at 1.5 amplitude and 9 Hz at 2 amplitude. Thus, as expected, the reconstruction that follows also coincides perfectly with the original signal. To provide a quantitative understanding of the success of L1, the error in reconstruction can be considered. The RMS error of L1 reconstruction was calculated to be 0.0730.

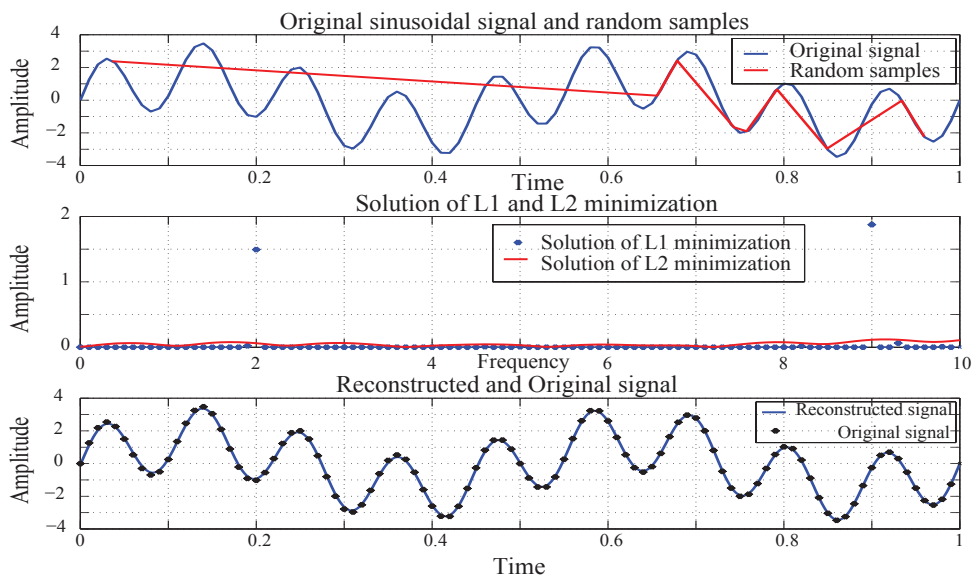


Figure 4.13: Frequency recovery and signal reconstruction - L1 minimization approach (attempt 2)

The next step is to consider a conventional FFT approach to the same problem and to compare its performance with that of L1. Figure 4.14 represents the result of taking an FFT approach towards the recovery and reconstruction problem.

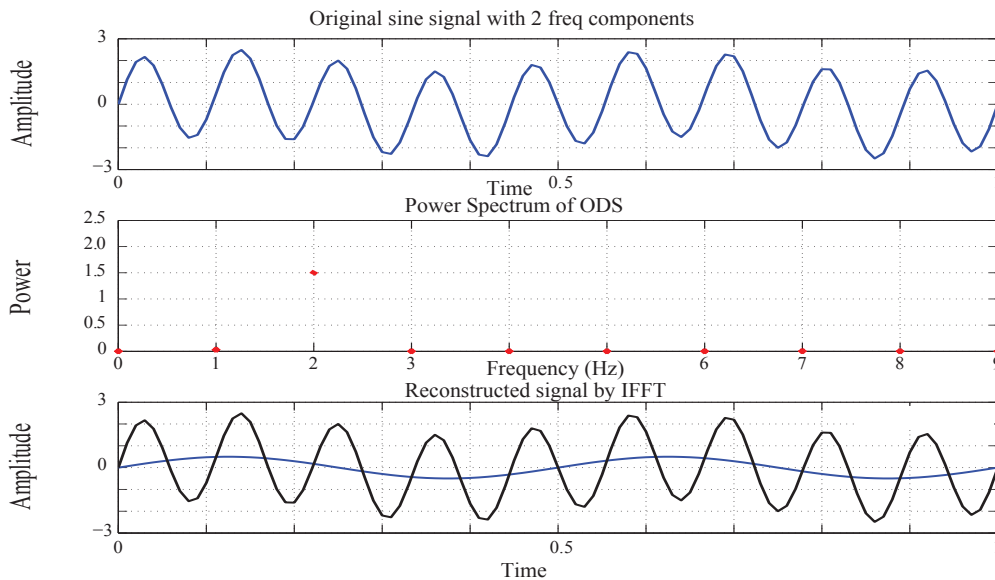


Figure 4.14: Frequency recovery and signal reconstruction - FFT approach (attempt 2)

It can be seen that only the 2 Hz frequency is recovered at an amplitude of 1.5. The 9 Hz frequency is lost. Hence, the reconstruction is also a failure due lack of accuracy in frequency recovery. The RMS error in reconstruction is 1.4538.

Similar to the previous scenario (sinusoid with 1 Hz and 4 Hz), it would be prudent to provide a quantification of performance of L1 minimization as compared to FFT. The error in reconstruction for both the L1 and FFT methods are represented in figure 4.15. It should be noted that the reconstruction for L1 approach was performed using 9 random samples while that for FFT approach was performed using 18 regularly spaced samples.

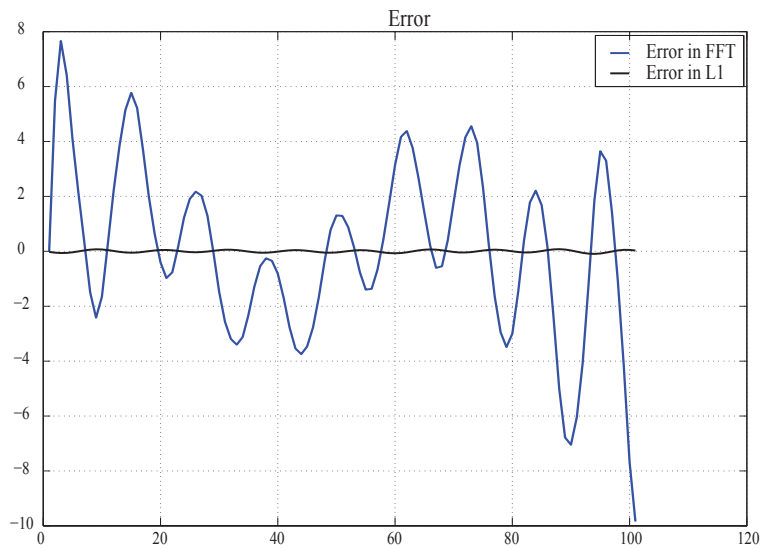


Figure 4.15: Error in reconstruction - L1 and FFT approaches (attempt 2)

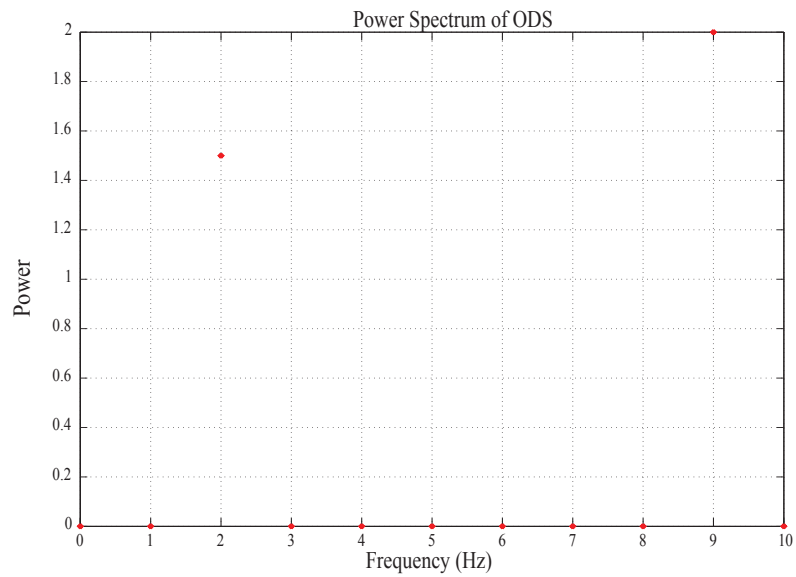


Figure 4.16: Frequency recovery - FFT approach (attempt 2)

The next step would be to attempt to better the signal reconstruction for FFT approach by increasing the sampling frequency. Figure 4.16 represents the frequencies recovered by FFT at a sampling frequency of 20 Hz. It can be seen that now both frequencies (2 Hz at 1.5 and 9 Hz at 2) are indeed recovered. Hence, the signal reconstruction is expected to be satisfactory. The visual comparison between the signal reconstructions is represented in figures 4.17,4.18 and 4.19.

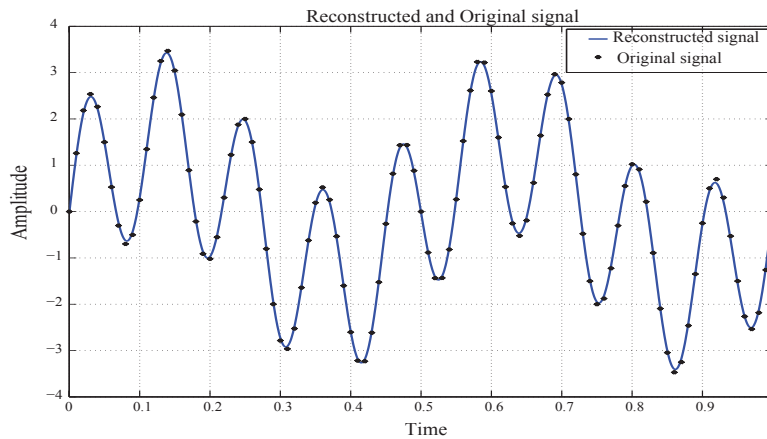


Figure 4.17: Signal reconstruction using L1 minimization (9 random samples)(attempt 2)

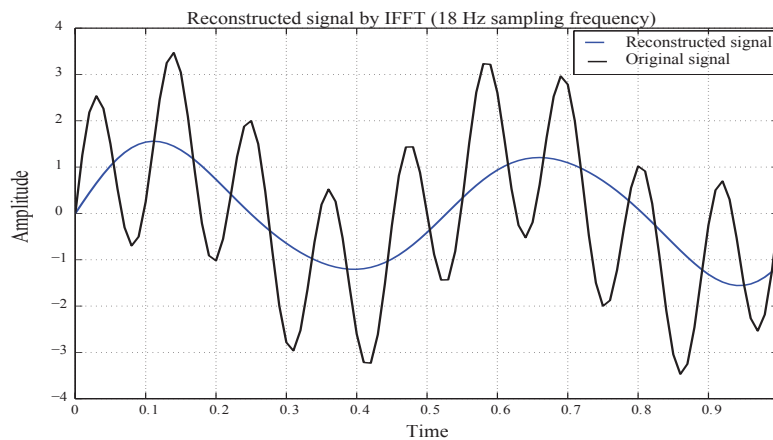


Figure 4.18: Signal reconstruction using FFT (Sampling frequency 18 Hz)(attempt 2)

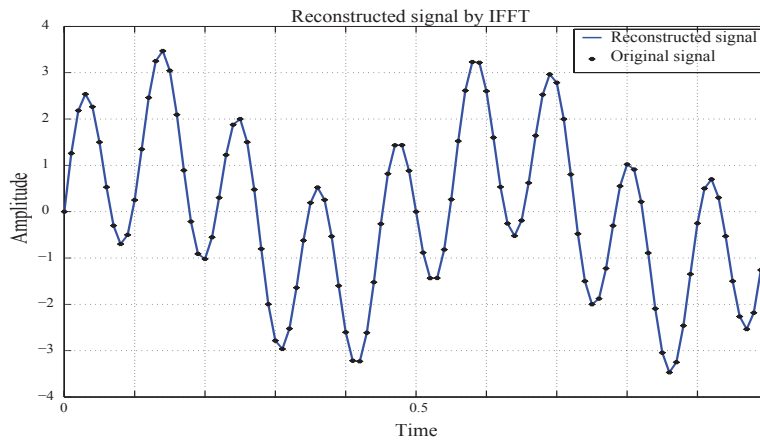


Figure 4.19: Signal reconstruction using FFT (Sampling frequency 20 Hz)(attempt 2)

As seen from the visual comparison, FFT does provide a very accurate reconstruction using 20 samples/s (with an RMS error of 0.0606). However, as stated before, this is considered waste of resources when L1 can provide an equally good result (RMS error 0.0730) with just 9 random samples.

4.4 Single degree of freedom system

In this section the performance of L1 minimization to recover the frequency of response and reconstruct the response of an SDOF linear system is discussed in detail. Two cases are considered here:

1. Unforced and undamped SDOF system (Undamaged and damaged cases)
2. Forced and damped SDOF system (Undamaged and damaged cases)

Each of these systems are discussed in separate subsections so as to make it easier for the reader to comprehend.

4.4.1 Unforced undamped SDOF system

Here, the recovery of frequency of response of an unforced and undamped SDOF linear system is discussed in detail. Further, from the components recovered, an attempt is made to reconstruct the response as well.

The SDOF system in question is represented by equation 4.5. The specifications of the system are listed in Table 4.6. As mentioned, in the undamaged case, the spring constant has a value of $K = 25Nm^{-1}$. Hence, the natural frequency of vibration of the system is at $\omega_n = 5rads^{-1}$ or $0.795Hz$.

$$M\ddot{x} + Kx = 0 \quad (4.5)$$

Table 4.6: Details of the SDOF system from equation 4.5

Mass (M)	1Kg
Spring constant (K)	$25Nm^{-1}$
Natural frequency (ω_n)	$5rads^{-1}$ or $0.795Hz$
Initial conditions	Velocity = $2ms^{-1}$, Displacement = 0
Type of forcing	Impact
Input excitation	Nil

Since this is an unforced system with only velocity as an initial condition, it can be interpreted as

vibration of a system after an impact. It would be prudent to note here that this system will by default oscillate at its natural frequency of vibration. The key to detecting damage here is therefore to recover this ω_n . Occurrence of a damage, modeled as a drop in K value results in a changed natural frequency ($\omega_{n,new}$) which can also be recovered from the new response.

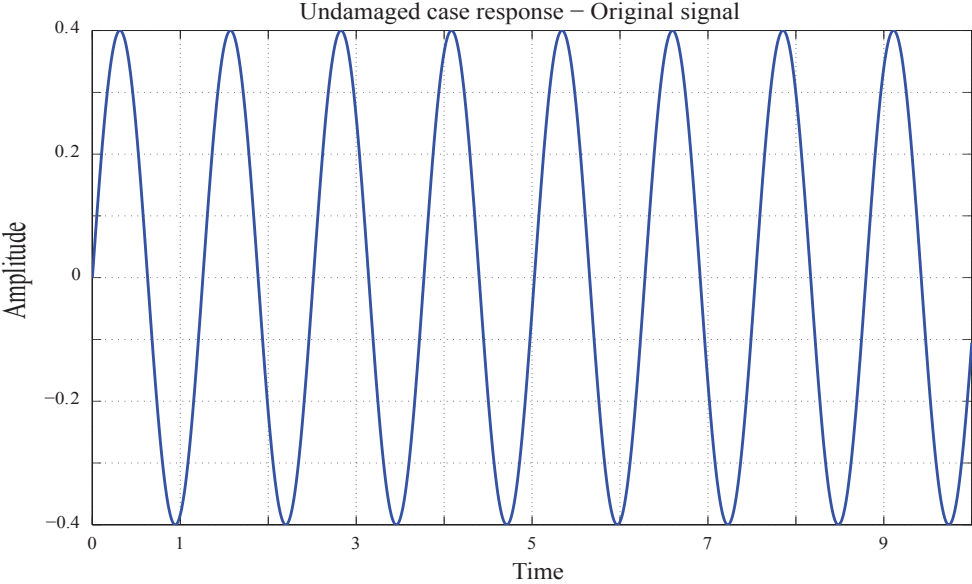


Figure 4.20: Original unforced response of the undamped SDOF system - Undamaged

Figure 4.20 shows the original response of the unforced and undamped system when there is no damage. For L1, the frequency range of operation is chosen to be $0 - 7Hz$ with a resolution of $0.1Hz$. Hence, as opposed to the conventional case where a total of 70 samples are required, L1 requires only $Slog(N)$, i.e. 4.2 samples. The frequency recovered from the L1 process and its corresponding reconstruction are given in Figure 4.21 and Figure 4.22 respectively. It can be observed that the $\omega_n = 0.795Hz$ is recovered at an amplitude of about 0.4. This is unquestionably proved by reconstruction where the original and reconstructed responses almost completely coincide.

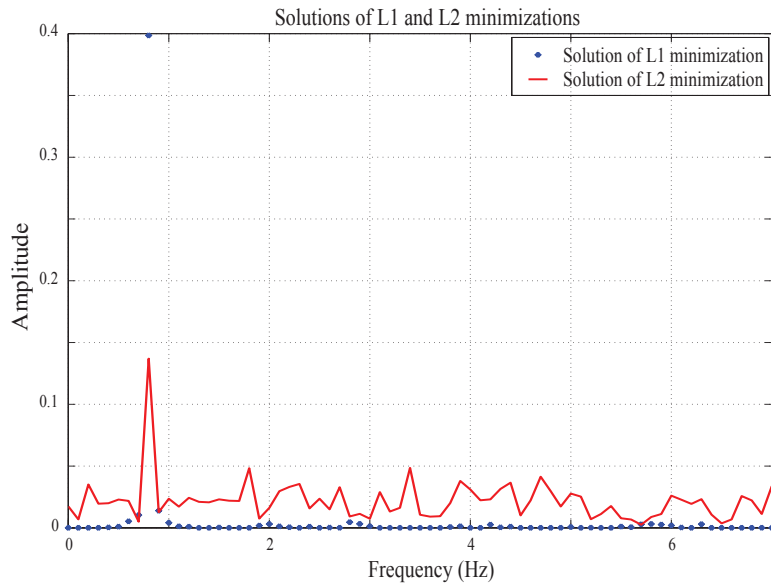


Figure 4.21: Frequency recovered from L1 minimization and L2 minimization - undamaged

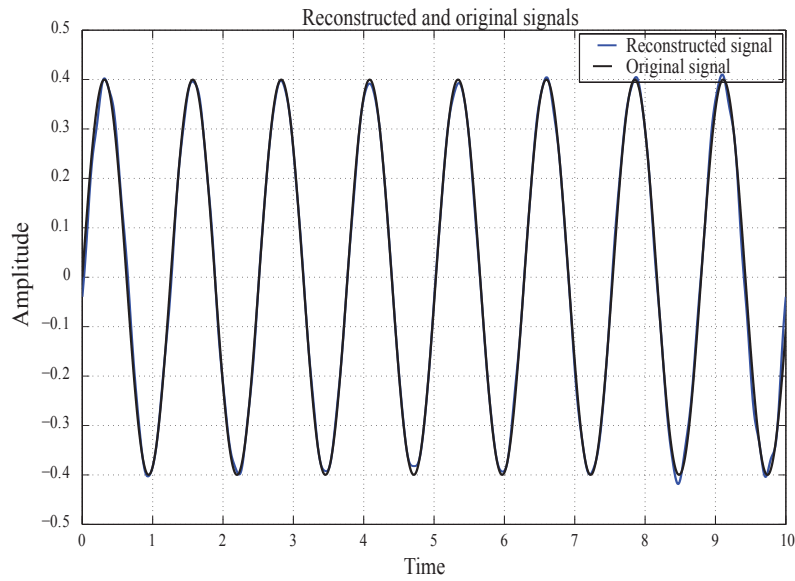


Figure 4.22: Reconstructed response and original response overlapped - Undamaged

Now, the damaged case is considered. In order to induce damage in the system, the value of its spring constant K is changed from $25Nm^{-1}$ to $4Nm^{-1}$. Hence, the natural frequency is now changed to $\omega_{n,new} = 2rads^{-1}$ or $0.31Hz$. Therefore, in order to detect the damage, L1 minimization must be able to recover this frequency and thus reconstruct the damaged case response. It should be kept in mind that while doing so, the number of samples are retained from the undamaged case.

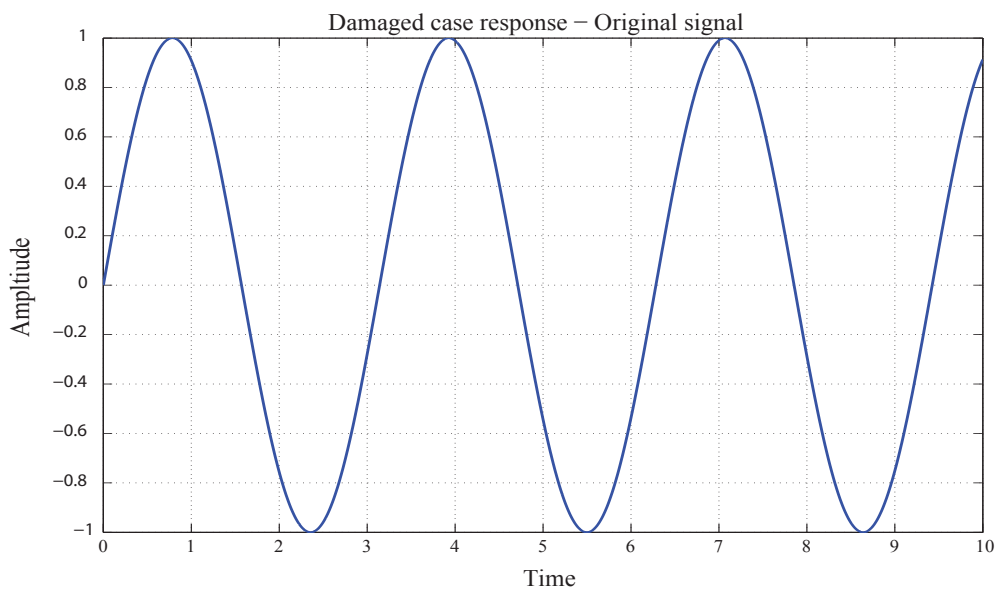


Figure 4.23: Original unforced response of the undamped SDOF system - Damaged

Figure 4.23 illustrates the response of the SDOF system after introducing damage. It can be quite obviously seen that the frequency of oscillation has decreased as compared to the undamaged case. This is expected due to the drop in the K value of the system. The frequency recovered by L1 process is depicted in Figure 4.24.

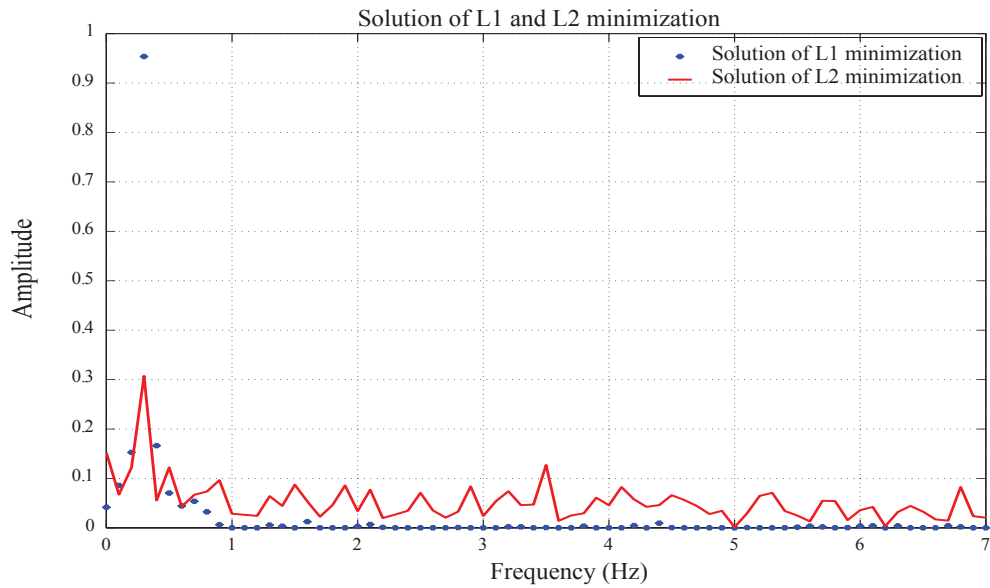


Figure 4.24: Frequency recovered from L1 minimization and L2 minimization - Damaged

As observed, the changed natural frequency $\omega_{n,new}$ of 0.31Hz is indeed flawlessly recovered at an amplitude of about 1. The increase in the amplitude of vibration is attributed to the reduction the spring constant. It is therefore expected that reconstruction will be satisfactory. This can be seen from Figure 4.25, where the original and the reconstructed response of the damaged system are indeed coinciding with each other.

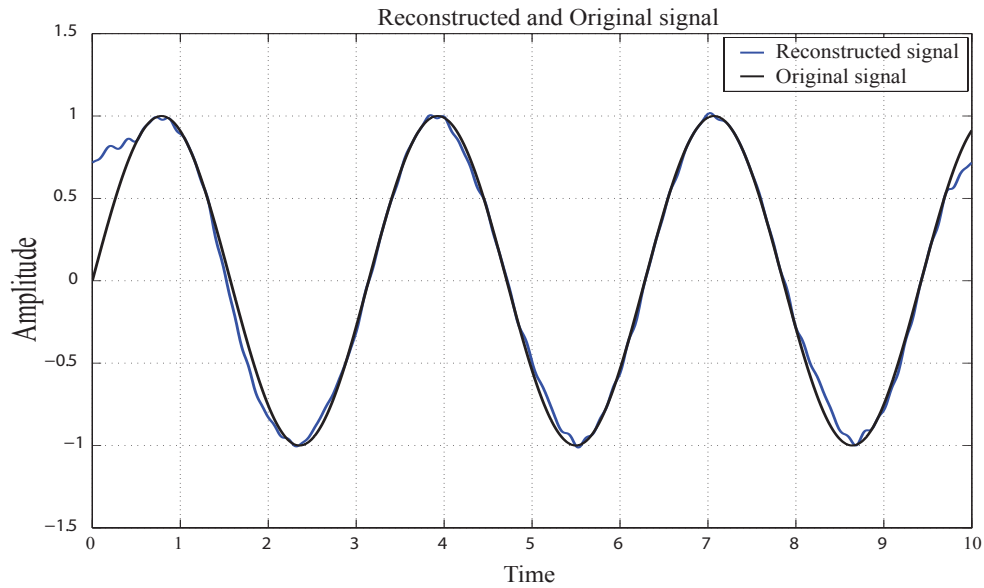


Figure 4.25: Reconstructed response and original response overlapped - Damaged

4.4.2 Forced damped SDOF system

This sub-section focuses on the recovery of signature frequencies and reconstruction of the response of a damped SDOF system under harmonic forcing. The system being dealt with is represented by equation 4.6.

$$M\ddot{x} + C\dot{x} + Kx = f(t) \quad (4.6)$$

where, the forcing function is harmonic and is represented by equation 4.7

$$f(t) = 8\sin(2\pi\omega t) \quad (4.7)$$

The specifications of the system are listed in table 4.7. As in the previous case (unforced and

undamped SDOF scenario), the undamaged system has a spring constant of $K = 25Nm^{-1}$, while the damaged system has a reduced value of $K = 4Nm^{-1}$.

Table 4.7: Details of the SDOF system from equation 4.6

Mass (M)	1Kg
Spring constant (K)	25Nm ⁻¹
Damping coefficient (C)	3Nsm ⁻¹
Natural frequency (ω_n)	5rads ⁻¹ or 0.795Hz
Initial conditions	Velocity = 0, Displacement = 0
Type of forcing	Sinusoidal (harmonic)
Input excitation	8sin(2 π t)

Figure 4.28 illustrates the forced response of the undamaged damped SDOF system. Being linear, as expected, it oscillates at the frequency of excitation once the system reaches steady state. In the beginning however, there are multiple frequencies present owing to transience.

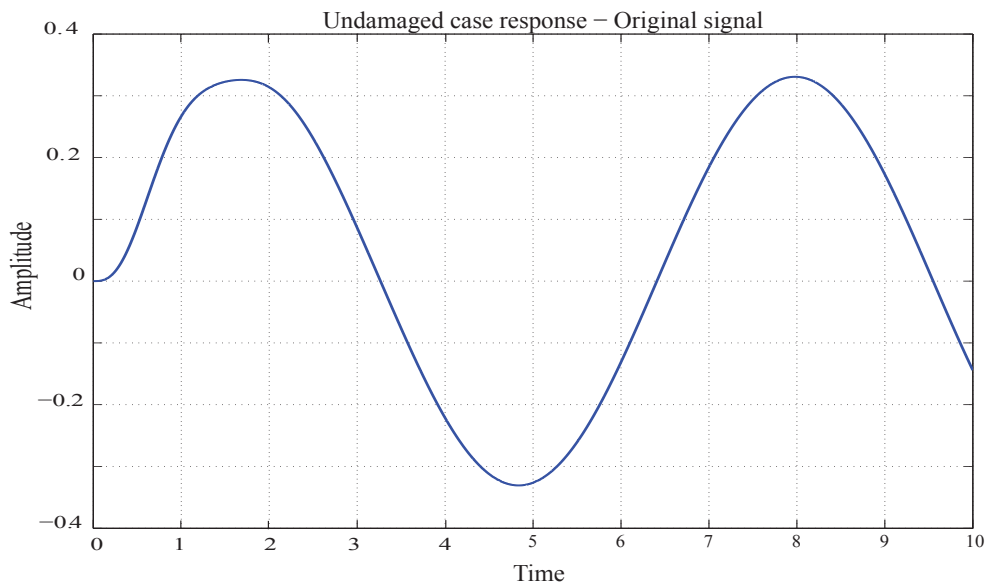


Figure 4.26: Original forced response of the damped SDOF system - Undamaged

Figure 4.27 indicates the frequencies recovered from the response using 4 random samples from $t_{initial} = 0s$ to $t_{final} = 10s$. Since the signal is expected to contain only one frequency, the number of samples for L1 is calculated using equation 3.6, i.e. 4.2 samples. As in the previous scenario, the frequency range of operation is chosen to be $0 - 7Hz$ with a resolution of $0.1Hz$.

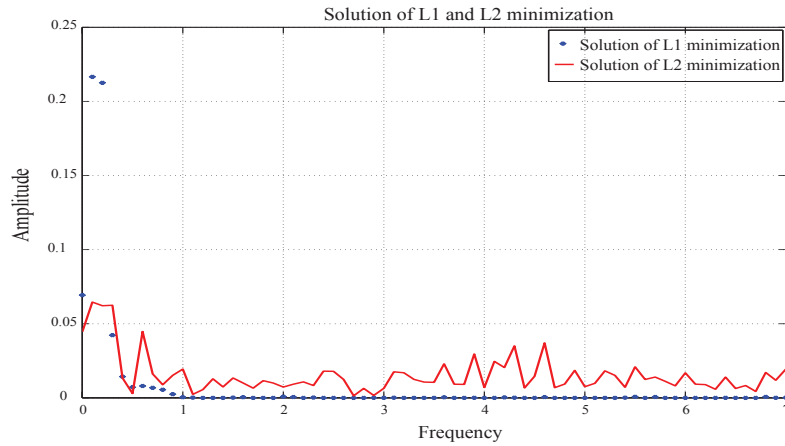


Figure 4.27: Solutions of L1 and L2 minimizations - Forced damped SDOF system - Undamaged

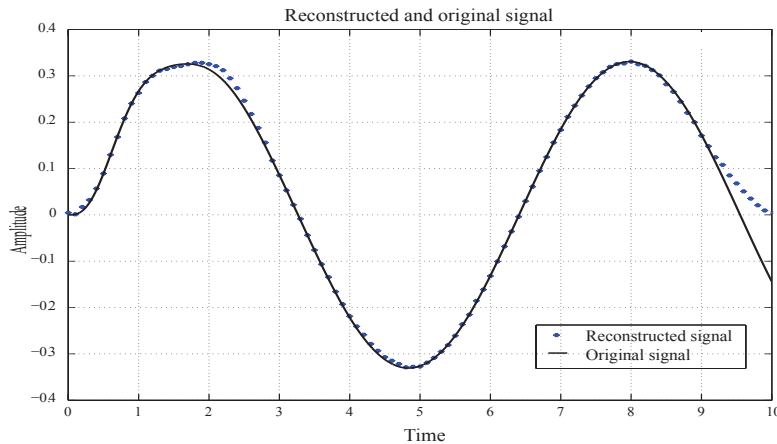


Figure 4.28: Reconstructed response - Undamaged

The frequency recovered from the L1 process and its corresponding reconstruction are given in Figure 4.27 and Figure 4.28 respectively.

Next, the damaged case is considered. It is important to mention that the damage detection criteria differs from the unforced SDOF scenario. Just like in the unforced case, introducing damage by changing the value of K will indeed bring about a change in the natural frequency of vibration of the system. However, unlike in the unforced situation, here, the system oscillates only at the excitation frequency which does not change with a change in K. Therefore, what could be the signature of damage? It is pretty obvious that the reduction in K value can be looked at as a spring that has stretched so that its amplitude of oscillation increases. Hence, it can be argued that the damage would indeed portray itself as an increase in the amplitude of the system's response. Capturing this increase in amplitude is the key to detecting damage in the system. In the healthy case, the amplitude of vibration was 0.33 which was indeed reconstructed with acceptable precision (refer figure 4.28).

Figure 4.29 illustrates the response of the damaged SDOF system. It can be observed that in compliance with the claim, the frequency of the response shows no change, only the amplitude is drastically increased. As opposed to the undamaged amplitude of 0.33, in the damaged case, the amplitude of vibration is 1.8, that is almost 6 times the undamaged amplitude. This can be attributed to the drastic decrease in the K value from $25Nm^{-1}$ to $4Nm^{-1}$.

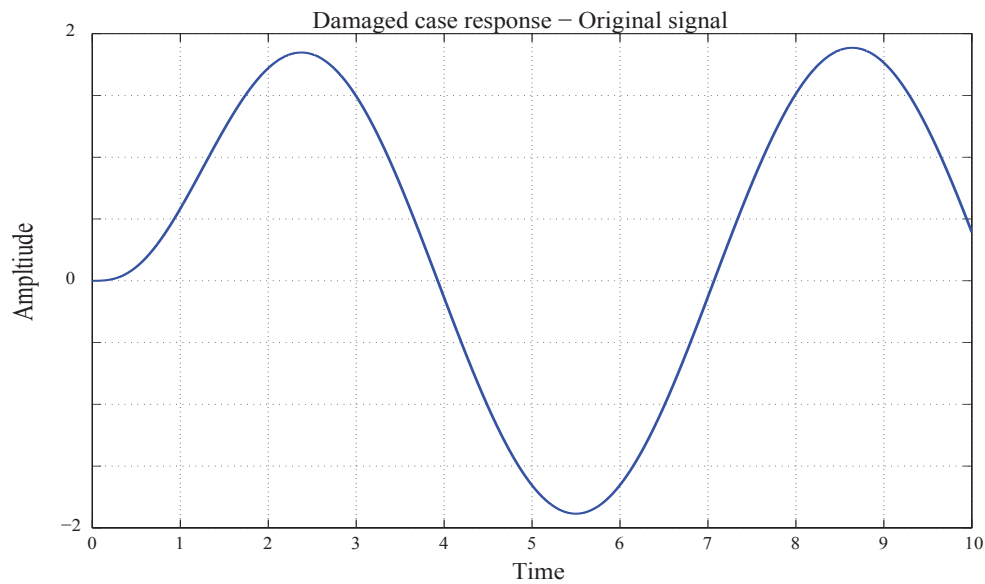


Figure 4.29: Original response of the SDOF forced system - Damaged

To reiterate the signature of damage in the forced linear system, refer to figure 4.30. It can be seen that frequencies recovered are similar to the ones from undamaged case. However, it is evident that the amplitudes at which these frequencies occur are higher. Effectively, this means that the amount to which these frequencies are present in the response has increased. This is tune with the increase in the amplitude of vibration that is tied to the occurrence of damage.

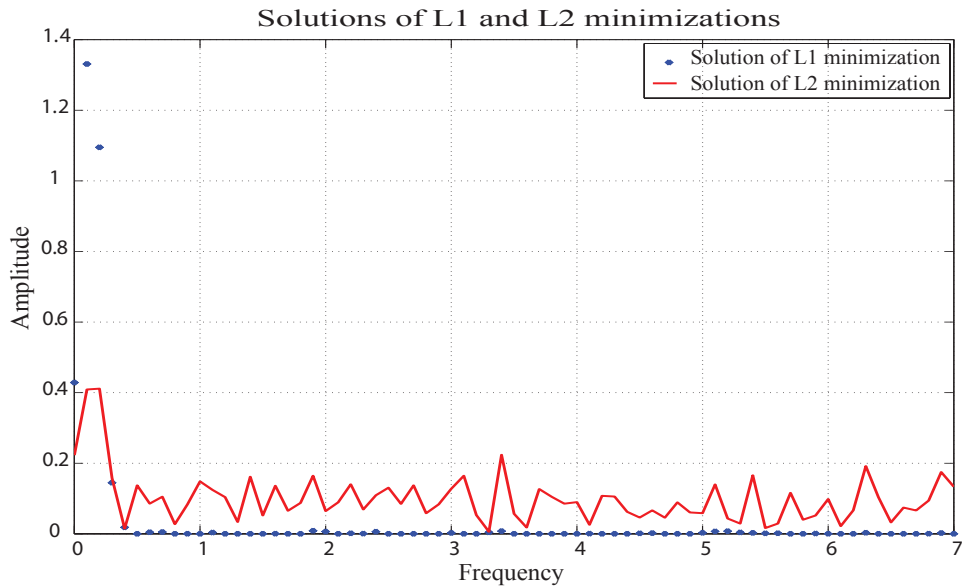


Figure 4.30: Solutions of the L1 and L2 minimizations - Damaged

The final step here is to attempt reconstruction of the signal and comparing it to the original signal to check if it provides any intelligible details that help to detect the presence of damage. This is illustrated in figure 4.31. From the figure, it can be observed that even though the reconstruction is not a replica of the original response, it does capture the sinusoidal nature of the signal and most importantly, the amplitude of the response.

The amplitude of the reconstructed response is at 1.8. This is indeed sufficient information to conclude that there is a damage in the system.

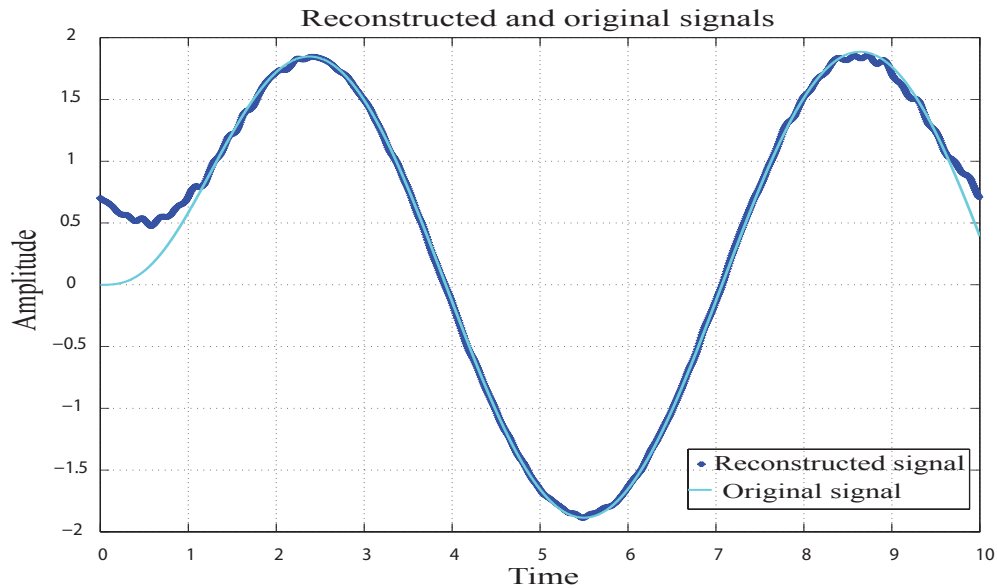


Figure 4.31: Reconstructed response - Damaged

It would be wise to take a minute to compare the performance of L1 minimization approach for the reconstruction of the responses of the SDOF system for the unforced and forced cases. It is quite evident from the results that in case of free vibration (unforced response with initial conditions), it was much easier to recover the exact frequencies of oscillation. In the forced case however, it was observed that although only one frequency was expected to be recovered (excitation frequency), two frequency components close to each other were showing up. This can be attributed to the fact that during transience it can become complicated for the L1 approach to capture the exact frequencies using very less number of samples. It can therefore be argued that with more number of frequencies to be recovered, it might be expected that L1 may not exactly capture the frequencies present in the signal. Instead, it would populate frequencies around the expected region. This pitfall is made up during reconstruction, where L1 reconstructed signal indeed matches the original signal very closely.

4.5 L1 minimization for signals with multiple frequencies

This section explores how L1 minimization performs when it encounters a signal with a lot of frequencies in it. The objective of performing this test simulation is to gauge how robust L1 minimization is when applying to these types of complicated signals.

The multiple frequency signal that is going to be dealt with is a chirp signal whose frequency linearly varies with time. The range of frequencies contained in it varies from 1 - 2.5 Hz at a uniform rate of $\frac{2}{12} Hz/s$ with an amplitude of one. This signal is illustrated in figure 4.32.

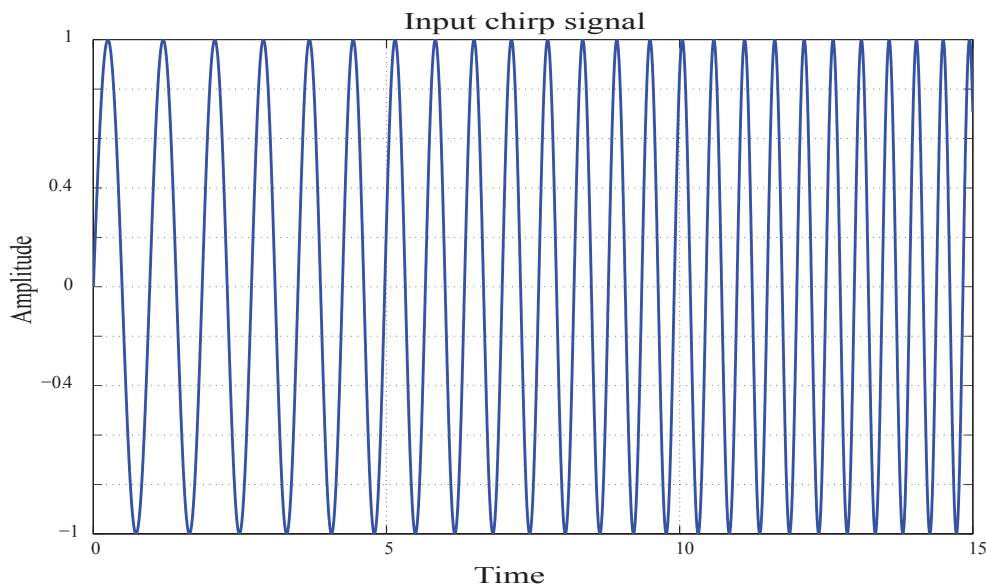


Figure 4.32: Input chirp signal

This input is used to excite an SDOF linear system with the specifications mentioned in table 4.8. The response of the system to this input is recorded and an attempt is made to recover the frequencies present in it and go a step further to perform reconstruction - all this taking an L1

minimization approach. The response of the system to the chirp excitation is shown in figure 4.33.

Table 4.8: Specifications of the SDOF system for the chirp excitation

Mass (M)	1Kg
Spring constant (K)	25Nm ⁻¹
Damping (C)	3Nsm ⁻¹
Damping coefficient (ζ)	0.3
Natural frequency (ω_n)	5rads ⁻¹

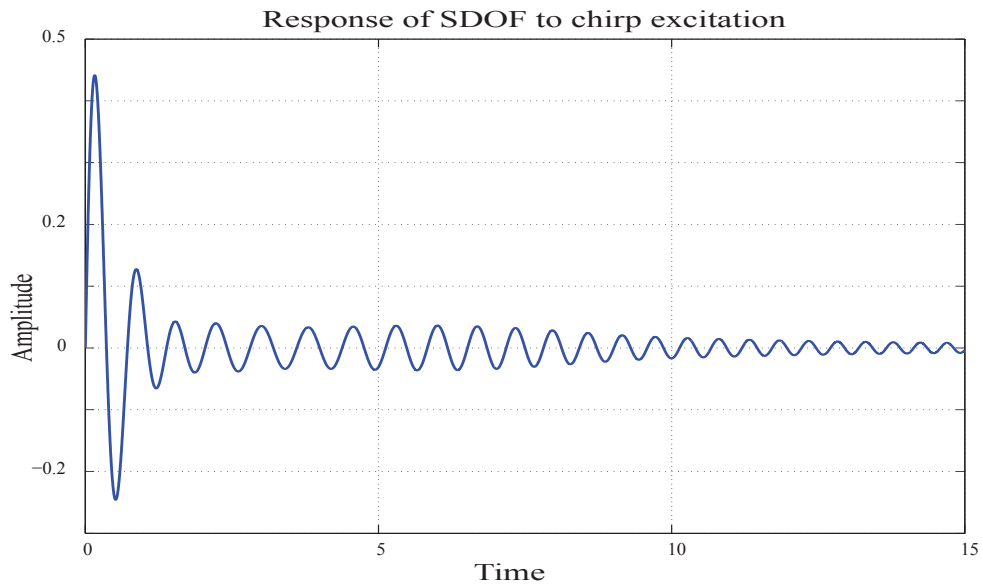


Figure 4.33: Original response of the SDOF system to the chirp input

Before applying L1 minimization, it is necessary to decide on the important parameters such as frequency range of operation, frequency resolution and the number of frequency components to be recovered. In all of the previous situations, the number of frequencies contained in the signal

to be reconstructed was already known. Based on that, rest of the parameters were decided upon. In this case however, only the frequency content span of the signal is known, i.e. the response (of the linear system) will contain frequencies ranging from 1 - 2.5 Hz over the entire time interval. Therefore, the frequency range and resolution are set first. The range is chosen from 0 - 5 Hz with a resolution of 0.001 Hz. Therefore conventionally, 5000 samples are required for recovery and reconstruction. Once these are fixed, the number of samples can be chosen depending upon the number of frequency components that are desired for recovery. In this test, 30 samples are chosen to be able to recover about 3-4 predominant frequencies. The frequency recovery and signal is illustrated in figure 4.34.

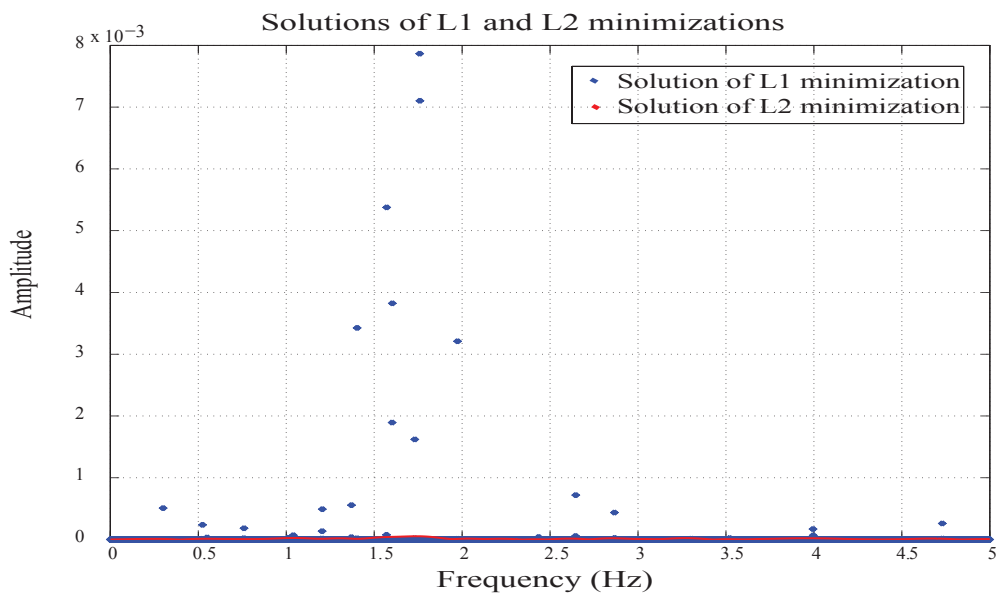


Figure 4.34: Solutions of L1 and L2 minimizations - Chirp input response of SDOF system

From the figure, it is evident that the 3-4 predominant frequencies are not recovered specifically. However, frequency components are indeed populated within that range. It has to be admitted that this does not provide highly intelligible information to assess the signal. The next step is to try

signal reconstruction from the populated frequencies.

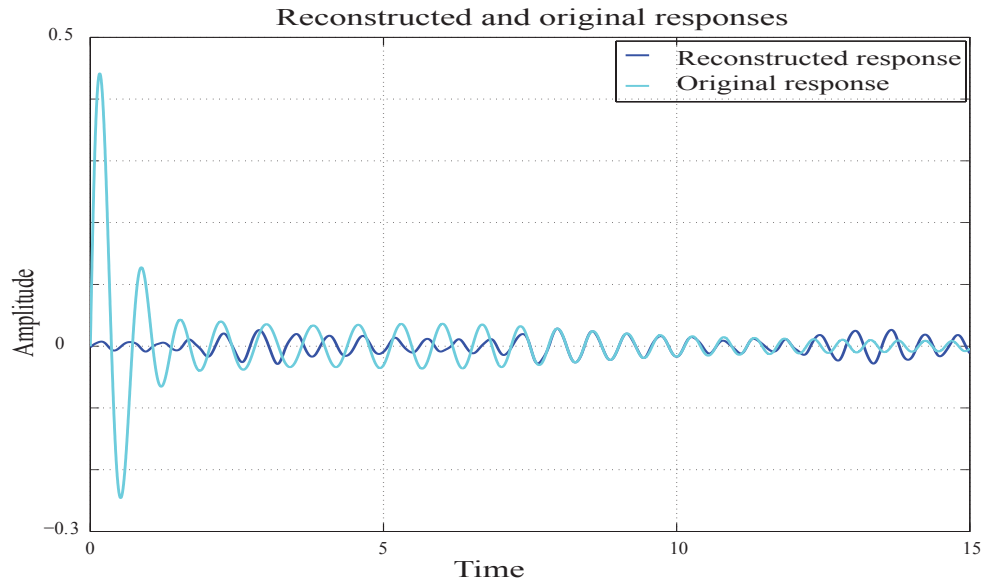


Figure 4.35: Reconstructed response of SDOF system - Chirp excitation

Shown in figure 4.35 are the reconstructed and original responses of the same linear SDOF system to the chirp excitation superimposed on each other. From the figure, it can be concluded that the reconstruction of the signal is not of very high accuracy either. However, it does provide a superficial idea of the nature of response. Also, it should be noted that from $t = 7\text{s}$ to $t = 12\text{s}$, the reconstructed and the original responses superimpose on each other. This is the interval for which the signal is captured.

In comparison to the recovery and reconstruction of signals with lesser frequency content, this performance does not fair well. However, for the same signal, use of the conventional sampling would require a very high sampling rate. Even theoretically, the signal has to be sampled at a minimum of 5 Hz to avoid any anti-aliasing. Since the signal is captured for 10 seconds, a minimum 50

samples are required. However, as seen previously, practical applications require that the sampling frequency is way higher than just twice the highest frequency content of the signal. This effectively means that the number of samples must be at least a minimum of 100 over 10 seconds. In addition, if the resolution is considered as well, as mentioned earlier, conventional technique would require about 5000 sinusoids. L1 on the other hand uses only 30 random samples over 10 seconds for frequency recovery and signal reconstruction.

The fact that the components recovered employing this technique do fall in the expected frequency range, L1 can be concluded to be robust. One fortunate situation to be mentioned here is that in real world applications, especially for structural health monitoring, the number of spatial frequencies in the response of an undamaged structure is not that many. Hence, as claimed previously, when a bizarre recovery is obtained, it can very well be concluded as the presence of damage in the structure.

4.6 Modeshape reconstruction using L1 minimization

In the literature survey, various techniques were explored in order to efficiently and effectively monitor the health of a structure. Most state of the art techniques employ temporal frequency based methods such as recovery of natural frequency of vibration of the structure, analyzing the transmissibility function between the degrees of freedom, measuring the transmission coefficient and so on. On the other hand, feasibility of using modeshapes of a vibrating structure in order to detect damage was also discussed. This section focuses its attention on recovering the natural frequencies and reconstructing the modeshapes of a structure that is under vibration.

Modeshape, as the name suggests is the shape that the structure will take while vibrating at a particular mode. Mode, here represents a natural frequency of the system or structure being examined.

As already seen, an N degree freedom system will have N natural frequencies of vibration, i.e. it will have N modes of vibration. Therefore, if the system or structure is excited at one of its modes, then the shape it takes while vibrating will be represented by a specific modeshape.

The question then is what will happen if the structure is excited as a combination of more than one modal frequencies? The answer is straight forward. It will vibrate as a combination of all the concerned modeshapes. Similarly, when the excitation frequency lies between two modal frequencies, the resulting shape of vibration of the structure will be a combination of both the modeshapes in proportion to the amount each frequency is present in the excitation.

While considering modeshapes, it is important to keep in mind that the lower frequencies or the lower modeshapes are significant in the response of a vibrating structure. This is because, the higher modeshapes correspond to higher frequencies which die out quickly. Hence, it can be argued that for testing purposes, examination of the first modeshape is indeed sufficient. It should also be kept in mind that a finite element approach (FEM) is employed to obtain the modeshapes. The structure being considered is a simply supported beam whose specifications are listed in table ??.

Table 4.9: Specifications of the simply supported beam

Number of elements (N)	100
Elemental mass(m)	1Kg
elemental stiffness (k)	$25Nm^{-1}$

Figure 4.36 illustrates both the healthy and damaged modeshape of a simply supported beam corresponding to the first natural frequency.

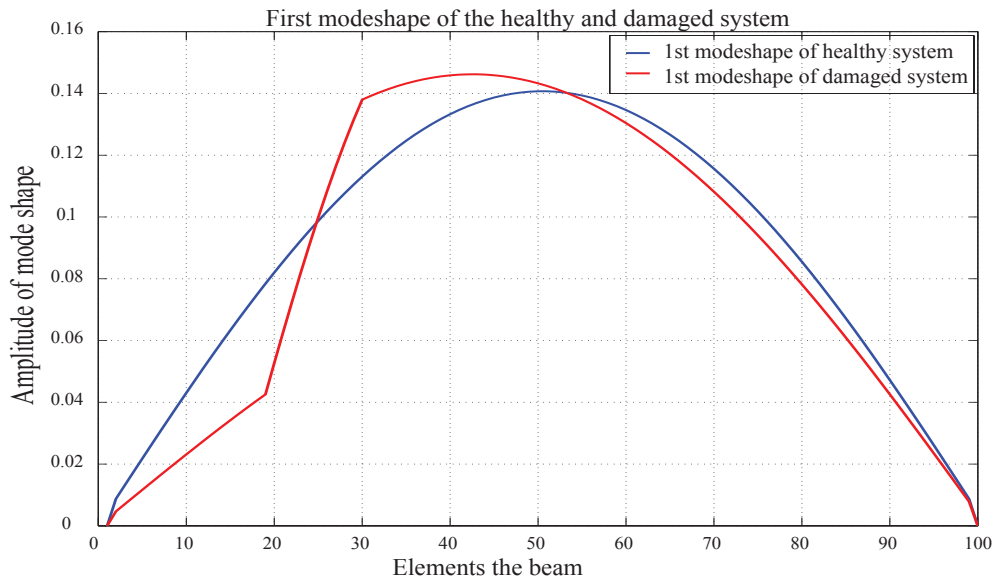


Figure 4.36: Analytical first modeshape of a simply supported beam - Healthy and damaged cases

As seen from the figure, the damage to the beam extends from DOF 20 to DOF 30. It is wise to mention here that once again the damage to the simply supported beam is simulated as a reduction in the stiffness (K) spread over ten elements. This is because it is necessary to match the real world situation, where a crack on the beam will not correspond to a single element or a single degree of freedom. Further, this implies that when the number of DOF is increased, more number of elements are to be considered in order to simulate the same damage.

Our interest lies in the recovery and reconstruction of the first modeshape of the beam in the damaged scenario. Figure 4.37 shows the first modeshape of the damaged SS beam with 10 random samples.

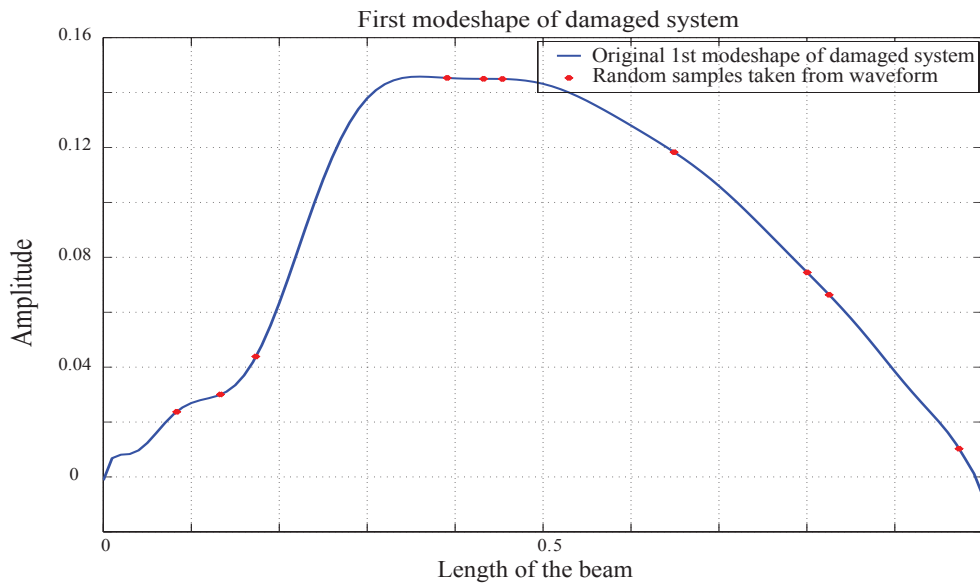


Figure 4.37: Damaged first modeshape of the SS beam with 10 random samples

In order to perform L1 minimization, the frequency range to be swept across is fixed at 0-10 Hz with a resolution of 0.1 Hz. Hence, conventionally, about 100 samples are required per second. Assuming that during damage additional higher frequencies are produced, there are about 2 frequencies to be recovered over the specified range. Hence, about 10 sampling points are chosen at random over the waveform (modeshape). Figure 4.38 illustrates the solutions to the L1 and L2 minimizations.

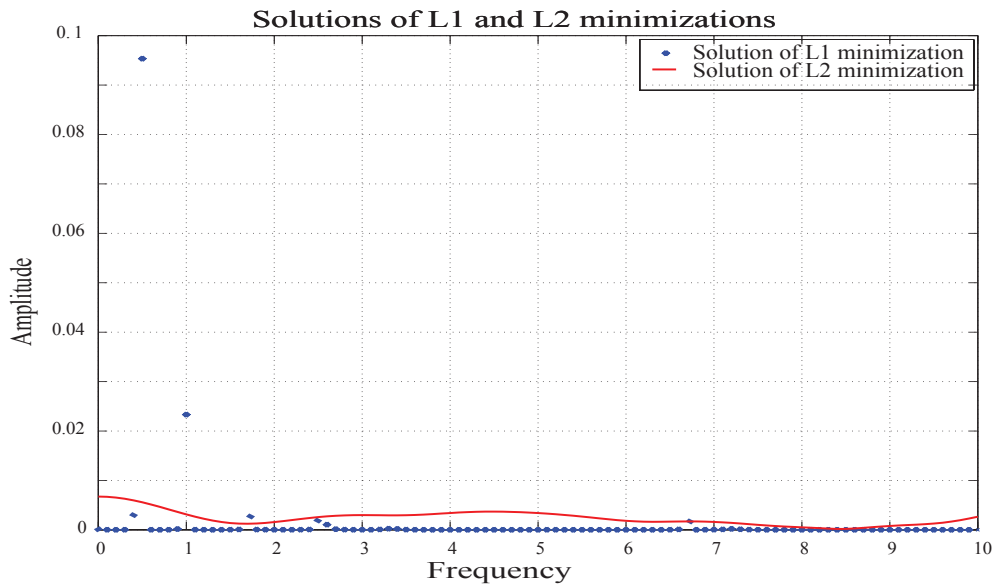


Figure 4.38: Solutions to the L1 and L2 minimizations

From the figure it is evident that two higher order frequencies are introduced into the waveform as a result of damage. This indeed is in compliance with the earlier argument. While the healthy first mode is of a frequency of 0.155 rads^{-1} or 0.025 Hz , it can be seen that the damage indicating frequencies are 0.5 Hz at an amplitude of 0.095 and 1 Hz at an amplitude of 0.025 . It should also be noted that due to the presence of these extra frequencies, the modeshape deviates from its ideal form.

Now that the frequencies have been successfully recovered, the next step is to reconstruct the damage indicating modeshape. The result of this attempt is quite satisfactory and is represented by figure 4.39.

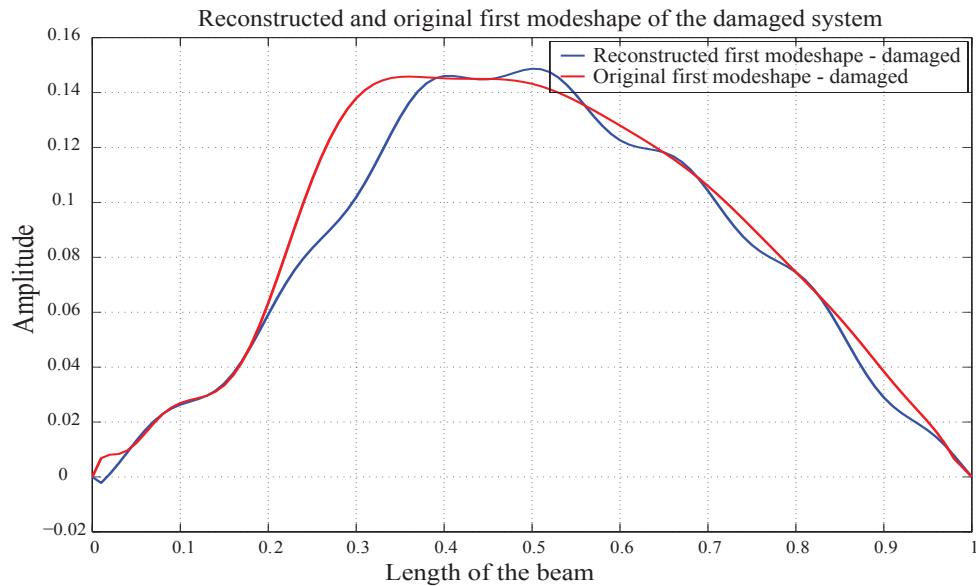


Figure 4.39: Reconstructed 1st modeshape and its original superimposed - Damaged



It is clear from the figure that L1 minimization indeed provides a very acceptable reconstruction of the modeshape (waveform) when the damaged SS beam undergoes vibration. Although in this simulation, the damage is quite severely reflected, it can very well be argued that the location of the damage may not be exactly evident from the reconstruction, had the damage been any less severe. It may be counter-argued that a damage would be considered as one, only when it is beyond a particular level of severity that causes interruption of service of the structure. This however does not affect the fact that the L1 reconstruction does in fact provides a tell tale sign of damage itself.

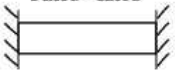
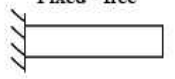
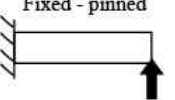

4.7 Comparison of modeshape - Analytical versus Finite Element Method

This section focuses on matching the analytical solution to obtaining a modeshape to a finite element (FEM) approach for the same. If the resultant error is very minimal that it can be approximated to zero, then the FEM approach adopted so far can be validated.

In the previous section, the structure under examination was a simply supported beam. Therefore, it would only be appropriate to compare the analytical and FEM solution to the eigenvalue problem of a simply supported beam. It can be argued that a structure such as a bridge need not necessarily be a mere SS beam. However, if the FEM approach for the SS beam is indeed valid, modeling of all other types of beams is a simple alteration of the boundary conditions. At this point, it would be wise to list out the boundary conditions and the characteristic equations of the different types of beams that are commonly used in practice (refer table 4.10).

Table 4.10: Boundary conditions of different types of beams [99]

Beam type	Boundary conditions	Frequency equation	Modeshape equation
<p>Simply supported</p> 	$w(0) = 0$ $EI \frac{\partial^2 w(0)}{\partial x^2} = 0$ $w(L) = 0$ $EI \frac{\partial^2 w(L)}{\partial x^2} = 0$	$\sin \beta_n l = 0$	$W_n(x) = C_n [\sin \beta_n x]$
<p>Free - free</p> 	$\frac{\partial EI \frac{\partial^2 w(0)}{\partial x^2}}{\partial x} = 0$ $EI \frac{\partial^2 w(0)}{\partial x^2} = 0$ $\frac{\partial EI \frac{\partial^2 w(L)}{\partial x^2}}{\partial x} = 0$ $EI \frac{\partial^2 w(L)}{\partial x^2} = 0$	$\cos \beta_n l \cdot \cosh \beta_n l = 1$	$W_n(x) = C_n [\sin \beta_n x + \sinh \beta_n x + \alpha_n (\cos \beta_n x + \cosh \beta_n x)]$

 <p>Fixed - fixed</p>	$w(0) = 0$ $EI \frac{\partial^2 w(0)}{\partial x^2} = 0$ $w(L) = 0$ $EI \frac{\partial^2 w(L)}{\partial x^2} = 0$	$\cos\beta_n l \cdot \cosh\beta_n l = 1$	$W_n(x) = C_n [\sinh\beta_n x - \sin\beta_n x + \alpha_n (\cosh\beta_n x - \cos\beta_n x)]$
 <p>Fixed - free</p>	$w(0) = 0$ $EI \frac{\partial^2 w(0)}{\partial x^2} = 0$ $w(L) = 0$ $EI \frac{\partial^2 w(L)}{\partial x^2} = 0$	$\cos\beta_n l \cdot \cosh\beta_n l = -1$	$W_n(x) = C_n [\sin\beta_n x - \sinh\beta_n x - \alpha_n (\cos\beta_n x - \cosh\beta_n x)]$
 <p>Fixed - pinned</p>	$w(0) = 0$ $EI \frac{\partial^2 w(0)}{\partial x^2} = 0$ $w(L) = 0$ $EI \frac{\partial^2 w(L)}{\partial x^2} = 0$	$\tan\beta_n l - \tanh\beta_n l = 0$	$W_n(x) = C_n [\sin\beta_n x - \sinh\beta_n x + \alpha_n (\cosh\beta_n x - \cos\beta_n x)]$
 <p>Pinned - free</p>	$w(0) = 0$ $EI \frac{\partial^2 w(0)}{\partial x^2} = 0$ $w(L) = 0$ $EI \frac{\partial^2 w(L)}{\partial x^2} = 0$	$\tan\beta_n l - \tanh\beta_n l = 0$	$W_n(x) = C_n [\sin\beta_n x + \alpha_n \sinh\beta_n x]$

Now let us look at the error between the analytical and FEM solution to the eigenvalue value problem of a simply supported beam. For the FEM approach, the SS beam of unit length is divided into 100 elements. It is excited at mid - length with various forcing frequencies and an amplitude of 5. Each forcing frequency excites a particular mode. It is also worthy to note that for ease of computation, the material density, area of cross section, the rigidity modulus and the area moment of inertia of the beam are also unity. Once the K and M matrices are established, the FEM solution to the eigenvalue value problem is obtained using MatLab.

The analytical solution to obtaining the modeshapes of the SS beam is expressed by equation 4.8.

$$w(x, t) = \frac{2f_0}{\rho A l} \sum_{n=1}^{\infty} \frac{1}{\omega_n^2 - \omega^2} \sin \frac{n\pi a}{l} \sin \frac{n\pi x}{l} \sin \omega t \quad (4.8)$$

The results of this attempt are illustrated in figures 4.40, 4.41, 4.42, 4.43 and 4.44.

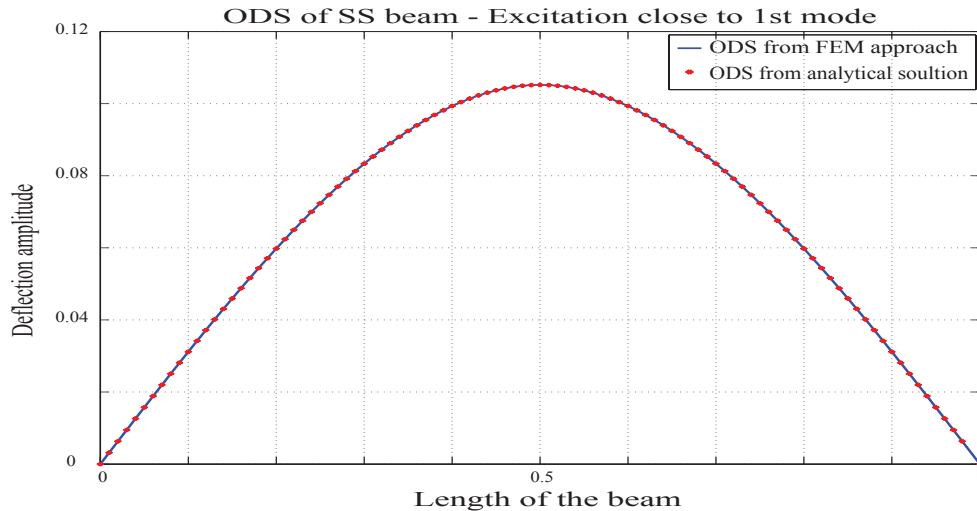


Figure 4.40: Analytical Vs FEM solution - Mode shape 1 (SS beam)

Figure 4.40 illustrates the comparison of the first modeshape of the simply supported beam using both the above mentioned approaches. The excitation frequency is 1 rads^{-1} . It can be observed that the two plots superimpose on top of each other.

The second modeshape of the same beam is illustrated in figure 4.41. It is obtained by excitation at a frequency of 33 rads^{-1} . However it should be noted that since this is the second modeshape, forcing at mid length will not produce displacement because of the presence of a node at the center of the beam. Hence, for this modeshape, the excitation can be at any point except at the center. For this simulation, the excitation was at one-fourth the beam length. As in the previous case, it can be visually observed that the error is very minimal that the modeshape from the two approaches are indeed coinciding.

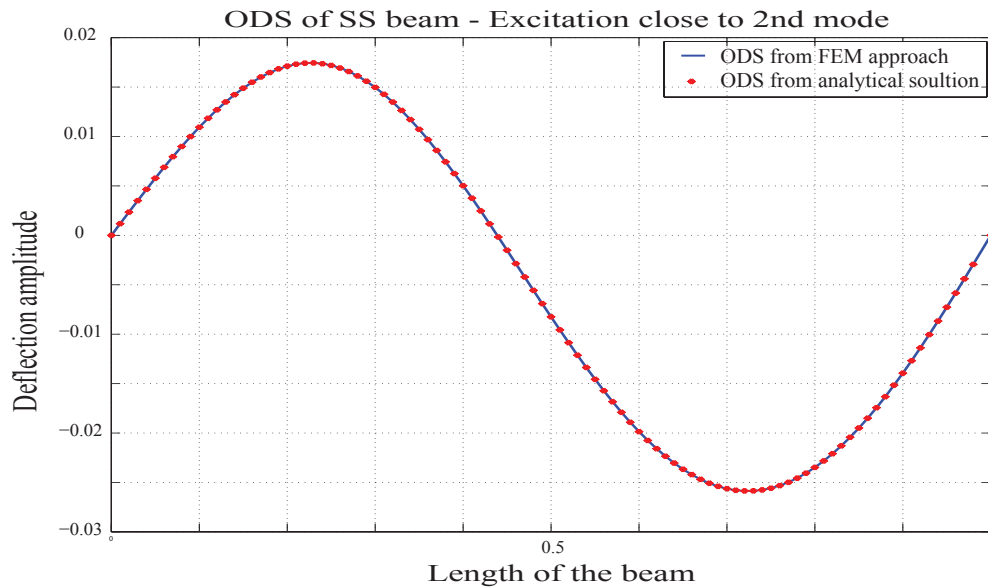


Figure 4.41: Analytical Vs FEM solution - Mode shape 2 (SS beam)

The third, fourth and fifth modeshapes of the simply supported beam obtained using both the FEM as well as analytical approaches are illustrated in figures 4.42, 4.43 and 4.44 respectively. As in the earlier two cases, the excitation for each mode is performed at specific frequencies of 85 rads^{-1} , 111 rads^{-1} and 230 rads^{-1} respectively. It can be observed that all the modeshapes using both approaches are clearly spot on.

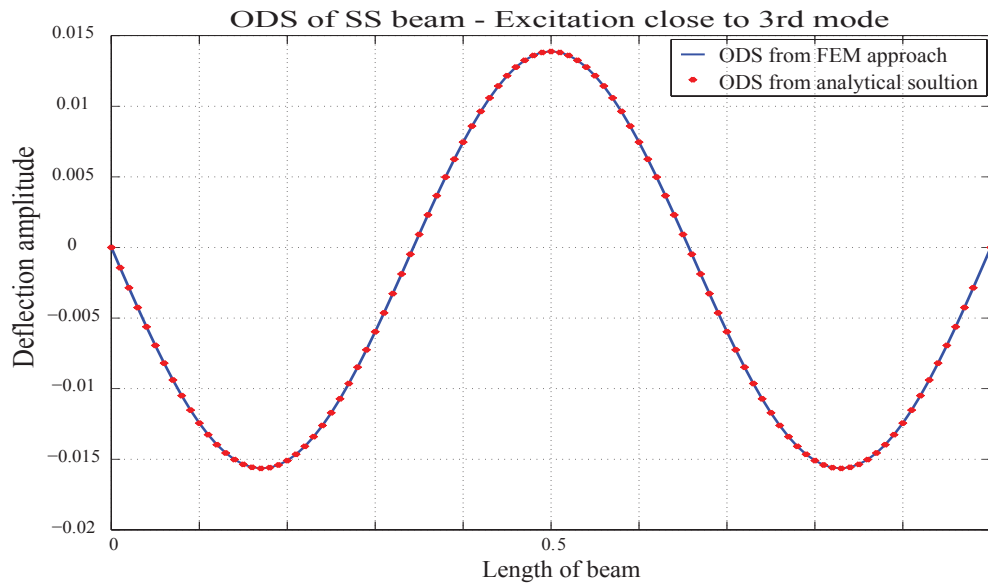


Figure 4.42: Analytical Vs FEM solution - Mode shape 3 (SS beam)

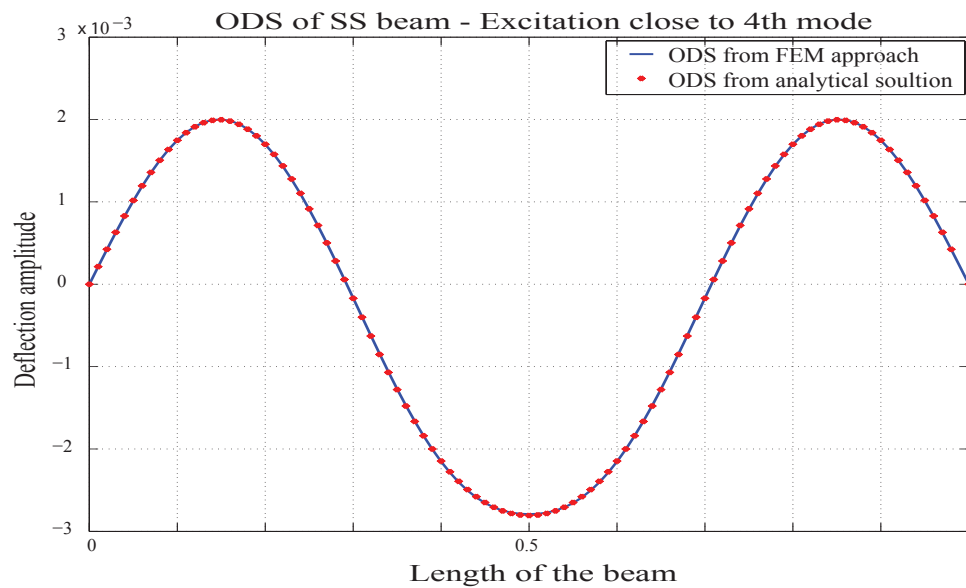


Figure 4.43: Analytical Vs FEM solution - Mode shape 4 (SS beam)

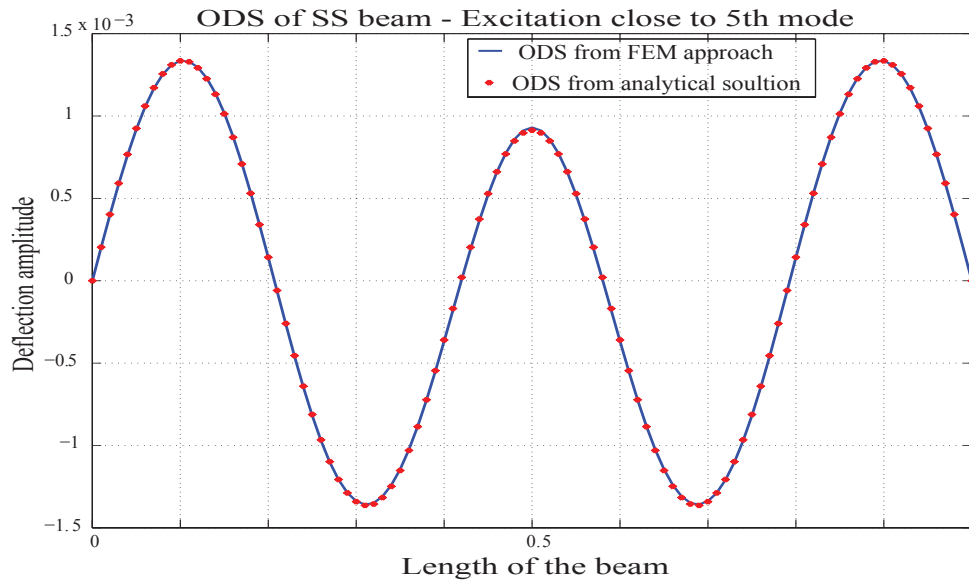


Figure 4.44: Analytical Vs FEM solution - Mode shape 5 (SS beam)

4.8 Investigation of Operational deflection shapes

This section is devoted to analyzing the operational deflection shapes of beams with standard boundary conditions and testing their feasibility in damage detection and location. Specifically, a simply supported beam and a fixed-fixed beam are examined. Further, the ODS are reconstructed using L1 minimization to validate the viability of the approach in the field.

4.8.1 ODS of a simply supported beam

The ODS of a simply supported beam is first examined. The SS beam chosen for testing is modeled using FEM analysis and is divided into 100 elements. The beam is uniform and of unit length, unit rigidity modulus and unit ρA . It is harmonically excited at the center of its span with an

amplitude of 5 and a frequency of 2rads^{-1} . As discussed earlier, the ODS is usually a mixture of several modes of vibration of the structure. In case of an impact for instance, the ODS can be quite unpredictable since a lot of modes may be excited at the same time. In case of harmonic forcing however, the ODS can be manipulated to containing larger proportion of a specific mode by appropriately choosing the excitation frequency. In this particular scenario, we aim to keeping the ODS very close to the first mode of vibration. The first natural frequency of the SS beam chosen is 9.86rads^{-1} . Hence, it would be a safe bet to excite the beam at a frequency lower than its first mode. Hence the choice of excitation frequency.

Before proceeding further, it is important to note that the number of samples, sampling points, frequency range of operation and resolution are kept the same for both the healthy as well as damaged scenarios. This is to match the realistic situation where a system once installed will function without many alterations during its lifetime. In other words, once the number of sensors are decided and are embedded on a structure, it would be unwise and practically impossible to make further changes to the system. Also, since there is no knowledge of whether or not a damage has occurred (prior to its detection of course), chances are, the same number of samples (may be even the same samples) are routinely collected and analyzed.

Figure 4.45 illustrates the ODS of the SS beam with 10 random samples. Because the excitation frequency is kept below its first mode of vibration, only a simple sine-like curve is expected.

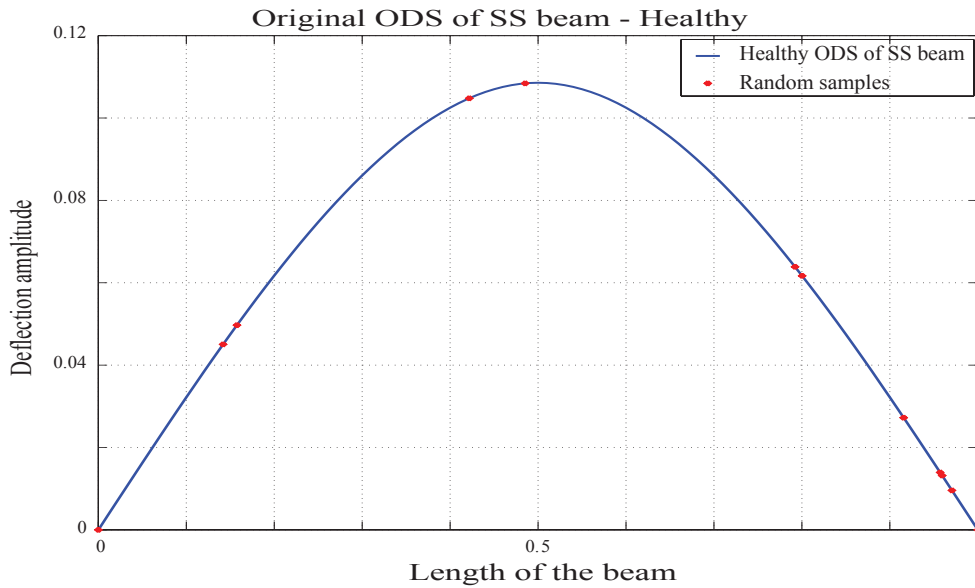


Figure 4.45: ODS of a simply supported beam - Healthy (with 10 random samples)

Such an ODS has a spatial frequency of 0.5 Hz (because the beam is of unit length). But, it is not really a sine wave of a single frequency. To allow for any additional frequencies that might be present in the undamaged case as well (may be of very low amplitude), the number of frequencies to be recovered can be fixed at 2. With that in mind, CS dictates that we use a frequency range of operation of 0-10 Hz with 0.1Hz frequency resolution. Using the appropriate equation 3.6 we conclude that we would indeed need 10 samples for successful signal reconstruction. Now, it must be kept in mind that in case of ODS, we focus on the spatial domain. Hence here, x number of samples per second translates to x number of samples per unit length. In accordance with the ODS obtained, the spatial frequency to be recovered is expected to be at 0.5 Hz or at least lie in its closest proximity.

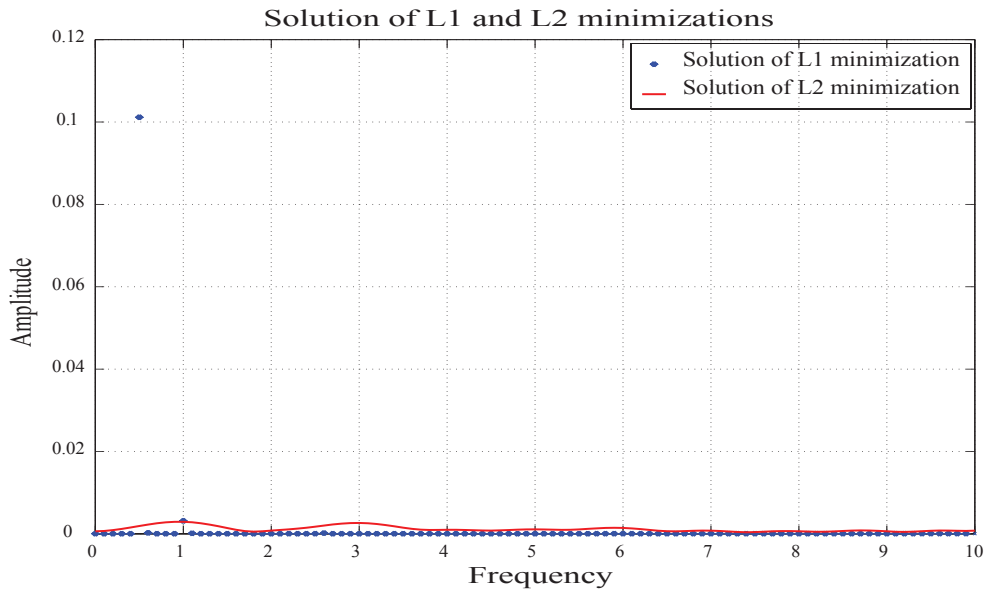


Figure 4.46: L1 and L2 minimization solutions

Figure 4.46 indicates the solutions of both L1 and L2 minimizations. It can be observed that the frequency recovery was indeed successful because the only dominant frequency component obtained as a solution to the L1 minimization problem is at 0.5 Hz. All other frequencies are more or less close to zero and hence can be easily neglected.

Successful recovery of predominant frequencies are the first step to ensuring not just the satisfactory performance of CS as an effective tool for optimization, but in this case, the proper health of the beam itself. As far as the SS beam has no irregularities or deformations in its structure, excitation below the first mode will unfailingly trigger an ODS that will have a spatial frequency of 0.5 Hz. The next step to ensuring good health of the beam is to reconstruct the ODS (spatial signal) from the recovered frequency. This reconstruction and its comparison to the original ODS are illustrated in figure 4.47.

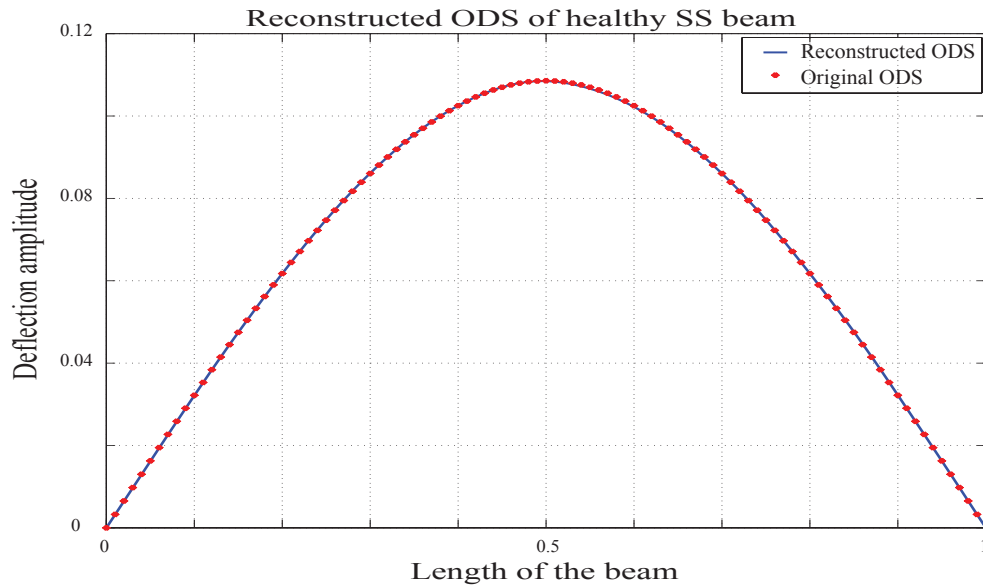


Figure 4.47: Reconstructed ODS of the SS beam - Healthy

It can be observed in figure 4.47 that the reconstructed and the original deflection shapes are almost coinciding with each other. Hence the approach can be validated as an effective technique in monitoring the health of the beam.

The next scenario to be examined is when the beam is damaged, or when a damage is introduced into the beam. In SDOF and multi-DOF systems, damage was simulated as a change in the value of one or more stiffness coefficients. As explained in the earlier sections, a reduction in K translates as the structure becoming looser and vibrating more violently, while an increase in K presents a situation where the structure becomes more rigid and hence vibrates minimally. Similarly, damage in a beam is being simulated as a change in the value of rigidity modulus (EI) over a certain span, i.e. in terms of FEM, it is distributed over a certain number of elements.

Specifically here, two cases of damage are explored, both of which suffer from a reduction in EI over different areas of the beam. This reduction will cause the beam to vibrate non-uniformly, i.e. the ODS will no longer resemble a sinusoid of frequency 0.5 Hz (spatially looking at it), but will be distorted. This distortion can very well be conceived as a signal with higher frequency components (damage). The damage cases being simulated on the SS beam are listed in table 4.11.

Table 4.11: Damage cases of SS beam

Scenario	Rigidity modulus (EI)	Number of elements
Healthy	1	N/A
Case 1	0.1	75-80
Case 2	0.1	25-35

The table 4.11 lists out the two damage cases to be simulated in terms of the elements that are involved. However, it would be easier to visualize a change in the EI (here, reduction) over a certain beam span. The SS beam of unit length is modeled using FEM and is divided in to 100 elements. Hence, simple math teaches that each element represents 0.01 units of the beam span. Therefore, for damage cases 1 and 2, where can we expect the damage to be reflected? The answer to this is listed in table 4.12.

Table 4.12: Elements to beam span reflection

Damaged elements	Beam span
75 - 80	0.75 - 0.80
25 - 35	0.25 - 0.35

4.8.1.1 Damage case 1 (Elements 75-80)- SS beam ODS

The first case of damage to be investigated is the reduction in EI from 1 to 0.1 over elements 75-80 of the simply supported beam. It is important to reiterate that the forcing conditions of the healthy SS beam are retained for the damaged case also. The damaged ODS of the beam is represented in figure 4.48. The damaged elements are also indicated on it.

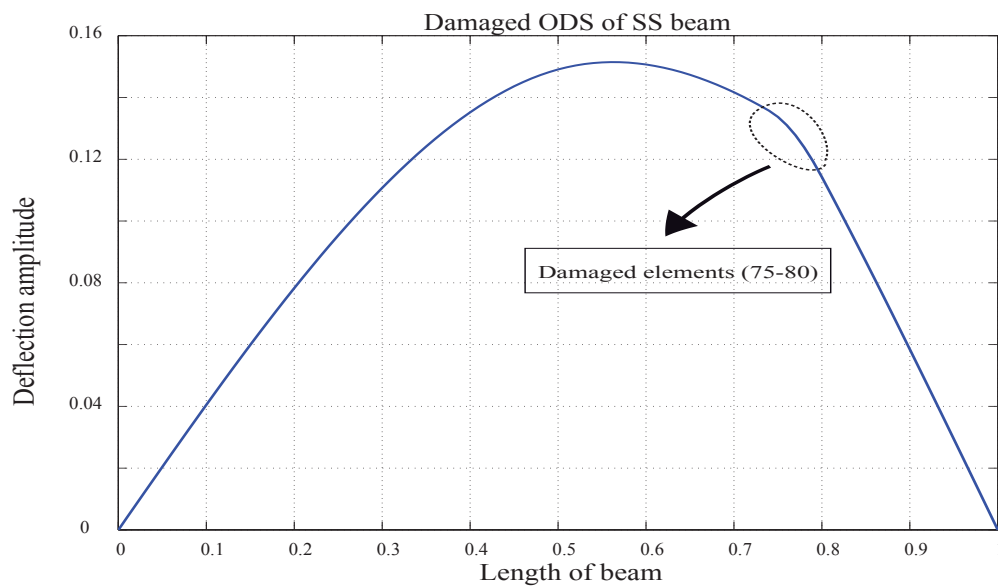


Figure 4.48: Damage case 1 - ODS of SS beam

As explained earlier, injection of damage in terms of reducing the stiffness or rigidity causes distortions in the vibration pattern of the beam. Hence, the damaged ODS will represent a sinusoidal signal infiltrated with higher frequency components. Therefore, a tell-tale sign of damage are the presence of extra frequencies during recovery using L1 minimization. As seen before, the healthy SS beam has spatial frequency of only 0.5 Hz under the specified forcing conditions. With damage on the other hand, more frequencies (higher) are expected to show up in the L1 recovery.

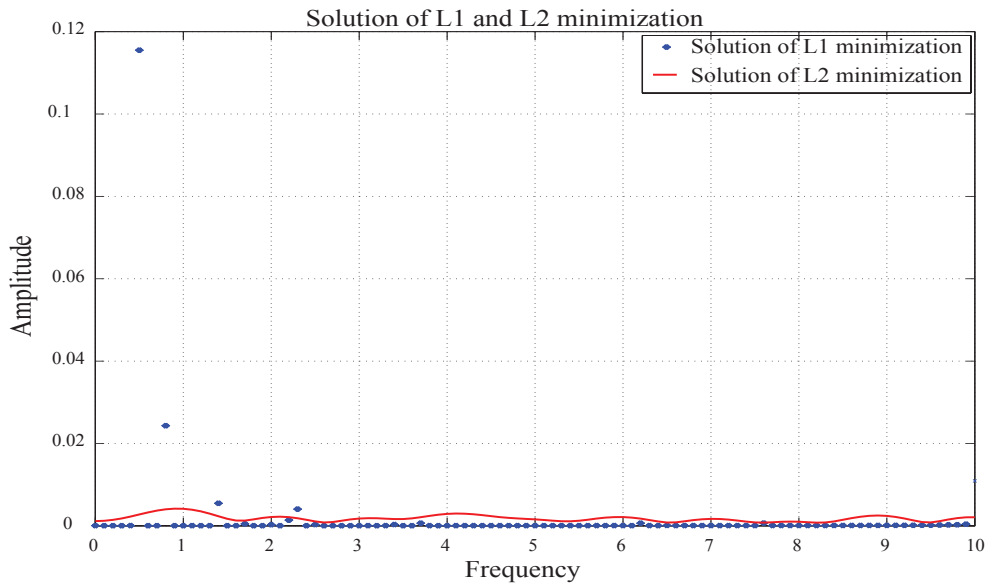


Figure 4.49: Extra frequencies recovered - Damage case 1 of SS beam

In accordance with the above claim, extra frequencies recovered do show up in the L1 recovery process and these are represented shown in figure 4.49. In addition to the 0.5 Hz frequency, a higher harmonic of 0.6 Hz is also present at an appreciable amplitude.

Figure 4.50 illustrates the reconstructed damaged ODS of the simply supported beam (case 1). Due to the evident distortion in the ODS, it is very clear that the beam has been damaged. The damaged area (potential) is indicated in the figure. It can also be observed that the ODS is not very smooth between 0.2 m - 0.3 m. So how do we conclude on the potentially damaged area? The answer comes from the shift of the ODS itself. It can be seen from the figure that the ODS seems to have shifted (or is more inclined) towards the end of the beam. Hence, the distortion around that region of the beam may be concluded as having a greater chance of being damaged.

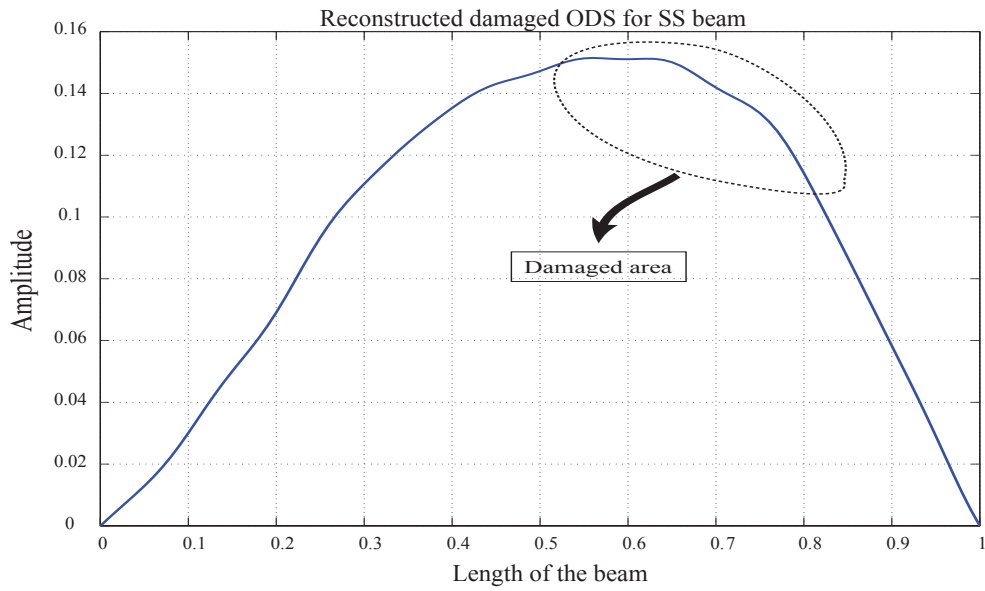


Figure 4.50: Reconstructed ODS - Damage case 1 of SS beam

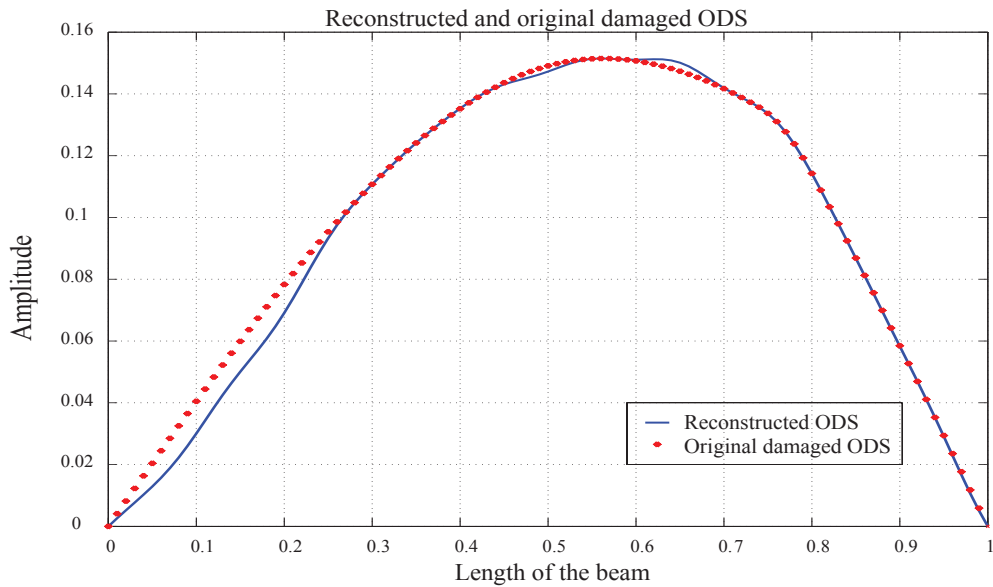


Figure 4.51: Reconstructed ODS compared to original ODS - Damage case 1 of SS beam

Figure 4.51 provides a visual comparison between the damaged original ODS of the SS beam and its reconstruction. This simulation attempts to reiterate that L1 minimization (CS) is indeed successful in reconstructing a spatial wave with minimal error.

4.8.1.2 Damage case 2 (Elements 25-35) - SS beam ODS

In the previous section, the ODS of the SS beam with damage towards the end of the beam was investigated. It was observed that while damage was indicated by the extra frequencies recovered during the L1 minimization process, the reconstruction helped to narrow down the location of damage on the beam. The next step is to check if the detection and location techniques be valid for damage elsewhere on the beam also. For this reason, a second case of damage is considered.

In this scenario, the EI of the SS beam is once again reduced from 1 to 0.1, but this time, over elements 25-35 of the simply supported beam. It is important to reiterate that the forcing conditions of the healthy SS beam are retained for this damaged case also. The damaged ODS of the beam is represented in figure 4.52. The damaged elements are also indicated on it.

As in the previous case, frequency recovery from the damaged ODS brings out the higher frequency components. These are indicated in figure 4.53. In case 2, higher frequencies of 0.6 Hz, 1.5 Hz and 1.6 Hz are recovered in addition to the 0.5 Hz (all spatial frequencies) at appreciable amplitudes. It can be reasoned also that the higher frequency components that show up in the L1 recovery process are entirely dependent on the shape the distorted ODS takes. This in turn is influenced by the extent of damage (i.e. number of elements involved in the damage), change in EI and probably even the point of forcing. These scenarios are yet to be tested out. Nevertheless, it can be undoubtedly concluded that damage in the beam distorts the ODS which has a tell-tale signature - higher spatial frequency components.

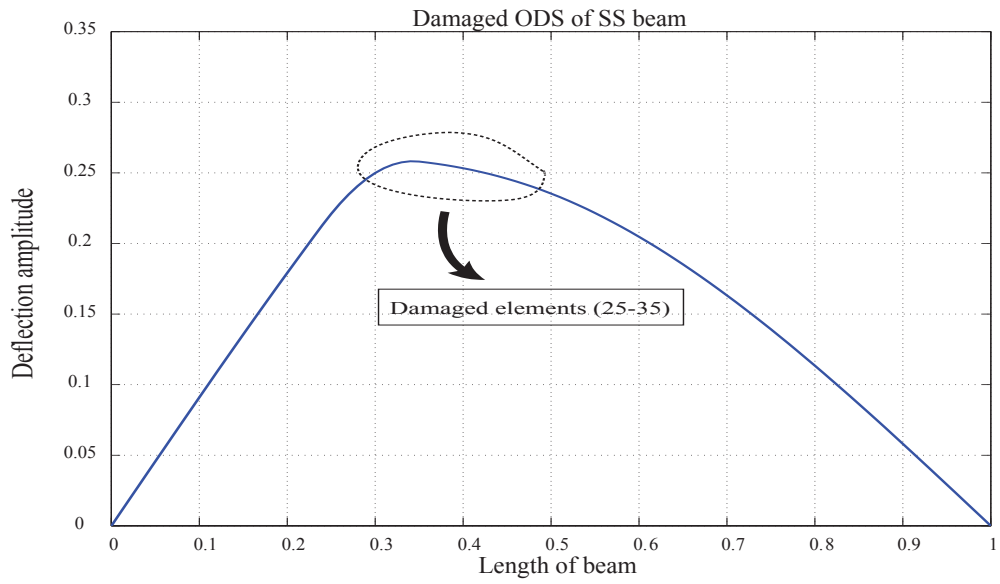


Figure 4.52: Damage case 2 - ODS of SS beam

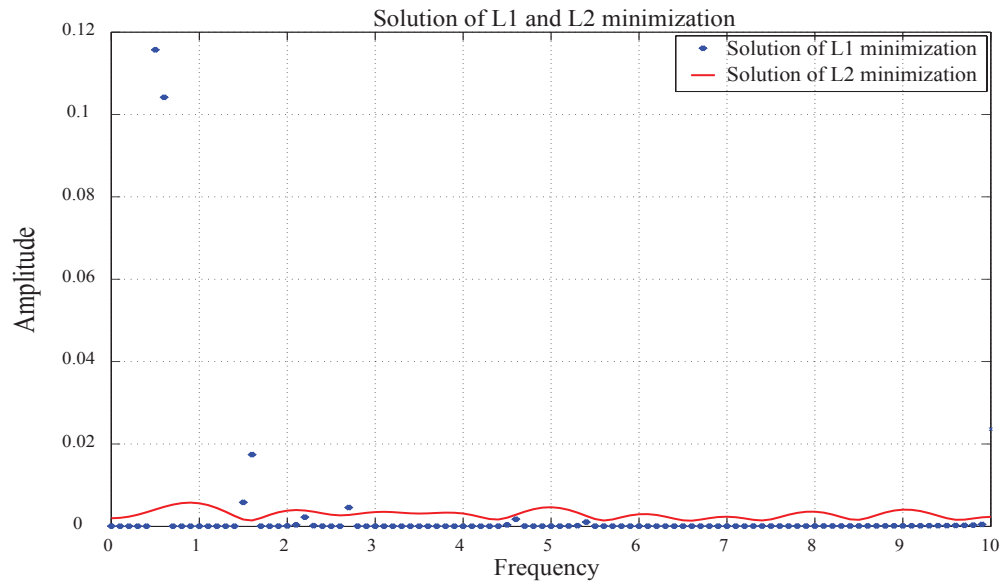


Figure 4.53: Extra frequencies recovered - Damage case 2 of SS beam

Figure 4.54 illustrates the reconstructed ODS of the damaged SS beam. As in damage case 1, the frequencies recovered using L1 minimization are used to obtain this almost flawless reconstruction. This also goes to show that the higher spatial frequencies from L1 recovery are indeed correct. The damaged area of the SS beam can be very evidently seen in the figure. A closer look at the ODS exposes distortions in other parts as well. However, as explained in damage case 1, the ODS here is shifted towards 0.2 m - 0.4 m of the beam thus suggesting higher chances of damaged in that region.

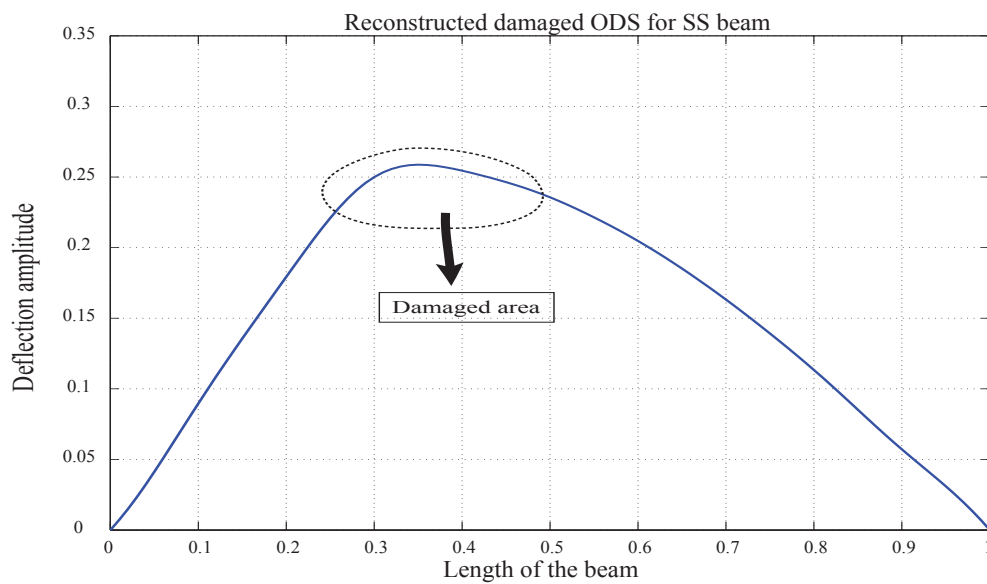


Figure 4.54: Reconstructed ODS - Damage case 2 of SS beam

The final step is to compare the originally distorted ODS of the SS beam in damage case 2 against its reconstruction. This is presented in figure 4.55. It can be observed the reconstruction is spot-on. In fact, as compared to damage case 1 where the same damage was distributed over elements 75-80, here, the error of reconstruction is much lower.

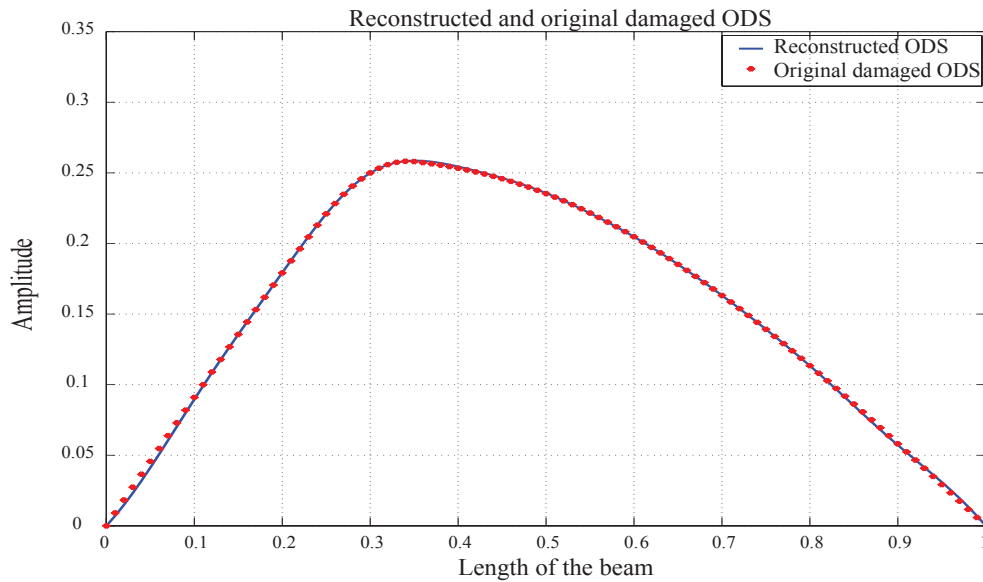


Figure 4.55: Reconstructed ODS compared to original ODS - Damage case 2 of SS beam

4.8.2 ODS of a fixed-fixed beam

A simply supported beam is a very simple scenario. We next move on to a slightly complex situation where the beam is fixed at both its ends. Such a beam has a transcendental solution with four terms - sine, cosine, hyperbolic sine and hyperbolic cosine components.

The ODS of a fixed-fixed beam is therefore examined to take one further step towards a more realistic structure. The FF beam chosen for testing is modeled using FEM analysis and is divided into 100 elements. The beam used here has the same properties as that of the SS beam used in the previous section, except for a change in the boundary conditions. It is harmonically excited at mid-length with an amplitude of 5 and a frequency of 2rads^{-1} . As in the case of SS beam, we aim to keeping the ODS very close to the first mode of vibration. For the FF beam considered, the first

natural frequency is at 22rads^{-1} .

Also, it is important to mention here that the number of samples, sampling points, frequency range of operation and resolution are kept the same for both the healthy as well as damaged scenarios. The reason behind such a choice has already been explained in the case of SS beam - to match realistic data acquisition environment.

Figure 4.56 illustrates the ODS of the FF beam with 12 random samples. Since the excitation is below the first mode of vibration, the ODS is expected to contain a greater percentage of first mode like pattern, i.e. resemble a simply sinusoid of frequency 0.5 Hz (spatially speaking!). However, because both ends of the beam are fixed, the healthy (undistorted) ODS should resemble a single frequency sine signal with 0 amplitude for a short period before zero crossing. This behavior is clearly evident in figure 4.56.

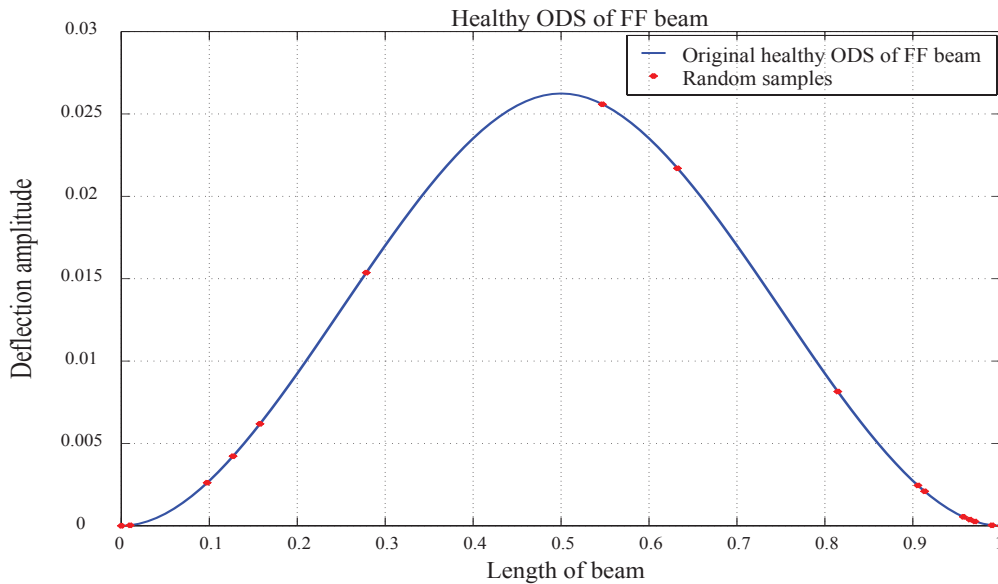


Figure 4.56: ODS of a fixed-fixed beam - Healthy (with random samples)

The next question to address is how many frequency components are expected to be recovered using L1 minimization? The FF beam ODS shown above is definitely not a sine wave of single frequency. Since both the ends are fixed, even in the damaged case, more than one frequency is expected to be present. Also, it may not (will not) have a predominant 0.5 Hz component as in the case of SS beam. To allow for tolerance, the number of frequencies to be recovered is fixed at 3. The frequency range of operation is chosen to be 0-7 Hz with a resolution of 0.1 Hz. Using the appropriate equation 3.6 we conclude that we would indeed need 12 samples per unit length for successful signal reconstruction.

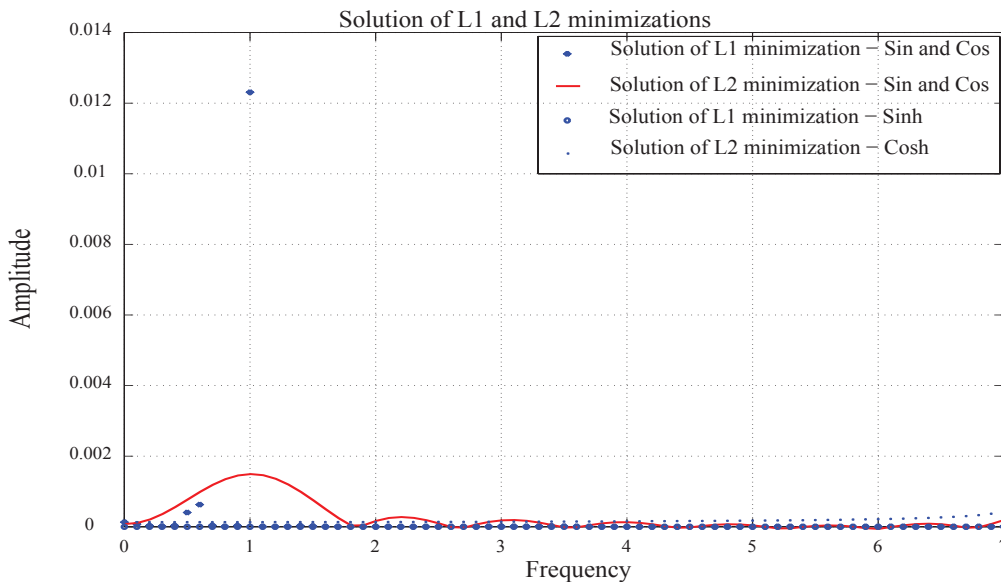


Figure 4.57: L1 and L2 minimization solutions

Figure 4.57 illustrates the frequencies that are recovered by L1 minimization using 12 random samples along the span of the beam. In comparison to the case of SS beam, here two more components are to be considered - the hyperbolic sine and cosines. This is owing to the transcendental characteristic equation of an FF beam. It can be observed from the figure that in accordance with

the above claim, the predominant frequency is at 1 Hz while couple of more components show up at very low amplitudes that they can ignored.

The final step is to check the reliability of using L1 to reconstruct the ODS from the recovered frequencies. This is illustrated in figure 4.58. It can be observed that the reconstructed ODS coincides almost completely with the original undamaged ODS. Hence L1 is a valid approach in case of a more realistic beam (FF) as well.

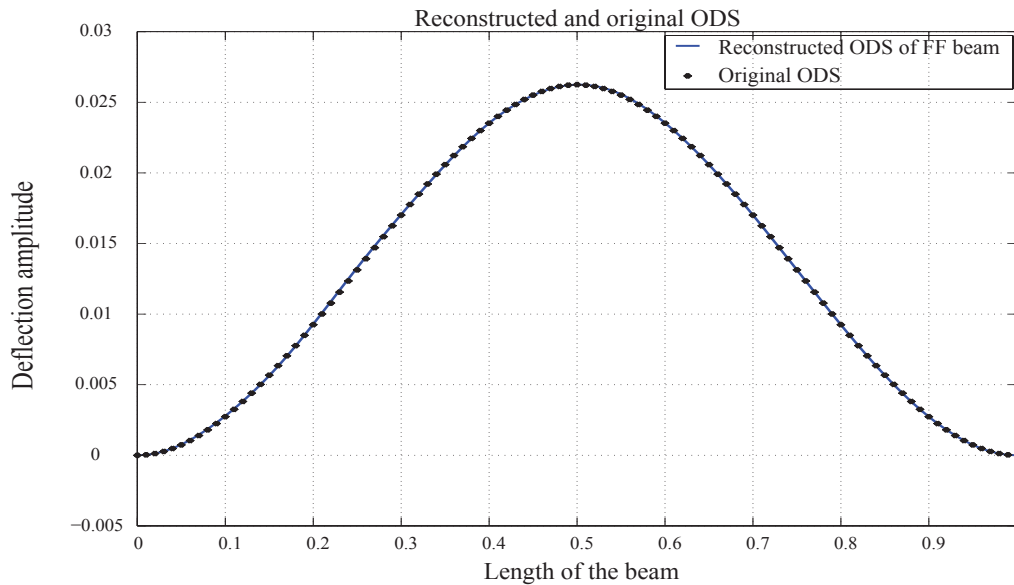


Figure 4.58: Reconstructed ODS of the FF beam - Healthy

Having obtained success in the undamaged situation, the next step is to use L1 recovery and reconstruction in case of damage in the FF beam. Similar to the case of an SS beam, the damage is characterized as a change (here, reduction) in the EI over a certain part of span.

A reduction in EI must cause higher amplitude vibrations in the elements involved, thus introducing higher harmonics in the ODS wave. The damage cases for the FF beam are listed in table 4.13.

Table 4.13: Damage cases of FF beam

Scenario	Rigidity modulus (EI)	Number of elements
Healthy	1	N/A
Case 1	0.1	68-78
Case 2	0.1	20-30

How the elements involved translates into a certain part of the beam span had already been explained in detail in section 4.9.1.1. These details for the FF beam are tabulated in table 4.14.

Table 4.14: Elements to beam span reflection

Damaged elements	Beam span
68-78	0.68 - 0.78
20 - 30	0.20 - 0.30

4.8.2.1 Damage case 1 (Elements 68-78)- FF beam ODS

The first case of damage to be investigated is the reduction in EI from 1 to 0.1 over elements 68-78 of the fixed-fixed beam. The forcing conditions such as type, amplitude, frequency and point of application of excitation is retained as in the undamaged case of the FF beam. The damaged ODS of the FF beam along with the damaged elements are indicated in figure 4.59.

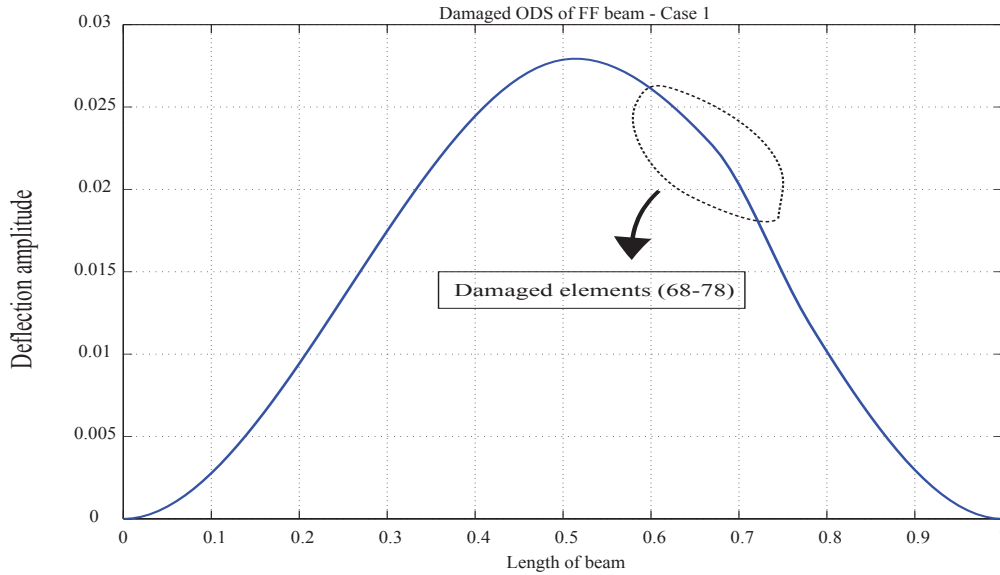


Figure 4.59: Damage case 1 - ODS of FF beam

From 12 randomly located samples over the entire length of the beam, frequency range of 0-7 Hz and resolution of 0.1 Hz, the L1 minimization operates over the distorted ODS to recover the extra frequencies (in addition to the 1 Hz) thus providing a clear signature for damage. These are represented in figure 4.60. From the damaged as well as the undamaged cases, it can be concluded that although there are hyperbolic components present in the characteristic equation of an FF beam, they do not play a very dominant role in frequency recovery. In fact, it would be important to note that one of the reasons for considering the hyperbolic components' recovery is a their probability of being predominant in the ODS wave. This was however proved negative from the results in both cases of the FF beam.

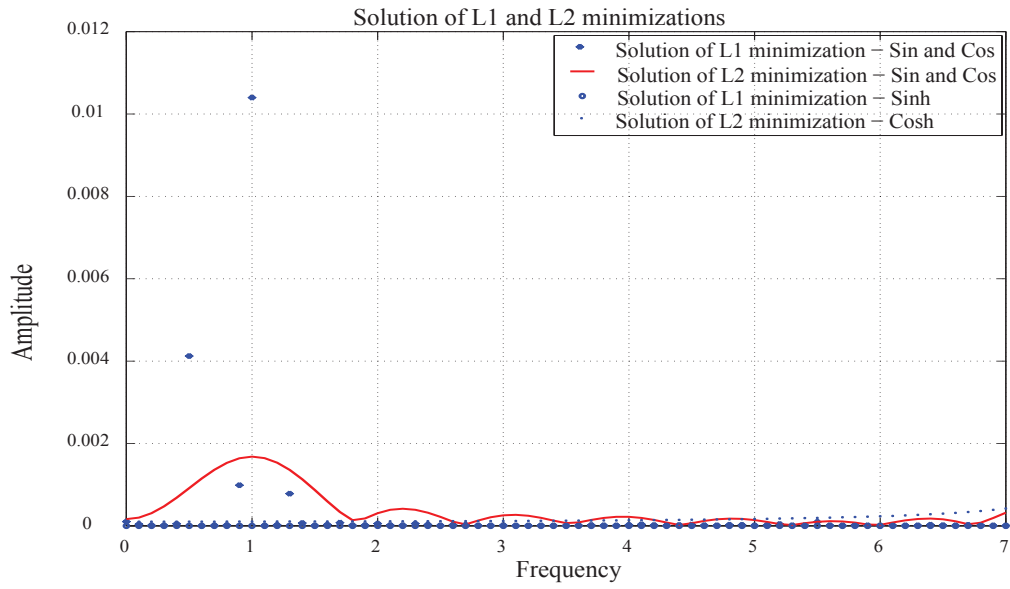


Figure 4.60: Extra frequencies recovered - Damage case 1 of FF beam

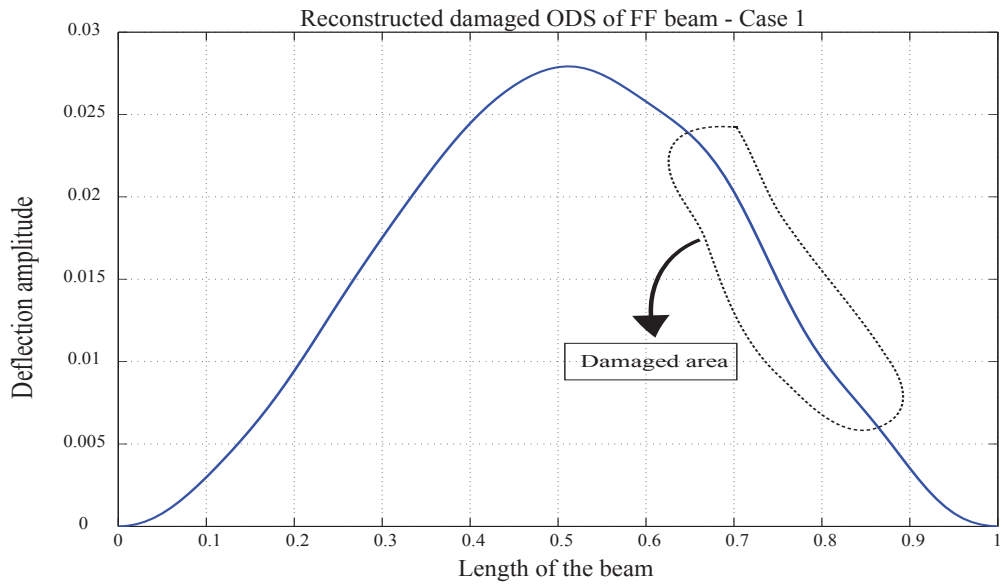


Figure 4.61: Reconstructed ODS - Damage case 1 of FF beam

The reconstructed ODS of the damaged FF beam (case 1) is illustrated in figure 4.61. The damaged area is also indicated. It can be observed from the reconstruction that distortions seem to extend a little further beyond the elements that were originally involved in the damage. This can be overlooked since it does help to narrow down the damage area even if not zero down to the elements specifically.

Figure 4.62 provides a visual perception on how the reconstructed ODS compares to the originally distorted ODS. It can be observed that the reconstruction indeed follows the original wave with very minimal error around the area of damage.

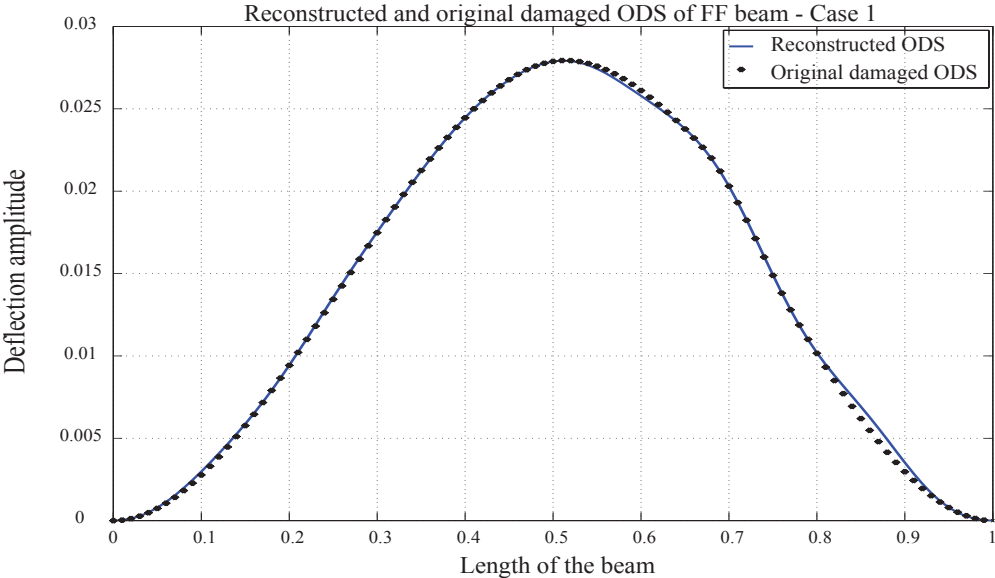


Figure 4.62: Reconstructed ODS compared to original ODS - Damage case 1 of FF beam

4.8.2.2 Damage case 2 (Elements 20-30) - FF beam ODS

Similar to an SS beam, in case of an FF beam another damage scenario is considered. This is performed to ensure that the L1 recovery and reconstruction of the distorted ODS is indeed valid for damage in any part of the FF beam.

The EI of the SS beam is once again reduced from 1 to 0.1, but this time, over elements 20-30 of the fixed-fixed beam. It is important to reiterate that the forcing conditions of the healthy FF beam are retained for this damaged case also. The damaged ODS of the beam is represented in figure 4.63. The damaged elements are also indicated on it.

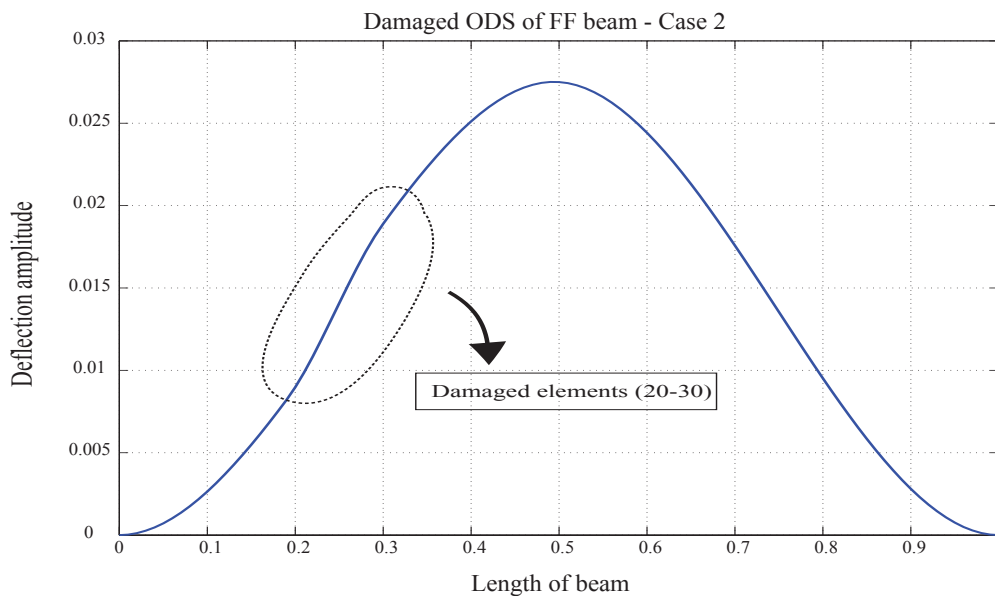


Figure 4.63: Damage case 2 - ODS of FF beam

The extra spatial frequencies that are recovered owing to introduction of damage are indicated in figure 4.63. Unlike case 1, case 2 damage produces spatial frequencies with less significant amplitudes. Therefore, one concern is that the signature of damage might not be very evident

from the recovery process in a practical sense. However, the hope is that presence of these extra frequencies will trigger distortion during the reconstruction of the ODS.

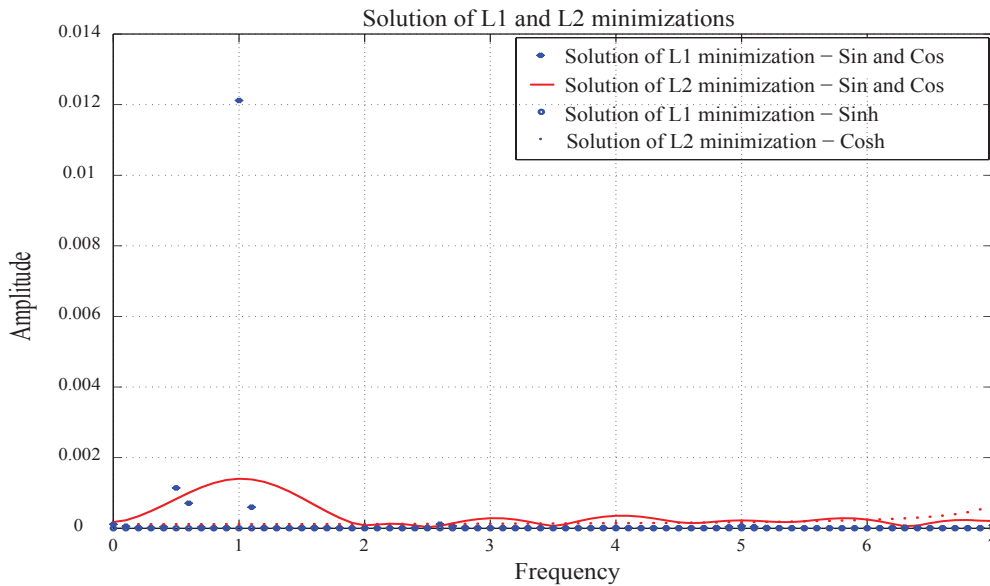


Figure 4.64: Extra frequencies recovered - Damage case 2 of FF beam

The reconstructed ODS is presented in figure 4.65. The damage is not strikingly evident. However, a closer look reveals the slight distortion (indicated by the circled area) in the ODS. Figure 4.66 illustrates how the reconstruction compares to the originally distorted ODS in case 2 of the damaged FF beam. It can be clearly seen that the reconstructed and the original ODS do coincide with each other almost flawlessly, suggesting that inherently, case 2 damage scenario was not severe enough to reflect very prominently in the ODS.

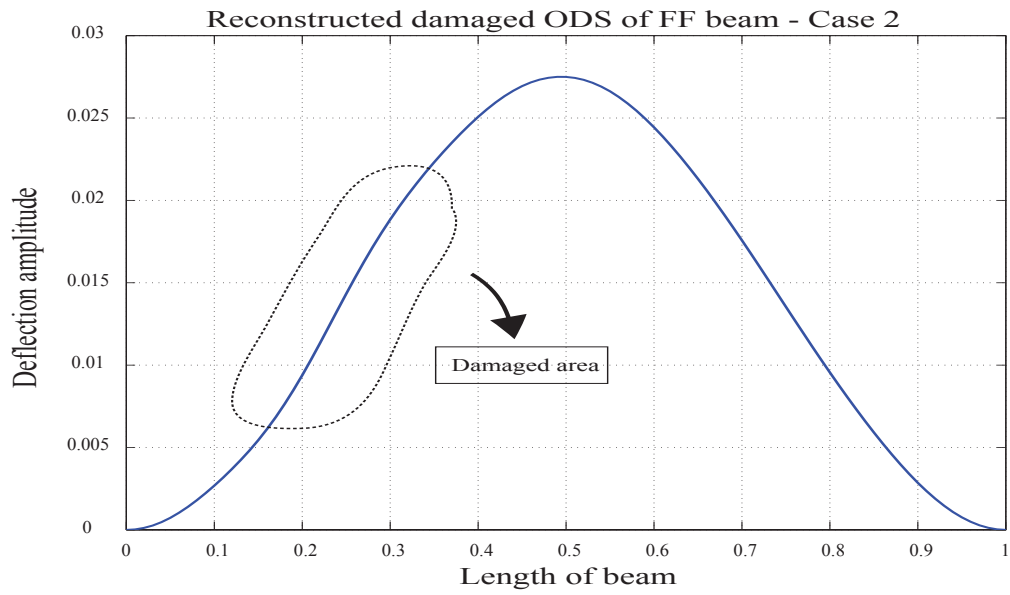


Figure 4.65: Reconstructed ODS - Damage case 2 of FF beam

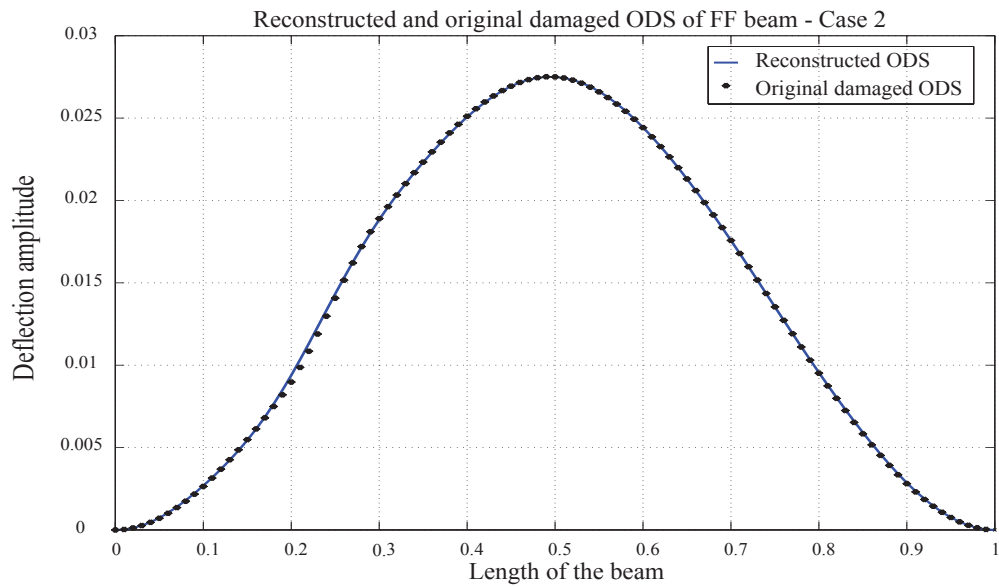


Figure 4.66: Reconstructed ODS compared to original ODS - Damage case 2 of FF beam

CHAPTER 5: CONCLUSION

Compressive sensing was studied for application to structural health monitoring. It was observed that L1 minimization, a basic tenet of compressive sensing, out-performed both fast fourier transform as well as L2 minimization methods in terms of frequency recovery and signal reconstruction. While FFT failed to recover the higher frequency components of a signal when sampled at the Nyquist rate, L1 minimization reliably extracted frequency components using reduced number of randomly placed samples. Furthermore, comparing and analyzing the results of L2 and L1 minimizations, it was clear that L1 produced better quality reconstruction for sparse signals.

L1 minimization was applied to the response of linear systems to observe changes in natural frequency of vibration and amplitude of vibration to detect damage. It was also used to reconstruct modeshapes of beam vibration under both healthy and damaged conditions to observe how damage was reflected. This amounted to extending L1 minimization to spatial reconstruction. In the spatial domain, L1 was used to reconstruct operational deflection shapes (ODS) of both simply supported (SS) beams and fixed-fixed (FF) beams under undamaged and damaged conditions. Presence of damage was evident which and reproduced in reconstruction.

It was concluded that L1 minimization or compressive sensing may potentially contribute significantly in reducing the number of samples/sensors used in damage detection procedures. One could also realize that the potential of CS can extend beyond structural health monitoring to other fields where the burden on data acquisition must be reduced.

LIST OF REFERENCES

- [1] Ajay Raghavan and Carlos E.S. Cesnik, *Review of Guided-wave Structural Health Monitoring*. The Shock and Vibration Digest; 39; 91, DOI:10.1177/0583102406075428, 2007.
- [2] Peter C. Chang, Alison Flatau and S.C. Liu *Review Paper: Health Monitoring of Civil Infrastructure*. Structural Health Monitoring; 2:257, DOI:10.1177/1475921703036169, 2003.
- [3] Chance, J.C., Tomlinson, J.R. and Worden, K. *A Simplified approach to the numerical and experimental modelling of the dynamics of a cracked beam*. Proceedings of the 12th International Modal Analysis Conference, pp.778–785, 1994.
- [4] Toksoy, T. and Aktan, A.E. *Bridge-condition assessment by modal flexibility*. Experimental Mechanics, 34, 271–278, 1994.
- [5] Zhang, Z. and Aktan, A.E. *The damaged indices for constructed facilities*. Proceedings of the 13th International Modal Analysis Conference, pp.1520–1529, 1995.
- [6] Wu, M., Chen, X. and Liu, R. *Highway crack monitoring system*. Proceedings of the SPIE Conference, Sandiego pp.18–21, 2002.
- [7] Rasim O. Guldiken, Onursal Onen, Mustafa Gul and F. Necati Catbas. *A structural health monitoring system with ultrasonic MEMS transducers*. Sensors and smart structures technologies for civil, mechanical and aerospace systems, Proceedings of SPIE, Vol. 7981, 79810F–1, 2011.
- [8] Akash Jain, David W. Greve and Irving J. Oppenheim. *A MEMS transducer for ultrasonic flaw detection*. ISARC, Washington D.C, 2002.

- [9] Mousumi Majumder, Tarun Kumar Gangopadhyay, Ashim Kumar Chakraborty, Kamal Dasgupta and D.K. Battacharya. *Fibre Bragg Gratings in structural health monitoring - Present status and applications*. Sensors and Actuators A: Physical, Volume 147, Issue 1 pp 150 – 164, 2008.
- [10] F Necati Catbas, Hasan B Gokce and Mustafa Gul. *Non-parametric analysis of structural health monitoring data for identification and localization of changes: Concept, lab and real-life studies*. Structural Health Monitoring, 11:613 DOI: 10.1177/1475921712451955, 2012.
- [11] Adam J. Brzezinski, Sunil Kukreja, Jun Ni and Dennis S. Bernstein. *Sensor - Only fault detection using pseudo transfer function identification*. American Control Conference, Marriott Waterfront, Baltimore, MD, USA, 2010.
- [12] Richard Marquez, Addison-Rios-Bolivar and Eduardo Teles. *A transfer function approach to fault diagnosis for linear systems: inversion and low-pass filters*. Proceedings of the 15th International Workshop Principles Diagnosis, pp 105–110, Carcassonne, 2004.
- [13] E. Peter Carden and Paul Fanning. *Vibration based condition monitoring: A review*. Structural Health Monitoring, 3: 355, DOI: 10.1177/1475921704047500, 2004.
- [14] Farrar C.R., and Doebling, S.W. *Damage Detection II: field applications to large structures*. NATO Science Series, Dordrecht, Netherlands: Kulwer Academic Publishers, 1999.
- [15] Ghoshal, A., Sundaresan, M.J., Schulz, M.J. and Pai, P.F. *Structural health monitoring techniques for wind turbine blades*. Journal of Wind Engineering and Industrial Aerodynamics, 85, 309–324, 2000.
- [16] Aktan, A.E., Catbas, F.N., Grimmelsman, K.A. and Tsikos, C.J. *Issues in infrastructure health monitoring for management*. Journal of Engineering Mechanics, 126(7), 711–724, 2000.

- [17] Aktan, A.E., Farhey, D.N., Helmicki, A.J., Brown, D.L., Hunt, V.J., Lee, K.-L and Levi, A. *Structural identification for condition assessment: Experimental arts*. Journal of Structural Engineering, 123(12), 1674–1684, 1997.
- [18] Alaylioglu, H. and Alaylioglu, A. *Finite element and experimental bases of a practical bridge management and maintenance system*. Computers and Structures, 73, 281–293, 1999.
- [19] Catbas, F.N. and Aktan, A.E. *Condition and damage assessment: Issues and some promising indices*. Journal of Structural Engineering, 128(8), 1026–1036, 2002.
- [20] Fryba, L. and Pirner, M. *Load tests and modal analysis of bridges*. Engineering Structures, 23, 102–109, 2001.
- [21] Maia, N.M.M. and Silva, J.M.M. (eds) *Theoretical and Experimental Modal Analysis*. England: Research studies Press, Ltd., 1997.
- [22] J. Pereira, W. Heylen, S. Lammens, and P. Sas. *Influence of the number of frequency points and resonance frequencies on model updating techniques for health condition monitoring and damage detection of flexible structures*. Proceedings of the 13th IMAC, pp 1273–1281, 1995.
- [23] J. Pereira, W. Heylen, S. Lammens, and P. Sas. *Model updating and failure detection based on experimental FRF's: Case study on space frame structure*. ISMA19 - Tools for Noise and Vibration Analysis, pp 669–681, 1994.
- [24] Richardson, M. and Mannan, M.A. *Detection and location of structural cracks using FRF measurements*. Proceeding of the 8th International Modal Analysis Conference, pp 512–518, 1990.
- [25] Morassi, A. *Identification of a crack in a rod based on changes in a pair of natural frequencies*. Journal of Sound and Vibration, 242(4), 577–596, 2001.

- [26] I. Trendafilova, W. Heylen. *Fault localization in structures from remote FRF measurements. Influence of the measurement points*. Proceedings of the 23rd International Conference on Noise and Vibration, Leuven, Belgium, 149–156, 1998.
- [27] Adams, R.D., Cawley, P., Pye, C.J. and Stone, B.J. *A vibration technique for non-destructively assessing the integrity of structures*. Journal of Mechanical Engineering Science, 20(2), 93–100, 1978.
- [28] Samman, M.M. and Biswas, M. *Vibration testing for nondestructive evaluation of bridges. I: Theory*. Journal of Structural Engineering, 120(1), 269-289, 1994a.
- [29] Samman, M.M. and Biswas, M. *Vibration testing for nondestructive evaluation of bridges. II: Results*. Journal of Structural Engineering, 120(1), 290-306, 1994b.
- [30] Cawley, P. and Adams, R.D. *The location of defects in structures from measurements of natural frequencies*. Journal of Strain Analysis, 14(2), 49-57, 1979.
- [31] Salawu, O.S. *Detection of structural damage through changes in frequency: a review*. Engineering Structures, 19(9), 718-723, 1997.
- [32] Banks, H.T., Inman, D.J., Leo, D.J. and Wang, Y. *An experimentally validated damage detection theory in smart structures*. Journal of Sound and Vibration, 191(5), 859-880, 1996.
- [33] Kessler, S.S., Spearing, S.M., Atalla, M.J., Cesnik, C.E.S and Soutis, C. *Damage detection in composite materials using frequency response methods*. Composites Part B: Engineering, 33, 87-95, 2002.
- [34] Chen, H.L., Spyrakos, C.C. and Venkatesh, G. *Evaluating structural deterioration by dynamic response*. Journal of Structural Engineering, 121(8), 1197-1204, 1995.
- [35] Farrar, C.R., Baker, W.E., Bell, T.M., Cone, K.M., Darling, T.W., Duffey, T.A., Eklund, A. and Miglori, A. *Dynamic characterization and damage detection in the I-40 bridge over the*

Rio Grande. Los Alamos National Laboratory Report LA-12767-MS, Los Alamos National Laboratory, P.O. Box 1193, Los Alamos, NM, 87544, USA, 1994.

- [36] Law, S.S., Ward, H.S., Shi, G.B., Chen, R.Z., Waldron, P. and Taylor, C. *Dynamic assessment of bridge load-carrying capacities. I*. Journal of Structural Engineering, 121(3), 478-487, 1995a.
- [37] Law, S.S., Ward, H.S., Shi, G.B., Chen, R.Z., Waldron, P. and Taylor, C. *Dynamic assessment of bridge load-carrying capacities. II*. Journal of Structural Engineering, 121(3), 488-495, 1995b.
- [38] De Roeck, G., Peeters, B. and Maeck, J. *Dynamic monitoring of civil engineering structures*. Computational Methods for Shell and Spatial Structures, IASS-IACM 2000, Chania, Crete, Greece, 2000.
- [39] Ewins, D.J. *Modal Testing: Theory and Practice*. England: Research Studies Press Ltd., 1984.
- [40] Allemang, R.J. and Brown, D.L. *Correlation coefficient for modal vector analysis*. Proceedings, 1st International Modal Analysis Conference, Orlando, Florida, USA, pp. 110-116, 1982.
- [41] Lieven, N.A.J. and Ewins, D.J. *Spatial correlation of modespaces: the coordinate modal assurance criterion (COMAC)*. Proceedings of the 6th International Modal Analysis Conference, Kissimmee, Florida, USA, pp. 1063-1070, 1988.
- [42] Salawu, O.S. and Williams, C. *Bridge assessment using forced-vibration testing*. Journal of Structural Engineering, 121(2), 161-173, 1995.
- [43] Ren, W.-X. and De Roeck, G. *Structural damage identification using modal data. I: Simulation verification*. Journal of Structural Engineering, 128(1), 87-95, 2002a.

- [44] Ren, W.-X. and De Roeck, G. *Structural damage identification using modal data. II: Test verification*. Journal of Structural Engineering, 128(1), 96-104, 2002b.
- [45] Alampalli, S., Fu, G. and Dillon, E.W. *Signal versus noise in damage detection by experimental modal analysis*. Journal of Structural Engineering, 123(2), 237-245, 1997.
- [46] Rathcliffe, C.P. and Bagaria, W.J. *Vibration technique for locating delamination in a composite beam*. AIAA Journal, 36(6), 1074-1077, 1998.
- [47] Wahab, M.M.A. and De Roeck, G. *Damage detection in bridges using modal curvatures: applications to a real damage scenario*. Journal of Sound and Vibration, 226(2), 217-235, 1999.
- [48] Oh, B.H. and Jung, B.S. *Structural damage assessment with combined data of static and modal tests*. Journal of Structural Engineering, 124(8), 956-965, 1998.
- [49] Wahab, M.M.A. *Effect of modal curvatures on damage detection using model updating*. Mechanical Systems and Signal Processing, 15(2), 439-445, 2001.
- [50] Sampaio, R.P.C., Maia, N.M.M. and Silva, J.M.M. *Damage detection using the frequencyresponse- function curvature method*. Journal of Sound and Vibration, 226(5), 1029-1042, 1999.
- [51] Kim, J.-T. and Stubbs, N. *Model-uncertainty impact and damage-detection accuracy in plate girder*. Journal of Structural Engineering, 121(10), 1409-1417, 1995.
- [52] Shi, Z.Y., Law, S.S. and Zhang, L.M. *Damage localization by directly using incomplete mode shapes*. Journal of Engineering Mechanics, 126(6), 656 - 660, 2000c.
- [53] Waldron, K., Ghoshal, A., Schulz, M.J., Sundaresan, M.J., Ferguson, F., Pai, P.F. and Chung, J.H. *Damage detection using finite element and laser operational deflection shapes*. Finite Elements in Analysis and Design, 38, 193-226, 2002.

- [54] Kim, J.-T. and Stubbs, N. *Improved damage identification method based on modal information*. Journal of Sound and Vibration, 252(2), 223-238, 2002.
- [55] Chen, H.R. and Kiriakidis, A.C. *Stiffness evaluation and damage detection of ceramic candle filters*. Journal of Engineering Mechanics, 126(3), 308-319, 2000.
- [56] Stubbs, N. and Kim, J.-T. *Damage localization in structures without baseline modal parameters*. AIAA Journal, 34(8), 1644-1649, 1996.
- [57] Law, S.S., Shi, Z.Y. and Zhang, L.M. *Structural damage detection from incomplete and noisy modal test data*. Journal of Engineering Mechanics, 124(11), 1280-1288, 1998.
- [58] Worden, K., Manson, G. and Allman, D.J. *An experimental appraisal of the strain energy damage location method*. Damage Assessment of Structures, Proceedings of the 4th International Conference on Damage Assessment of Structures, Cardiff, Wales, UK, June, Key Engineering Materials, Vols. 204-205, pp. 35-46, 2001.
- [59] Peterson, S.T., McLean, D.I., Symans, M.D., Pollock, D.G., Cofer, W.F., Emerson, R.N. and Fridley, K.J. *Application of dynamic system identification to timber beams. I*. Journal of Structural Engineering, 127(40), 418-425, 2001a.
- [60] Peterson, S.T., McLean, D.I., Symans, M.D., Pollock, D.G., Cofer, W.F., Emerson, R.N. and Fridley, K.J. *Application of dynamic system identification to timber beams. II*. Journal of Structural Engineering, 127(4), 426-432, 2001b.
- [61] Mario Sols, Mario Algaba and Pedro Galvn. *Continuous wavelet analysis of mode shapes differences for damage detection*. Mechanical Systems and Signal Processing, 40(2), 645-666, 2013.
- [62] T. Mathworks, MatLab, 2011.

- [63] M. Rucka, K. Wilde. *Crack identification using wavelets on experimental static deflection profiles*. Eng. Struct. 28(2), 279-288, 2006.
- [64] U.P. Poudel, G. Fu, J. Ye. *Structural damage detection using digital video imaging technique and wavelet transformation*. Journal of Sound Vibration, 286(4-5), 869-895, 2005.
- [65] G. Strang, N. Truong. *Wavelets and Filter Banks*. Wellesley College Press, Cambridge, 1996.
- [66] A. Messina. *Refinements of damage detection methods based on wavelet analysis of dynamical shapes*. International Journal of Solids and Structures, 45(14-15), 4068-4097, 2008.
- [67] A. Gentile, A. Messina. *On the continuous wavelet transforms applied to discrete vibrational data for detecting open cracks in damaged beams*. International Journal of Solids and Structures, 40(2), 295-315, 2003.
- [68] Quan Wang, Xiaomin Deng. *Damage detection with spatial wavelets*. International Journal of Solids and Structures, 36, 3443-3468, 1999.
- [69] Dana Mackenzie. *Compressed Sensing Makes Every Pixel Count*. What's Happening in the Math. Sciences, AMS, 114-127, 2009.
- [70] Michael Lustig, David Donoho and John M. Pauly. *Sparse MRI: The Application of Compressed Sensing for Rapid MR Imaging*. Submitted to Magnetic Resonance in Medicine.
- [71] Jarvis Haupt and Robert Nowak. *Signal Reconstruction from Noisy Random Projections*. IEEE Trans. Inform. Theory, 52(9), pp. 4036-4048, 2006.
- [72] E. Candes, J. Romberg, and T. Tao. *Robust uncertainty principles: Exact signal reconstruction from highly incomplete frequency information*. IEEE Transactions on Information Theory, 52(2), pp. 489-509, 2006.

- [73] E. Candes and T. Tao *Near optimal signal recovery from random projections and universal encoding strategies*. Preprint, October, 2004.
- [74] D. L. Donoho. *Compressed sensing*. Preprint, September, 2004.
- [75] Jianwei Ma. *Compressed Sensing for Surface Characterization and Metrology*. IEEE Trans. Instrument and Measurement, 2009, to appear.
- [76] Richard Baraniuk and Philippe Steeghs. *Compressive Radar Imaging*. IEEE Radar Conference, Waltham, MA, April 2007.
- [77] Moshe Mishali, Yonina C. Eldar and Joel A. Tropp. *Efficient sampling of sparse wideband analog signals*. Proc. IEEE, 25th Conv., pp. 290-294, Dec. 2008
- [78] Mark A. Davenport, Jason N. Laska, John R. Treichler, and Richard G. Baraniuk. *The Pros and Cons of Compressive Sensing for Wideband Signal Acquisition: Noise Folding vs. Dynamic Range*. IEEE Trans. Signal Process. (2012), in press.
- [79] A. Beck and M. Teboulle. *A fast iterative shrinkagethresholding algorithm for linear inverse problems*. SIAM J. Imaging Sciences, vol. 2, no. 1, pp. 183-202, Jan. 2009.
- [80] Masaaki Nagahara, Daniel E. Quevedo, Takahiro Matsuda and Kazunori Hayashi. *Compressive sampling for networked feedback control*. IEEE International Conference on Acoustics, Speech and Signal Processing, pp 2733–2736, March 2012.
- [81] M. Unser. *Sampling 50 Years after Shannon*. Proceedings of the IEEE, Vol. 88, no. 4, pp. 569-587, 2000.
- [82] Massimo Fornasier and Holger Rauhut. *Compressive Sensing*. Handbook of Mathematical methods in Imaging, edited by Scherzer, O. Springer, to appear.

- [83] S. G. Mallat and Z. Zhang. *Matching pursuits with time-frequency dictionaries*. IEEE Trans. Signal Process., vol. 41, no. 12, pp. 3397-3415, 1993.
- [84] B. K. Natarajan. *Sparse approximate solutions to linear systems*. SIAM J. Comput., vol. 24, pp. 227-234, 1995.
- [85] S. S. Chen, D. L. Donoho, and M. A. Saunders. *Atomic decomposition by Basis Pursuit*. SIAM J. Sci. Comput., vol. 20, no. 1, pp. 33-61, 1999.
- [86] S. Boyd and L. Vandenberghe. *Convex Optimization*. Cambridge Univ. Press, 2004.
- [87] J. A. Tropp. *Greed is good: Algorithmic results for sparse approximation*. IEEE Trans. Inform. Theory, vol. 50, no. 10, pp. 2231-2242, 2004.
- [88] J. Tropp and D. Needell. *CoSaMP: Iterative signal recovery from incomplete and inaccurate samples*. Appl. Comput. Harmon. Anal., page 30, 2008.
- [89] Emmanuel J. Cands. *Compressive Sampling*. Proc. Int. Cong. Mathematicians, Madrid, Spain, vol. 3, 2006, pp. 1433-1452.
- [90] Mallat, S. *A Wavelet Tour of Signal Processing*. Academic Press, San Diego, CA, 1998.
- [91] R.G. Baraniuk. *Compressive sensing*. IEEE Signal Processing Mag., vol. 24, no. 4, pp. 118-120, 124, 2007.
- [92] Michael Lamoureux. *Tutorial on Compressive Sampling*. CSPG CSEG CWLS Convention, 2008.
- [93] R.G. Baraniuk, M. Davenport, R. DeVore, and M.B. Wakin. *A simple proof of the restricted isometry principle for random matrices (aka the Johnson-Lindenstrauss lemma meets compressed sensing)*. Constructive Approximation, 2007 [Online]. Available: <http://dsp.rice.edu/cs/jlcs-v03.pdf>

- [94] D. Takhar, V. Bansal, M. Wakin, M. Duarte, D. Baron, J. Laska, K.F. Kelly, and R.G. Baraniuk. *A compressed sensing camera: New theory and an implementation using digital micromirrors*. Proc. Comput. Imaging IV SPIE Electronic Imaging, San Jose, Jan. 2006.
- [95] . Bjrck. *Numerical Methods for Least Squares Problems*. SIAM. ISBN 978-0-89871-360-2, 1996.
- [96] C.R. Rao, H. Toutenburg, A. Fieger, C. Heumann, T. Nittner and S. Scheid. *Linear Models: Least Squares and Alternatives*. Springer Series in Statistics, 1999.
- [97] *Federal analysis: Over 7,700 bridges in danger of collapse*. Associated Press, September 16, 2013.
- [98] Grabianowski, Ed. *10 Reasons Why Bridges Collapse*. HowStuffWorks.com, 13 September 2011.
- [99] Singiresu S. Rao. *Mechanical Vibrations 4th edition*. Pearson Education, Inc. and Dorling Kindersley Publishing Inc., 2004.